IMPERIAL COLLEGE LONDON

Spectral Collocation Methods for Leaky Waves in Submerged and Buried Elastic Waveguides

by

Evripides Georgiades

A thesis submitted to Imperial College London for the degree of

Doctor of Philosophy

Department of Mechanical Engineering
Imperial College London
London SW7 2BX

January 2025

Declaration of originality

The content of this thesis is my own research work, which was completed with the supervision of Professor Michael Lowe and Professor Richard Craster. Wherever other work was used I clearly acknowledged, and provided references.

Evripides Georgiades

April 15, 2025

Copyright

In memory of my father

Στη μνήμη του πατέρα μου

Abstract

Leaky waves constitute an important class of guided waves that propagate in waveguides adjacent to infinite fluid or solid media. A mismatch in material properties between the waveguide and its surroundings causes the radiation of energy away from the waveguide and the attenuation of the propagating wave. Such waves are encountered in a wide range of settings, from non-destructive evaluation and submerged pipes to medical ultrasound and bone surrounded by tissue. Thus, a thorough understanding of the mechanisms underlying their propagation, and particularly of their dispersion curves, is essential for many applications. Despite this, the numerical schemes traditionally employed for the computation of these dispersion curves are significantly compromised by the complex wavenumbers associated with leaky waves and their exponential growth in amplitude away from the waveguide.

The work presented in this thesis proposes a spectral collocation method that overcomes those numerical challenges and aims towards a fully automated approach for the computation of leaky wave dispersion curves. To demonstrate the method, a typical situation is studied first: waves radiating from a straight elastic waveguide with a fluid on either side. The novelty of the work lies in the use of complex coordinate transformations that facilitate the numerical decay of the radiated field while also preserving all its physical characteristics; solving the leaky wave problem then becomes a matter of

solving a numerically decaying one in complex space.

Building on this approach, problems of increased complexity were subsequently investigated. These include the computation of leaky wave dispersion curves of waves in plates embedded in elastic media or submerged hollow cylinders, and the computation of scattered fields in closely linked underwater scattering response problems. The validity of the method was established through comparisons of predicted dispersion curves against those of commercially available software, numerical experiments with finite elements, and analytic formulations.

Acknowledgements

This thesis marks the end of a long journey that has been as much a process of academic discovery as one of personal development and perseverance. Despite it being my name on the title page, its completion would not have been possible without the direct or indirect contributions of so many, to whom I am deeply grateful.

First and foremost, I would like to extend my gratitude to my supervisors Mike Lowe and Richard Craster. I am forever indebted to you for the invaluable opportunity to work with such kind and brilliant minds, and for the knowledge I have inherited. Thank you for always being patient, encouraging and believing in me, even during times when I might have doubted myself. Your love for science is truly contagious and I will always look back on these last four years working alongside you with great fondness. You have set the bar for what it means to be an exceptional mentor remarkably high.

Many thanks also go out to the NDE group here at Imperial College London. I feel privileged to have been surrounded by all the smart and wonderful people of the group. I will forever treasure the countless conversations, academic or otherwise, the drinks, the dinners, the football and the late nights. A special thanks goes out to my dear friend Giorgos, for his support, encouragement, and most importantly, the cherished memories we've shared in the office and around the world; here's to many more.

I owe a heartfelt thank you to the most significant contributors of this thesis – my family. To my mum, Evi, your strength, love, and dedication have been the foundation of everything I've achieved. Looking back, I am certain I would not be writing this now if it weren't for all your sacrifices and support. I can never thank you enough but please know that I will be forever grateful for everything you've done for me. Likewise, I am deeply grateful to the rest of the family – my siblings Pantelis and Anna, my grandmas and grandpas, uncles and aunts, cousins, godson and everyone in-between – for their unconditional love and for so frequently providing support in ways they may not even realise.

Last but not least, I wish to extend my appreciation to all my friends outside academia, for always cheering me on and showing a keen interest in my work. Each one of you have played a role in shaping this thesis, and I carry your kindness and support with me as I move forward.

From the bottom of my heart, I thank you all!

Ευχαριστώ!

Contents

List of Figures

Chapter 1

Introduction

1.1 Motivation

A guided wave is one that propagates along a surface or within a bounded medium, known as a waveguide [1], and has its direction guided by the boundaries of the medium. Famous examples of such waves are seismic waves propagating around the surface of the earth, waves in a tensioned string, waves propagating along a pipe, or the "whispering gallery" waves travelling around a concave surface, first studied by Lord Rayleigh [2] for sound waves (whispers) travelling around the walls of the whispering gallery of St Paul's Cathedral in London; this thesis will focus on guided waves in waveguides.

Because the energy of guided waves is constrained within the boundaries of a waveguide, an important feature – and one of the reasons they are a popular choice for a wide range of applications within physics, biology, medicine and engineering – is that guided waves can travel very long distances. In recent years, amongst other things, they have been used to characterise material properties in pavements [3], to assess bone quality and thickness [4,5],

to monitor steam generating tubes in nuclear power plants [6], to direct the emission of light using optical waveguide antennas [7], to transmit mechanical energy in surface acoustic wave devices [8] – used as filters, oscillators and transformers in electronic circuits of household devices and mobile phones – or, within Non-Destructive Evaluation (NDE), to inspect pipelines [9], railway tracks [10] and structures of arbitrary numbers of layers, materials and geometries [11–14].

Although the use of guided waves is very broad and takes many forms, a common premiss prevails; a guided wave is excited at a particular location, propagates inside a structure, and is monitored. If a feature is present within that structure, either due to its geometry, like a weld or varying thickness, or a defect, like a crack in a pipe or a broken bone, the guided wave will interact with the feature and get scattered by it, ultimately altering what is monitored. By studying the monitored signal, insight into the nature of the interaction and the feature itself is gained.

In addition to their ability to travel long distances, guided waves are, in general, dispersive; their velocity varies with frequency. The variation of a guided wave's velocity with frequency can be drawn out in the form of a curve – its dispersion curve. In fact, there may be an infinite number of possible guided waves that can propagate along a waveguide, known as the modes of propagation, with each one having its very own dispersion curve and causing the material of the waveguide to oscillate in a unique way. The distribution of displacements or stresses in the direction normal to the direction of propagation, caused by a mode of known frequency and velocity, is referred to as its mode shape, and mode shapes, just like velocity, vary as one moves along a mode's dispersion curve. For guided waves in symmetric straight waveguides of finite thickness, the mode shapes are the profiles of displacement or stress through the thickness of the waveguide, and they are odd or even functions

of perpendicular distance from the centreline of the waveguide. Modes of odd mode shapes are regarded as the antisymmetric modes, while modes of even mode shapes are regarded as the symmetric modes.

In the context of NDE inspections, for effective inspections to take place, dispersion curves and their mode shapes are of paramount importance in identifying the appropriate choices of frequencies and modes [15] one should make. They are intrinsic to the structure under consideration and are properties that people often wish to calculate. As an example, Figure 1.1, presents the dispersion curves, as a plot of phase velocity against frequency, accompanied by some symmetric and antisymmetric mode shapes, of guided waves in a straight, 1 mm thick, aluminium waveguide in vacuum. Calculations were performed with the commercially available software Disperse [16].

A few important comments need to be made here. The first is that dispersion curves of Figure 1.1(a) are colour coded based on the nature of their mode shapes. Antisymmetric modes (labelled $A0, A1, \dots$) are coloured in blue, while symmetric modes (labelled $S0, S1, \dots$) are coloured in red. Examples of mode shapes of an antisymmetric and a symmetric mode, displaying the amplitude of oscillations in the direction normal to the direction of propagation, i.e. up and down, as a function of position though the thickness of the waveguide, are presented in Figures 1.1(b) and 1.1(c) respectively. The second is that multiple different modes can exist simultaneously in a waveguide at any chosen frequency; this could potentially pollute experimental results if not accounted for. The third and final comment is that no two dispersion curves are the same, with some curves being steeper than others – their velocities vary a lot with frequency – and some being almost flat at high frequencies – there is almost no dispersion here and their velocities remain constant for all frequencies.

In real life applications, one would typically work with wave packets or toneb-

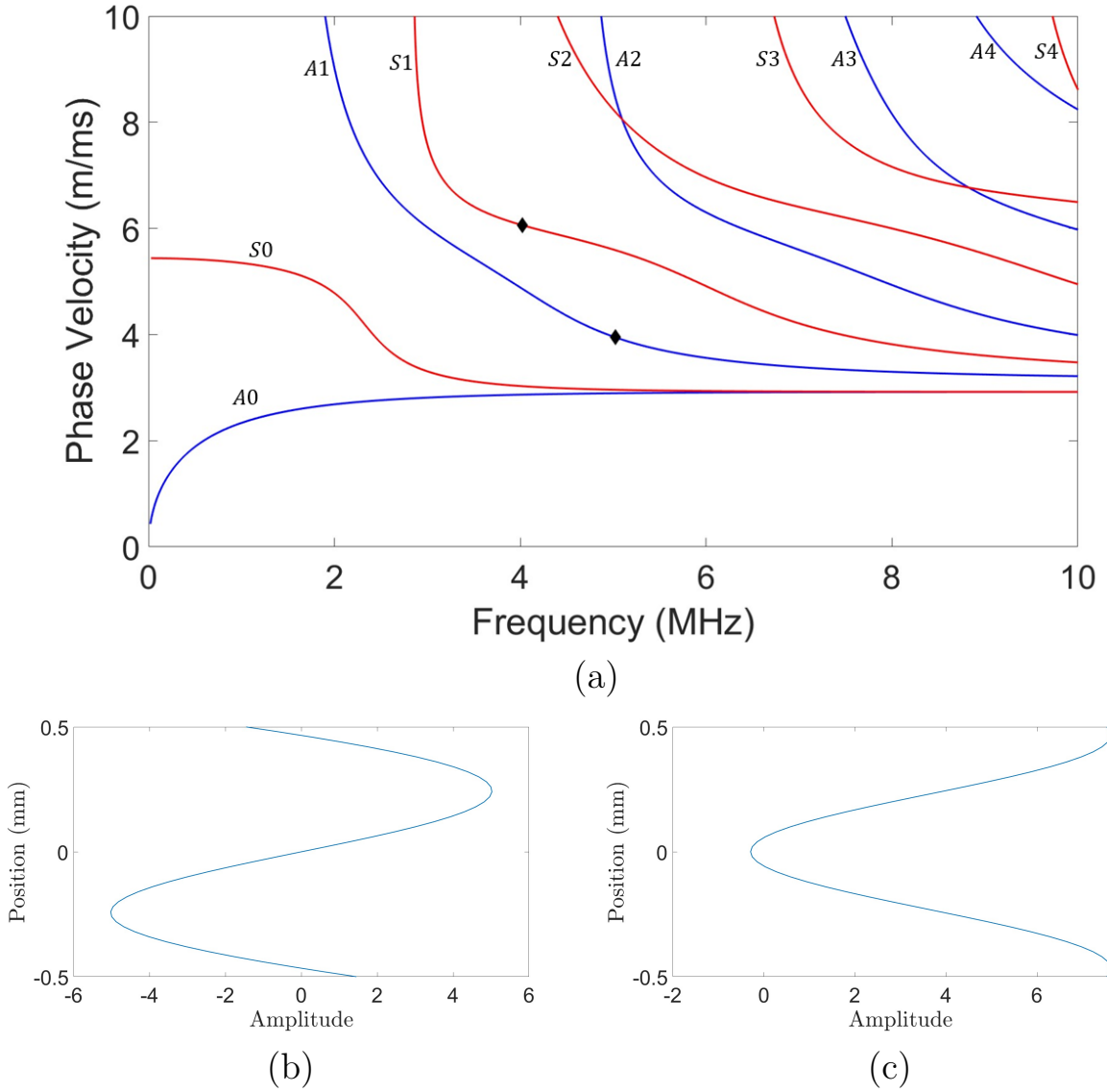

(a)

(b)

(c)

Figure 1.1: Dispersion curves and mode shapes calculated with DISPERSE [16], for a straight aluminium, 1 mm thick, waveguide in vacuum. Dispersion curves are shown in 1.1(a) as plots of phase velocity against frequency. Figures 1.1(b) and 1.1(c) display the mode shapes of an antisymmetric and a symmetric mode marked with ♦ in 1.1(a). Those are plotted as the amplitudes of displacements in the direction normal to the direction of propagation versus position across the thickness of the waveguide.

ursts, which are signals of finite length and multiple frequencies centred around a central frequency, f_c. When a mode is dispersive, low and high

frequency components of the wave packet will travel at different speeds, resulting in the change of its shape as the packet propagates along a waveguide. Figure 1.2 demonstrates this behaviour by presenting a wave packet of central frequency $f_c \approx 1.6$ MHz and its evolution as it propagates 1 m along a waveguide with and without dispersion. The length of the wave packet, in seconds, is five periods (5 cycles); a period is the time required for a complete oscillation and is defined as $T = 1/f_c$. For the non-dispersive propagation of Figure 1.2(a), a constant phase velocity is assumed and the wave packet can be seen to retain its original shape and amplitude, while for the dispersive propagation of Figure 1.2(b), phase velocity is chosen to vary in accordance to the $S0$ mode of Figure 1.1(a), and the wave packet can be seen to spread out and diminish in amplitude; a potentially undesirable feature when it comes to guided wave applications.

Consequently, to attain meaningful results in any guided waves application, it is crucial that one has a thorough understanding of the underlying complexities of a structure: the different guided modes that propagate along it, its dispersion curves, the modes that one may excite in and around the working frequency, and how those modes cause the vibration of the structure.

1.1.1 Computing Dispersion Curves

A great amount of research has gone into developing modelling techniques for guided waves and tools for the retrieval of their dispersion characteristics. Some techniques that are widely used today are briefly discussed in the following.

Partial Wave Root Finding (PWRF [17]), an approach traditionally used for computing the dispersion curves of guided waves, is depicted in Figure 1.3 for a simple case of an isotropic elastic waveguide of a single layer of finite thickness in vacuum; the method readily extends to multiple layers,

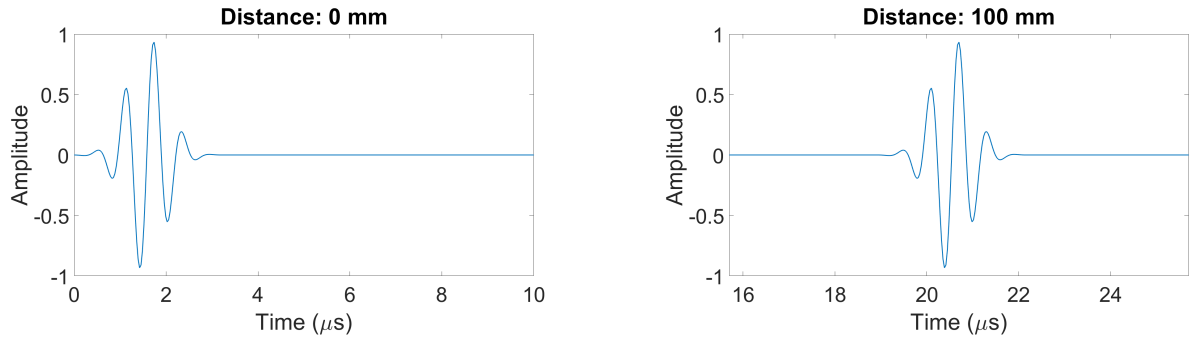

(a)

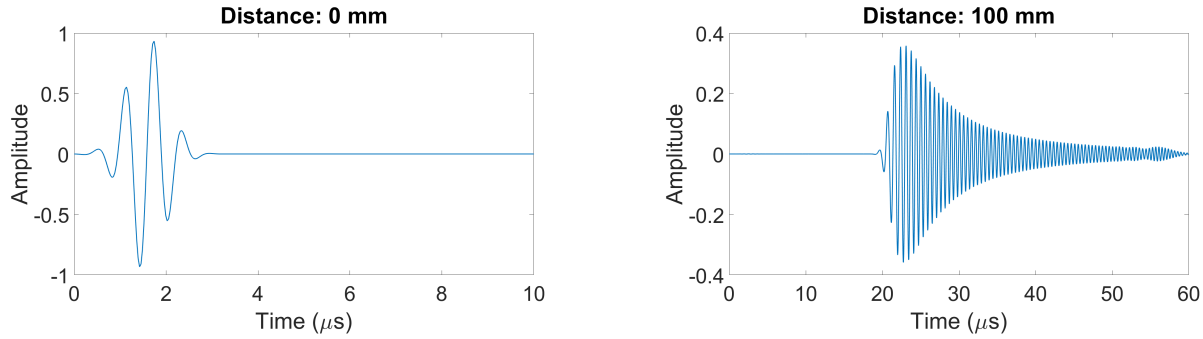

(b)

Figure 1.2: A 5-cycled wave packet of central frequency $f_c \approx 1.6$ MHz and the effect of dispersion as it propagates 1 m along a 1 mm thick aluminium waveguide. Propagation without dispersion is in 1.2(a) and propagation with dispersion ($S0$ mode), simulated with DISPERSE [16], is in 1.2(b).

fluids, damped materials, anisotropy, cylindrical waveguides and waveguides immersed or embedded in another material.

A guided wave in a straight waveguide of finite thickness and infinite extent in the x and z directions is composed as the superposition of partial waves. Those are bulk waves – waves that travel in the bulk of an unbounded medium and with their wave speeds and wavelengths (distance travelled in a single period) a material property of the medium – whose sum is such that boundary conditions, at the surfaces of the waveguide, are satisfied. Four bulk waves are shown here, two longitudinal (the direction of particle movement is parallel

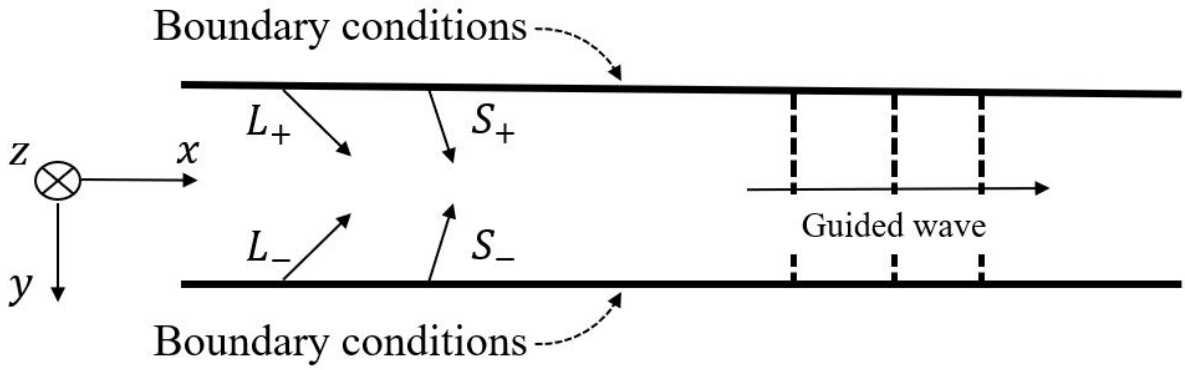

Figure 1.3: A guided wave as a superposition of pairs of longitudinal and shear waves in a straight isotropic waveguide of finite thickness.

to the direction of wave propagation) and two shear (the direction of particle movement is perpendicular to the direction of wave propagation), propagating in pairs up and down the waveguide.

Matrix methods [17], like the Transfer Matrix [18, 19] and Global Matrix [20] methods, allow the stresses and displacements at the two surfaces to be related with the four bulk waves, and the boundary condition equations of a system to be expressed as a matrix multiplication, in terms of the amplitudes of bulk waves and the phase velocity, c_{ph}, or equivalently the wavenumber of the guided wave along the direction of propagation, $k_x = \omega/c_{\mathrm{ph}}$. That reads

$$D(\omega, k_x)\boldsymbol{v} = \mathbf{0}, \tag{1.1}$$

with $\omega = 2\pi f$ and f the angular and linear frequencies of the guided wave, $\boldsymbol{v}$ a column vector of the bulk waves' amplitudes and D a matrix with each of its rows representing a boundary condition.

Non-trivial solutions of Eq. (1.1) require the vanishing of the determinant of D which is usually referred to as the characteristic function, $f(\omega, k_x)$, of the

problem [17]. The pairs (ω, k_x), for which

$$f(\omega, k_x) = 0, \tag{1.2}$$

determine the dispersion curves of the problem for a given set of boundary conditions. In its current form, Eq. (1.2) is a problem of two unknowns and to retrieve pairs (ω, k_x), one usually fixes one of frequency or wavenumber and employs a root-finding algorithm on Eq. (1.2) to find the other; in cases where the energy of the wave is dissipated or radiated away from the waveguide, k_x becomes complex and Eq. (1.2) is a problem of three unknowns that is harder to solve numerically. Performing this calculation for a range of frequencies or wavenumbers (frequency or wavenumber sweeps), allows for the dispersion curves of the system to be retrieved. The corresponding vectors, $\boldsymbol{v}$, obtained from subsequently solving Eq. (1.1), give the amplitudes of the bulk waves whose superposition makes up the wave field, i.e. the mode shapes are also retrieved.

An alternative to PWRF routines are the more recent methods based on a Semi-Analytical Finite Elements (SAFE) approach. An early popular work using SAFE was that of Gavric [21] on the study of waves propagating in a free rail. In that study, Finite Elements (FEs) were used for the discretisation of the waveguide domain and the differential equations of motion were converted into a solvable eigenvalue problem. This allowed for the algebraic retrieval of all the roots of the characteristic equation in the form of eigensolutions. SAFE allows for more flexibility when compared to the more traditional PWRF methods, as it can be used for spatially-irregular waveguides and complex structures where the latter becomes unstable. Examples of its use include the study of wave propagation in systems of viscoelastic media of arbitrary cross-section [22] and in axisymmetric damped waveguides [23].

In line with the idea of discretising the domain of the structure in question and then obtaining a solution of the dispersion relation in the form of eigenvalues of an algebraic eigenvalue problem, Spectral Collocation Methods (SCM) have also been employed in recent years for the solution of guided wave problems. Adamou and Craster [24] presented solutions for guided waves in simple cylindrical geometries, demonstrating their potential applications in the field of guided waves. Following that, Karpfinger *et al.* [25] successfully used spectral collocation to study multilayered cylindrical structures consisting of isotropic media, Zharnikov *et al.* [26] used SCM to study and plot the dispersion curves of an inhomogeneous anisotropic waveguide while Quintanilla *et al.* [27–29] utilised the flexibility of SCM for the study of flat and cylindrical multilayered viscoelastic and generally anisotropic systems. The use of SCM in physics can be very intuitive and numerically robust, making them an accessible tool for the algebraic solution of differential equations. The work presented in this thesis relies upon a SCM formulation, and for that reason a more detailed discussion on SCM follows in subsequent sections.

1.1.2 Leaky Waves

Very often, a structure under inspection comprises an elastic waveguide in contact with elastic or fluid media, whose material properties differ both from each other and from those of the waveguide. This behaviour is common in a wide range of settings, including reinforced concrete structures [30], seismology [31], adhesive joints and fibre composites [32,33], immersed or buried pipes [14,34–37] and biological structures such as bones surrounded by tissue [38–40]. In those scenarios, energy is no longer necessarily confined within the boundaries of a waveguide but rather radiates into the adjacent media, causing a loss of amplitude of the guided wave along the direction of propagation; the attenuation of the wave due to radiation. These propagating and

radiating waves are known as leaky guided waves, and they will be the focus of the work presented in this thesis.

Assuming no other forms of wave damping due to the material of the waveguide, leaky waves are characterised by an initially counter-intuitive exponential growth of amplitude in the direction normal to the direction of propagation and complex wavenumbers, which contrasts with the real valued wavenumbers needed to represent guided waves in a waveguide in vacuum. The real part of the wavenumber of leaky waves reveals information about the velocity of the waves while the imaginary part corresponds to their attenuation due to radiation.

To better understand why leaky waves exponentially grow in the normal direction, consider the following discussion for a flat waveguide in contact with fluid, taken from [41] and accompanying schematic in Figure 1.4. Suppose that a leaky wave is propagating along an elastic waveguide in contact with fluid and has wavenumber k_x along the x direction (the direction of propagation). The waveguide is taken to have finite thickness and infinite extent along the x direction. Suppose also that one is interested in monitoring the displacement field along the perpendicular direction above an observation point, P, located on the waveguide. The energy observed above P is the energy that has leaked from points preceding the point of observation; the higher up the dashed line drawn above P in Figure 1.4, the further back one needs to go in the x direction to find the point where the observable energy has leaked from. Consequently, in the far-field, the observed energy was radiated from points located infinitely far away from P. As the leaky wave attenuates as it propagates along the waveguide, it loses energy in the direction of propagation, i.e. while moving to the right. Equivalently, the leaky wave may be perceived as gaining energy in the opposite direction. This implies that more energy is radiated from points lying further back along the

waveguide and thus more energy is observed higher up the line of observation and in the far-field. On this basis the exponential growth observed is a consequence of energy conservation.

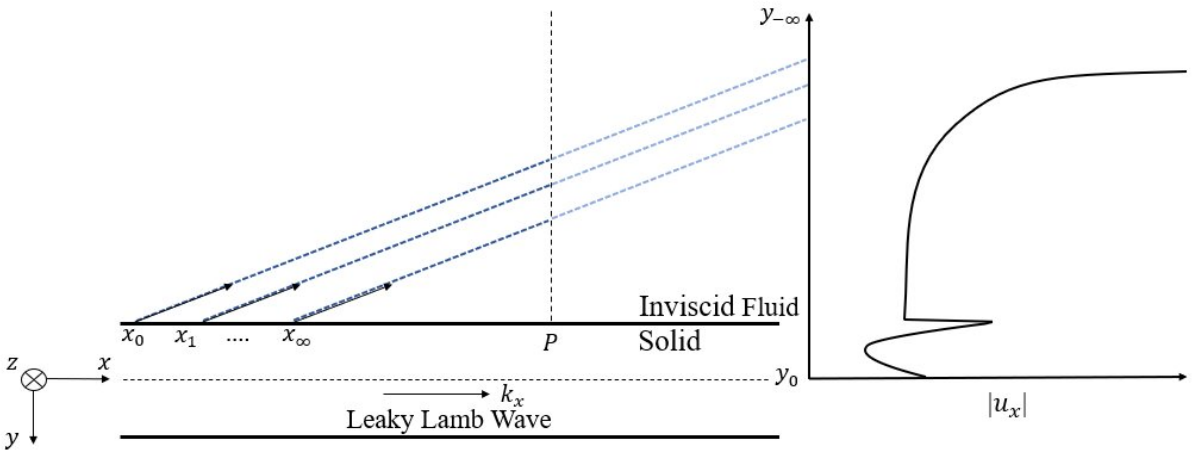

Figure 1.4: The exponential growth of leaky Lamb waves, as a result of energy radiation at a fluid-solid interface [41].

The techniques discussed in the previous section can be seen to produce excellent results for modelling wave propagation in structures made of an arbitrary number of layers and materials in vacuum, however, when solving for leaky systems, their performance is compromised by the unbounded nature of the domain and the exponential growth and complex-valued wavenumbers of leaky waves. Associated numerical challenges are discussed next.

Leaky waves radiate at an angle away from the waveguide and require additional wavenumbers, along the direction normal to the waveguide, to be described. Those wavenumbers may be expressed as non-linear (square root) functions of the wavenumber along the direction of propagation. When spatially discretising the waveguide domain to formulate the problem as an eigenvalue problem, with SAFE or SCM, and accounting for the media adjacent to the waveguide through modified interface conditions, non-linear terms start

to appear. These cause the resulting eigenvalue problems to be non-linear and careful treatments are required to compute their solutions [42–44]. Unfortunately, these are often problem-specific treatments and do not generalise to other problems or geometries.

One may instead express the problem as a linear eigenvalue problem by discretising the domain of the adjacent unbounded media in addition to the waveguide domain. Due to finite computational resources, an infinite domain cannot be modelled directly. Instead, finite domains, surrounded by artificial absorbing regions that attenuate outgoing waves, are often used, replicating in this way waves moving away from the waveguide and towards infinity. Examples of such artificial layers are the stiffness-reducing absorbing layers [45,46] and the Perfectly Matched Layers (PMLs) [47–49]. When outgoing leaky waves are modelled, special care needs to be taken because of their exponentially growing nature, as, if not effectively absorbed in an artificial absorbing region, they may pollute the computational domain with numerical reflections.

Finally, numerical schemes, like PWRF, that attempt to retrieve dispersion curves as zeros of the determinant of a matrix formulation of the problem, are susceptible to spurious solutions when matrices become computationally ill-conditioned. This is the case for some matrix formulations (e.g. Transfer Matrix [18]), when the product of layer thickness with frequency is large, due to the existence of coefficients that grow and coefficients that decay within the matrices – the "large fd" problem [50] – or when solving for the wave modes of multilayered waveguides near any of the bulk wave speeds involved in the system. In those scenarios, careful filtering needs to be applied to discard spurious solutions; a task that becomes increasingly difficult especially when filtering around genuine modes. In addition to ill-conditioned matrices, due to the nature of root-finding algorithms, PWRF methods may sometimes fail

to capture roots of the characteristic equation. This limitation is amplified when solving for leaky waves, as their complex wavenumber is particularly demanding for root-finding algorithms; as mentioned earlier, one effectively has three unknowns to solve for – frequency and the real and imaginary parts of wavenumber – but only one equation. Fine tuning of the convergence parameters of root-finding algorithms usually fixes the problem, however, it requires empirical knowledge of the existence of the mode that was missed in the first place.

Numerically modelling and solving for the dispersion curves of leaky waves are challenging problems; they may require handling non-linear eigenvalue problems, the fine tuning of absorption parameters and *a priori* knowledge of the existence of modes that might have been missed. The work presented in this thesis proposes a methodology, based on SCM, for the retrieval of the full set of dispersion curves of leaky waves and their mode shapes, that bypasses the challenges described above and moves in the direction of a "black-box" modelling technique for leaky waves that is easy to implement and does not require any user intervention.

1.2 Elastic waves

In this section, an overview of the fundamental principles of sound wave propagation and accompanying equations of motion are presented for waves in a flat, elastic and isotropic waveguide.

Consider guided waves propagating in a flat waveguide of infinite extent in the x and z directions and of finite thickness, $2d$, in the y direction, made of a homogeneous, linear-elastic and isotropic material, able to support both compressive and shearing motion [51]. The material of the waveguide is taken to have density ρ, and longitudinal and transverse wave speeds respectively

given by

$$c_l = \sqrt{\frac{\lambda + 2\mu}{\rho}} \quad \text{and} \quad c_t = \sqrt{\frac{\mu}{\rho}}, \tag{1.3}$$

where λ and μ are Lamé's elastic stiffness constants. The product of the material's density and longitudinal wave speed is referred to as its acoustic impedance [52], while the product of its density and transverse wave speed are referred to as its shear impedance [53]. The system is depicted in Figure 1.5, alongside the axis orientation.

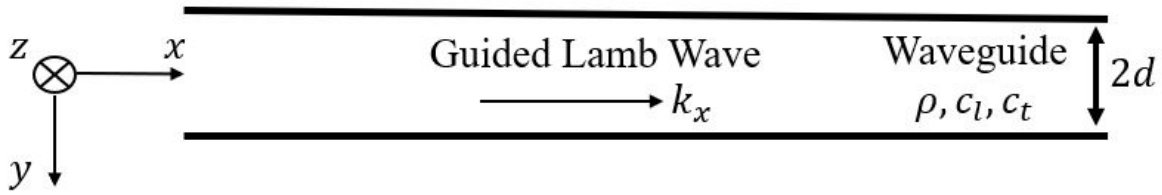

Figure 1.5: Guided Lamb waves propagating in a flat waveguide in vacuum.

To develop the equations of motion for an infinite elastic solid, the discussion in [17] is followed. Let us begin with an infinitesimal square element of the waveguide. Lamb waves [54], of wavenumber k_x, are assumed propagating in the waveguide, causing only in-plane displacements $\bar{\boldsymbol{u}} = (\bar{u}_x, \bar{u}_y)$ in the waveguide, with $\bar{u}_z = 0$. By application of Newton's second law, equilibrium requires that

$$\rho \frac{\partial^2 \bar{u}_x}{\partial t^2} = \frac{\partial \bar{\sigma}_x}{\partial x} + \frac{\partial \bar{\sigma}_{xy}}{\partial y}, \tag{1.4}$$

$$\rho \frac{\partial^2 \bar{u}_y}{\partial t^2} = \frac{\partial \bar{\sigma}_{xy}}{\partial x} + \frac{\partial \bar{\sigma}_y}{\partial y}, \tag{1.5}$$

where $\bar{\sigma}_x, \bar{\sigma}_y$ and $\bar{\sigma}_{xy}$ are the normal and shear stresses acting on the edges of the square. Hooke's law for linear elastic materials allows us to write the con-

stitutive stress-strain and strain-displacement relations for the infinitesimal square element as

$$\bar{\sigma}_x = \lambda\Delta + 2\mu\bar{\varepsilon}_x, \qquad \bar{\sigma}_y = \lambda\Delta + 2\mu\bar{\varepsilon}_y, \qquad \bar{\sigma}_{xy} = \mu\bar{\varepsilon}_{xy}, \tag{1.6}$$

$$\bar{\varepsilon}_x = \frac{\partial \bar{u}_x}{\partial x}, \qquad \bar{\varepsilon}_y = \frac{\partial \bar{u}_y}{\partial y}, \qquad \bar{\varepsilon}_{xy} = \frac{\partial \bar{u}_y}{\partial x} + \frac{\partial \bar{u}_y}{\partial x}. \tag{1.7}$$

where $\Delta = \bar{\varepsilon}_x + \bar{\varepsilon}_y$ is the change in area of the element. Substituting Eq. (1.7) into (1.6) gives the stress-displacement relations

$$\bar{\sigma}_x = \lambda\frac{\partial \bar{u}_x}{\partial x} + (\lambda + 2\mu)\frac{\partial \bar{u}_y}{\partial y}, \tag{1.8}$$

$$\bar{\sigma}_y = \lambda\frac{\partial \bar{u}_y}{\partial y} + (\lambda + 2\mu)\frac{\partial \bar{u}_x}{\partial x}, \tag{1.9}$$

$$\bar{\sigma}_{xy} = \mu\left(\frac{\partial \bar{u}_y}{\partial x} + \frac{\partial \bar{u}_x}{\partial y}\right), \tag{1.10}$$

Subsequently substituting Eqs. (1.8)-(1.10) and then those into Eqs. (1.4) and (1.5), gives the equations of motion as

$$\rho\frac{\partial^2 \bar{u}_x}{\partial t^2} = (\lambda + \mu)\frac{\partial}{\partial x}\left(\frac{\partial \bar{u}_x}{\partial x} + \frac{\partial \bar{u}_y}{\partial y}\right) + \mu\nabla^2\bar{u}_x, \tag{1.11}$$

$$\rho\frac{\partial^2 \bar{u}_y}{\partial t^2} = (\lambda + \mu)\frac{\partial}{\partial y}\left(\frac{\partial \bar{u}_x}{\partial x} + \frac{\partial \bar{u}_y}{\partial y}\right) + \mu\nabla^2\bar{u}_y. \tag{1.12}$$

The above may be expressed in vector form as

$$\rho\frac{\partial^2 \bar{\boldsymbol{u}}}{\partial t^2} = (\lambda + \mu)\,\boldsymbol{\nabla}\left(\boldsymbol{\nabla}\cdot\bar{\boldsymbol{u}}\right) + \mu\nabla^2\bar{\boldsymbol{u}}, \tag{1.13}$$

with the operators $\boldsymbol{\nabla} = (\partial/\partial x, \partial/\partial y)$ and $\nabla^2 = (\partial^2/\partial x^2 + \partial^2/\partial y^2)$.

For the time and space harmonic waves of this two-dimensional problem, the displacements $\bar{u}_x$, $\bar{u}_y$ are functions of three variables, x, y and t, while for a

given angular frequency ω, a common $\exp\left[i\left(k_x x - \omega t\right)\right]$ term is assumed in all displacement, stress and strain fields. Explicitly,

$$\bar{u}_x\left(x, y, t\right) = u_x\left(y\right)\exp\left[i\left(k_x x - \omega t\right)\right], \tag{1.14}$$

$$\bar{u}_y\left(x, y, t\right) = u_y\left(y\right)\exp\left[i\left(k_x x - \omega t\right)\right], \tag{1.15}$$

with $\boldsymbol{u} = \left(u_x, u_y\right)$ the y-dependent components of $\bar{\boldsymbol{u}} = \left(\bar{u}_x, \bar{u}_y\right)$ and similarly for stresses and strains.

Substituting Eqs. (1.14) and (1.15) into Eqs. (1.8)-(1.10) and Eqs. (1.11) and (1.12) allows the stresses and equations of motion to be express in terms of u_x and u_y, as

$$\sigma_x = \left(\lambda + 2\mu\right)ik_x u_x + \lambda\frac{\partial u_y}{\partial y}, \tag{1.16}$$

$$\sigma_y = \left(\lambda + 2\mu\right)\frac{\partial u_y}{\partial y} + \lambda ik_x u_x, \tag{1.17}$$

$$\sigma_{xy} = \mu\left(ik_x u_y + \frac{\partial u_x}{\partial y}\right), \tag{1.18}$$

and

$$\rho\omega^2 u_x - \left(\lambda + 2\mu\right)k_x^2 u_x + \left(\lambda + \mu\right)ik_x\frac{\partial u_y}{\partial y} + \mu\frac{\partial^2 u_x}{\partial y^2} = 0, \tag{1.19}$$

$$\rho\omega^2 u_y - \mu k_x^2 u_y + \left(\lambda + \mu\right)ik_x\frac{\partial u_x}{\partial y} + \left(\lambda + 2\mu\right)\frac{\partial^2 u_y}{\partial y^2} = 0, \tag{1.20}$$

respectively. Note that for the case of a fluid medium, the coupled equations of motion from elasticity reduce to a single, simplified wave equation, because fluids can only support waves of compressive polarisations (longitudinal waves), as opposed to both compressive and shear polarisations (longitudinal and shear waves) supported by elastic media.

1.3 Spectral Collocation Methods

SCMs are readily used today for the high accuracy numerical solution of Ordinary Differential Equations (ODEs) and Partial Differential Equations (PDEs), connected with problems in wave physics, fluid mechanics, complex analysis and other fields. They are the solution method of choice for retrieving the dispersion curves of leaky waves in this thesis and to that end a brief overview of the fundamental principles and techniques, taken from [55], is presented here.

Start by considering a set of grid points $\{x_j\}_{j=1}^N$ in some domain $\mathcal{C}$, and corresponding function values $\boldsymbol{g} = \{g(x_j)\}_{j=1}^N$, for a function g defined over $\mathcal{C}$. The set $\{x_j\}_{j=1}^N$ is taken to span over the domain $\mathcal{C}$, effectively discretising it, and the points x_j, for $j = 1, \ldots, N$, will be referred to as collocation points in $\mathcal{C}$.

Suppose that one wishes to evaluate the derivatives of g on the set of collocation points, up to the l^{th} derivative $\boldsymbol{g}^{(l)} = \{g^{(l)}(x_j)\}_{j=1}^N$. Spectral methods [55–58] suggest that this may be achieved by introducing weighted interpolants,

$$g(x) \approx p_{N-1}(x) = \sum_{j=1}^{N} \frac{\alpha(x)}{\alpha(x_j)} \psi_j(x) g_j, \tag{1.21}$$

where $\alpha(x)$ is a weight function, $g_j = g(x_j)$ and $\{\psi_j(x)\}_{j=1}^N$ are a set of interpolating functions that satisfy $\psi_j(x_k) = \delta_{jk}$ (Kronecker delta). Due to the choice of interpolating functions and weights, the function $p_{N-1}(x)$ interpolates $g(x)$, in the sense that

$$g(x_j) = p_{N-1}(x_j), \text{ for } j = 1, \ldots, N. \tag{1.22}$$

Differentiating both sides of Eq. 1.21, it follows that

$$g'(x_k) \approx \sum_{j=1}^{N} \frac{d}{dx}\left[\frac{\alpha(x)}{\alpha(x_j)}\psi_j(x)\right]_{x=x_k} g_j, \tag{1.23}$$

and more generally, the l^{th} derivative of g may be approximated by

$$g^{(l)}(x_k) \approx \sum_{j=1}^{N} \frac{d^l}{dx^l}\left[\frac{\alpha(x)}{\alpha(x_j)}\psi_j(x)\right]_{x=x_k} g_j, \tag{1.24}$$

for $k = 1, \ldots, N$. It is convenient to express Eq. (1.24) in matrix form as

$$\boldsymbol{g}^{(l)} \approx D_{\mathcal{C}}^{(l)} \boldsymbol{g}, \tag{1.25}$$

where $D_{\mathcal{C}}^{(l)}$ is an $N \times N$ differentiation matrix in $\mathcal{C}$, given explicitly as

$$D_{\mathcal{C}}^{(l)} = \begin{pmatrix} \frac{d^l}{dx^l}\left[\frac{\alpha(x)}{\alpha(x_1)}\psi_1(x)\right]_{x=x_1} & \cdots & \frac{d^l}{dx^l}\left[\frac{\alpha(x)}{\alpha(x_N)}\psi_N(x)\right]_{x=x_1} \\ \vdots & \ddots & \vdots \\ \frac{d^l}{dx^l}\left[\frac{\alpha(x)}{\alpha(x_1)}\psi_1(x)\right]_{x=x_N} & \cdots & \frac{d^l}{dx^l}\left[\frac{\alpha(x)}{\alpha(x_N)}\psi_N(x)\right]_{x=x_N} \end{pmatrix}. \tag{1.26}$$

The interpolating functions above are free to be chosen to serve the problem at hand [55]. For periodic domains, trigonometric polynomial functions on an equispaced grid of collocation points are usually the interpolating functions of choice; the resulting spectral methods are known as the "Fourier" methods. When domains are non-periodic, however, algebraic polynomials of order $N-1$ and irregular grids of collocation points are preferred; the "Chebyshev" methods. In both cases, the interpolants are global functions, as opposed to piece-wise polynomials used by other methods, leading to much higher accuracy, known as spectral accuracy, and faster convergence rates for smooth solutions [58].

In practice, when an ODE or PDE is to be solved for an unknown function that is defined over a given domain, SCM may be employed to obtain a discretised form of the equation allowing it to be solved numerically. To do so, one must spatially discretise the domain of the function with a grid of collocation points and obtain the corresponding differentiation matrices. The following example, discretising a linear ODE using Chebyshev methods, demonstrates how that may be achieved.

Consider the following boundary value problem [55]

$$\frac{d^2g}{dx^2} = \frac{e^{2x}}{4}, \qquad -2 < x < 2, \qquad g(\pm 2) = 0. \tag{1.27}$$

This is a Poisson equation, with a Dirichlet zero boundary condition and a solution $g(x) = [e^{2x} - \frac{x}{2}\sinh(4) - \cosh(4)]/16$. To solve it numerically with spectral methods, one may start with the N Gauss-Chebyshev-Lobatto collocation points in the interval $[-1, 1]$, given by

$$s_j = -\cos\left(\frac{(j-1)\pi}{N-1}\right), \text{ for } j = 1, \ldots, N. \tag{1.28}$$

The corresponding $N \times N$ differentiation matrices, $D^{(l)}$, based on Chebyshev interpolating polynomials, are efficiently computed by the differentiation matrix suite of Weideman and Reddy [58]. Recall that to be able to differentiate the function g, defined over $-2 < x < 2$, a grid of points in $[-2, 2]$ is needed, while only a set of collocation points in $[-1, 1]$ is proposed here. To get a set of Chebyshev collocation points spanning over the desired domain, one may simply use the set $\{x_j\}_{j=1}^{N}$, defined as

$$x_j = 2s_j. \tag{1.29}$$

By the chain rule, for a change of variables $x = 2s$,

$$\frac{dg}{dx} = 2\frac{dg}{ds}, \qquad \frac{d^2g}{dx^2} = 2^2\frac{d^2g}{ds^2}, \qquad \text{etc.} \tag{1.30}$$

Consequently, differentiation matrices in the interval $[-2, 2]$, for the collocation points $\{x_j\}_{j=1}^N$ read

$$D_{\mathcal{P}}^{(l)} = \left(\frac{1}{2}\right)^l D^{(l)}. \tag{1.31}$$

The Poisson equation of Eq. (1.27), without accounting for boundary conditions, may then be discretised as

$$D_{\mathcal{P}}^{(2)}\boldsymbol{g} = \boldsymbol{f}, \tag{1.32}$$

where $\boldsymbol{f} = [e^{2x_1}/4, \ldots, e^{2x_N}/4]^T$ is a column vector of N entries.

The Dirichlet zero boundary conditions of this problem requires the vanishing of the solution at the two collocation points $x_1 = -2$ and $x_N = 2$, or equivalently $g(x_1) = g(x_N) = 0$. To impose the boundary conditions to the discrete problem, one must replace the first and last rows of $D_{\mathcal{P}}^{(2)}$, corresponding to x_1 and x_N respectively, with $[1, 0, \ldots, 0]$ and $[0, \ldots, 0, 1]$ – denoting the new matrix with $\tilde{D}_{\mathcal{P}}^{(2)}$ – and also modify $\boldsymbol{f}$ to $\tilde{\boldsymbol{f}} = [0, e^{2x_2}/4, \ldots, e^{2x_{N-1}}/4, 0]^T$. The new matrix equation reads

$$\tilde{D}_{\mathcal{P}}^{(2)}\boldsymbol{g} = \tilde{\boldsymbol{f}}. \tag{1.33}$$

In the matrix multiplication at the LHS of Eq. (1.32), the $N \times N$ matrix $\tilde{D}_{\mathcal{P}}^{(2)}$ is multiplied with an $N \times 1$ column vector, resulting in a new $N \times 1$ column vector whose first and last entries are $g(x_1)$ and $g(x_N)$ respectively. Those are exactly the entries that are set to zero on the RHS in $\tilde{\boldsymbol{f}}$, effectively imposing the desired boundary conditions to the discrete problem.

The solution, $\boldsymbol{g}$, is retrieved with spectral accuracy as

$$\boldsymbol{g} = [\tilde{D}_{\mathcal{P}}^{(2)}]^{-1}\tilde{\boldsymbol{f}}. \tag{1.34}$$

It should be noted that although the example presented here is a rather "simple" one, it serves to demonstrate how one might go about discretising an equation with SCM. In general, discretising more complex equations will result in more complex forms for Eq. (1.33). As will be demonstrated in the chapters to follow, the discretisation of the equations of interest in this thesis, like the coupled elastic wave Eqs. (1.19) and (1.20), will result in polynomial eigenvalue problems in wavenumber and boundary conditions in terms of stresses and displacements.

1.4 Finite Element Modelling

Some of the results presented in this thesis were validated against FE simulations. This section introduces some of the principles of discretisation followed by the FE software of choice and a methodology for preferentially exciting modes of interest.

1.4.1 FE Discretisation

All FE simulations presented in this thesis were completed using the high-fidelity Graphics Processing Unit (GPU)-based FE software Pogo [59]. Given a structure to be investigated, Pogo, like other FE packages, discretises the domain by modelling it as a series of elements of finite size, and possibly different cross-sectional areas, connected by nodes [60]. Given an initial condition for a set of nodes – a boundary condition – displacements are propagated from each node to the next through interpolating functions, known as shape

functions. This achieves a piecewise approximation of the displacement field in space. Bilinear shape functions are used in Pogo, while for the purposes of this thesis, square elements of four nodes each were used. Nodes were free to move in the x and y directions but not the z, or equivalently, two degrees of freedom per node are assumed.

The equation of elasticity for a general model with damping terms, given in matrix form due to the spatial discretisation of the domain reads [60]

$$\boldsymbol{M}\ddot{\boldsymbol{U}} + \boldsymbol{C}\dot{\boldsymbol{U}} + \boldsymbol{K}\boldsymbol{U} = \boldsymbol{F}, \tag{1.35}$$

where $\boldsymbol{M}$, $\boldsymbol{C}$, $\boldsymbol{K}$ and $\boldsymbol{F}$ are the mass, damping, stiffness and applied force matrices, while $\boldsymbol{U}$, $\dot{\boldsymbol{U}}$ and $\ddot{\boldsymbol{U}}$ are the displacement, velocity and acceleration matrices respectively. Pogo uses the finite-difference method [61] to discretise Eq. (1.35) in time. With no material damping assumed for the simulations presented in this thesis, Eq. (1.35) is discretised in time as

$$\boldsymbol{M}\frac{\boldsymbol{U}^{m+1} - 2\boldsymbol{U}^{m} + \boldsymbol{U}^{m-1}}{\Delta t^2} + \boldsymbol{K}\boldsymbol{U}^{m} = \boldsymbol{F}, \tag{1.36}$$

where m stands for the m^{th} time step and Δt is the duration of a single time step. Knowing the displacement matrix at two consecutive time steps, $\boldsymbol{U}^{m}$ and $\boldsymbol{U}^{m-1}$, allows the solution to be propagated through time by solving for the displacement at the next time step, $\boldsymbol{U}^{m+1}$, in Eq. (1.36). The FE modelling approach described here follows the FE models used in other elastic wave propagation studies [62–64].

To simulate leaky waves, the discretisation of a waveguide of finite thickness and infinite length, adjacent to fluid or elastic spaces of both infinite length and thickness is required. To replicate the unbounded nature of such a structure, and to ensure that the exponential growth of leaky waves does

not pollute the computational domain with artificial reflections, a rectangular domain surrounded by stiffness-reducing absorbing layers should be used. Additionally, to accommodate for the different materials in the modelled structures, multiple material properties (Young's modulus, density, Poisson's ratio) should be passed onto the FE software, with each element of the domain being assigned with the material properties of the space it is a part of. An example of such a rectangular domain, surrounded by an absorbing region and containing different materials is shown in Figure 1.6

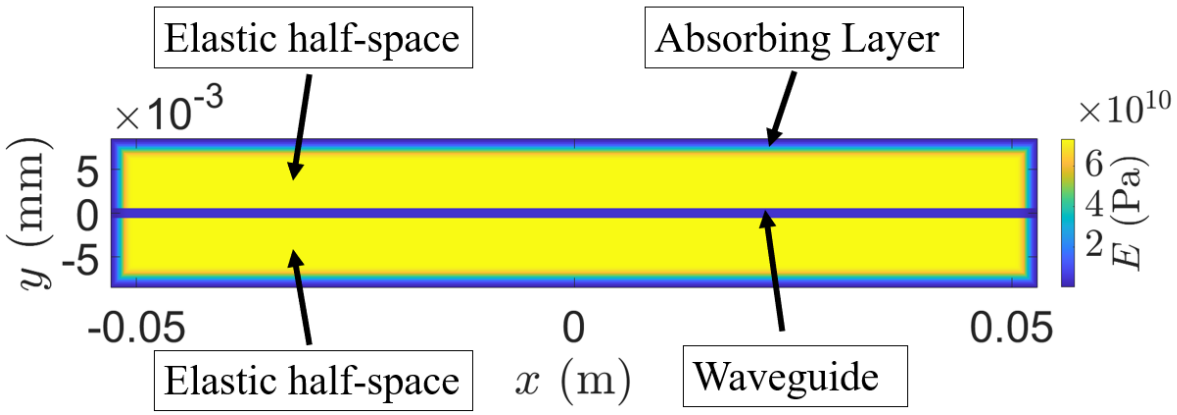

Figure 1.6: A rectangular FE domain showing a 1 mm waveguide embedded between two identical elastic half-spaces. The domain is surrounded by absorbing layers of gradually reducing Young's modulus, E.

1.4.2 Custom Excitations

To simplify the investigation of complex systems, such as the leaky systems of interest here, it is often desired to study various modes of the system separately. In the context of FE simulations, this may be achieved by precisely

controlling which guided modes are excited in the structure, preferentially exciting some modes and not others. The "centre mode shapes" technique of [65,66], used in the FE simulations of this thesis to selectively excite leaky modes, is briefly presented here.

Consider a vertical source line, comprised of multiple source nodes, defined in the middle of a rectangular domain – source nodes are nodes with predefined displacements and are used to excite the propagating wave in the model. Each source node has two degrees of freedom and an initial boundary condition may be imposed into the FE simulation by displacing each source node, left to right and up and down, with displacement amplitudes according to Hann-windowed tonebursts [67], like the wave packets of Figure 1.2.

These excitation tonebursts, as mentioned previously and by virtue of being windowed signals, contain multiple frequency components, of different amplitudes, and with each one constructively and destructively interfering with each other. The Fourier Transform (FT) [67] of a time-domain signal, $h(t)$, is the frequency-domain counterpart, $H(f)$, of $h(t)$, and describes the extent to which these frequency components are present in $h(t)$.

Functions $H(f)$ and $h(t)$ are two representations of the same function and one goes back and forth between the two representations through the Fourier transform equations [68]

$$H(f) = \int_{-\infty}^{\infty} h(t) e^{2\pi i f t}\, dt, \qquad h(t) = \int_{-\infty}^{\infty} H(f) e^{-2\pi i f t} df. \tag{1.37}$$

In most common situations, the signal $h(t)$ is sampled at evenly spaced intervals in time. Let Δt be the sampling interval and assume that $h(t)$ is sampled at N consecutive sampling points as

$$h_k = h(t_k), \qquad t_k = k\Delta t, \qquad k = 0, 1, \ldots, N-1, \tag{1.38}$$

Because of discrete sampling, the FT integrals of Eq. (1.37) may be approximated by the discrete Fourier transforms:

$$\begin{aligned} H(f_n) &= \sum_{k=0}^{N-1} h_k e^{2\pi i f_n t_k} \Delta t, \qquad f_n = \frac{n}{N\Delta t}, \qquad n = 0, \ldots, N-1, \\ H(f_n) &= H_n \Delta t, \qquad H_n = \sum_{k=0}^{N-1} h_k e^{2\pi i f_n t_k}, \end{aligned} \tag{1.39}$$

and

$$h_k = \frac{1}{N} \sum_{n=0}^{N-1} H_n e^{-2\pi i f_n t_k}. \tag{1.40}$$

In practice, MATLAB routines – the Fast Fourier Transform (FFT) and Inverse Fast Fourier Transform (IFFT) methods – allow one to go back and forth between the two discrete representations. An exemplar excitation signal of 5 cycles and 2 MHz central frequency is depicted in Figure 1.7(a), alongside the amplitude of its discrete FT in Figure 1.7(b).

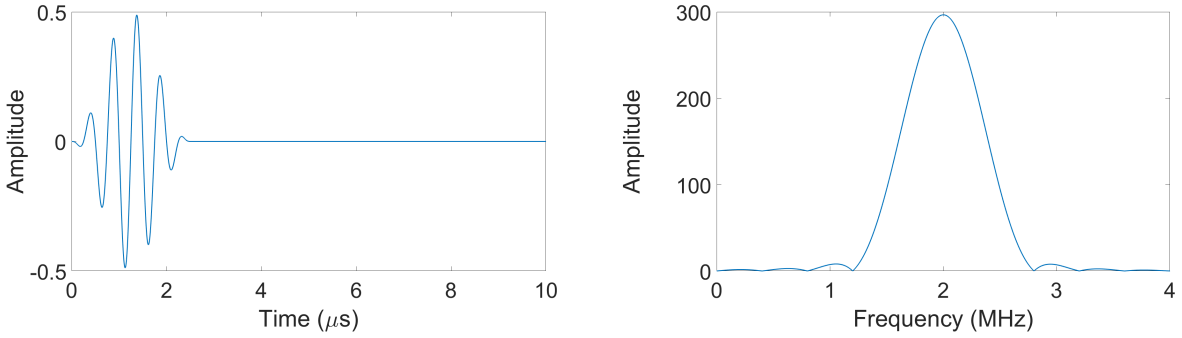

(a) (b)

Figure 1.7: Figure 1.7(a) depicts a Hann-windowed signal at $f = 2$ MHz. The amplitude of its FFT is shown in Figure 1.7(b).

To preferentially excite a guided mode with the "centre mode shapes" technique, excitation signals need to be chosen to displace source nodes along the source line in accordance to the mode shapes of the desired mode at the cen-

tral frequency. Denoting by y the perpendicular distance from the centreline of the rectangular FE domain, suppose that the desired mode to be excited has y-dependent mode shapes $\tilde{u}_x(y)$ and $\tilde{u}_y(y)$ at the central frequency. The discrete signals one must impose upon the source node located at a distance y from the centreline, along the x and y directions, say $h_x(t_k, y)$ and $h_y(t_k, y)$, should be those represented in the frequency domain by

$$H_x(f_n, y) = \tilde{u}_x(y) H_n \Delta t, \qquad H_y(f_n, y) = \tilde{u}_y(y) H_n \Delta t. \tag{1.41}$$

The "centre mode shapes" technique applies the same mode shapes, those of the central frequency, to all frequency components of the FFT of the excitation toneburst. That is, equivalent to assuming that the mode shapes of the mode of interest remain unchanged for frequencies around the central frequency. In reality and for most guided wave systems, however, mode shapes can vary rapidly with frequency, causing the approximation of using the central frequency mode shapes for all frequencies to fail. As noted in [65, 66], this will inevitably lead to the excitation of other, unwanted, modes at higher frequencies. Even though workarounds exist, like modulating each frequency component of a signal based on exact, frequency-dependent, mode shapes of the desired mode, the "centre mode shapes" technique was preferred due to its simplicity and the fact that it yielded excellent results in exciting modes predicted by the method proposed in this thesis.

1.5 Thesis Outline

Following this brief introduction of the background relevant to this thesis, Chapter 2 studies leaky waves radiating from a flat waveguide in contact with two, possibly dissimilar, fluid spaces. It presents the relevant theory and proposes a spatial discretisation of the domain through SCM. This allows

the leaky guided wave problem to be expressed as a polynomial eigenvalue problem whose eigenvalues are the dispersion curves of leaky wave modes of interest. Therein, a complex coordinate transformation bypasses the exponential growth of leaky waves by allowing the solution of a different, well behaved and numerically decaying, problem, which also encompasses all the physics of the leaky system. Dispersion curves and displacement fields computed with this SCM are validated against DISPERSE [16]. The methodology presented in this chapter is the backbone of this thesis and underpins the study of more challenging problems presented in subsequent chapters.

Chapter 3 proceeds to study the radiation of guided waves from a flat waveguide that is embedded between two elastic spaces. Due to the compressional and shear polarisations that a wave radiating into an elastic medium can have – with each one or both at the same time possibly exponentially growing – special care is taken when applying the methodology developed in the previous chapter to discretise the domain and solve for leaky waves in this context. Dispersion curves and mode shapes are again compared against DISPERSE curves wherever those were available. As an independent validation, dispersion curves of modes excited in a FE wave propagation model, using SCM predicted mode shapes as excitation inputs, are also presented. Agreement with FE results, even in cases where a DISPERSE prediction was not available, reinforced confidence of the versatility and accuracy of the proposed methodology.

Building upon previous work, Chapter 4 discusses the extension of the proposed methodology to cylindrical geometries and presents the theory underlying circumferential wave propagation in an elastic hollow cylinder immersed in fluid. Two different approaches of distinct physical meanings and dispersion curves are investigated in this chapter. Here, dispersion curves of real frequency against complex wavenumber and real wavenumber against com-

plex frequency are sought for. A common set of Bessel equations characterises both leaky systems and, in this chapter, it is discretised with the proposed SCM while both dispersion curve types are solved for. As no readily available validation tool exists, root searching on the characteristic equation of the problem is resorted to for the validation of both complex-wavenumber-against-real-frequency and real-wavenumber-against-complex-frequency dispersion curves predicted by the SCM. For the former, an additional investigation of two limiting cases of the immersed cylinder – a cylinder immersed in a fluid of low acoustic impedance and a cylinder of small curvature (almost flat) immersed in water – and a comparison of those against DISPERSE is also presented.

Chapter 5 investigates the application of SCM to study the response of immersed cylindrical targets subjected to incoming plane waves. The relevant theory is presented here, while a SCM, based on Chebyshev methods, is devised to predict the responses of the immersed elastic cylinder studied in Chapter 4. Analytical methods are subsequently employed to compute that same response at different frequencies, angles of incidence and angles of interest, and a comparison against SCM results is presented as validation. The direct link between the elastodynamic properties of the target, i.e. its real-wavenumber-against-complex-frequency dispersion curves computed in the previous chapter, with its response to the incoming wave is also investigated here.

Finally, Chapter 6 summarises the main findings of this work and discusses avenues of future investigation.

Chapter 2

Leaky Wave Radiation Into Fluids

2.1 Introduction

Ultrasonic guided waves are of enduring interest for NDE, where guided waves, such as Lamb waves [54], are utilised for the inspection or structural health monitoring of single or multilayered systems of plates or pipes [11–14]; the complexities and characteristics of Lamb wave propagation for different systems and media is of paramount importance in identifying the appropriate choices in terms of frequencies and modes [15]. The route to effective inspection techniques depends critically upon predictive models focused on identifying the dispersion curves and associated stress and displacement fields which have consequentially been the focus of much attention.

Leaky waves arise in immersed guiding structures: it is common for a structure of interest to consist of an elastic waveguide partially in contact or fully immersed in fluids. In this scenario the Lamb waves change their character as energy is no longer necessarily confined within the boundaries of a solid waveguide. When coupled to inviscid fluid(s) of infinite extent, two types of guided waves arise [48]. The first are guided waves remaining confined to the

solid and immediately-adjacent fluid, because their wave speeds are below the speed of bulk waves in the adjacent fluid(s); these include, at high frequencies, Scholte waves [69]; these are not of interest in this chapter. The second type of guided wave has energy leakage, in the form of acoustic energy radiation from the waveguide into the adjacent fluid(s), and occur when the guided wave's speed is above the fluid bulk wave speeds. As previously discussed, this leads to attenuation, i.e. decay in amplitude, along the waveguide, and modes in the fluid(s) whose amplitudes grow exponentially in the direction transverse to the waveguide; these leaky Lamb waves [32,70,71] will be the focus of the work presented in this chapter.

A key role in multiple areas of wave physics is played by leaky waves, for instance in guiding structures in electromagnetism [72] where a mismatch of refractive indices between waveguide and exterior medium leads to energy leakage and analogous leaky waves. A comprehensive recent review [73], in the electromagnetic waveguiding setting, usefully rationalises the phenomenon of the exponential growth of leaky waves and outlines applications in optics and electromagnetism. In acoustics and elasticity, leaky Rayleigh waves feature prominently in acoustic microscopy [74], in material characterisation of the waveguide [75] or of the exterior fluid [76], and underwater structural acoustics [77], while leaky Lamb waves [32,78] feature in the NDE of composites; there is therefore naturally considerable interest in their accurate identification.

A great amount of research went into developing modelling techniques for guided waves and tools for the retrieval of their dispersion characteristics, which are crucial for effective inspections to take place. Some notable techniques are the PWRF methods [17] that involve the matrix formulation [17–20] of the system in question, based in exact analytical field descriptions of partial bulk waves, and the subsequent employment of root-finding

routines for the evaluation of the roots of its characteristic equation, the SAFE methods [21–23, 37, 79] that discretise the cross-section of a structure with FE and algebraically retrieve dispersion curves as eigensolutions of a matrix representation of the differential equations of motion, and the SCMs [24, 43, 55, 80] that discretise the structure with collocation points and compute its dispersion curves algebraically by discretising the equations into generalised eigenvalue problems. These techniques are widely used today, and even though they can be seen to produce excellent results for modelling wave propagation in structures made of an arbitrary number of layers and materials in in vacuum, when solving for leaky systems, the performance of all of them is compromised by the unbounded nature of the domain and the exponential growth and complex-valued wavenumbers of leaky waves. Amongst other things, some formulations pose ill-defined problems (one has more unknowns to solve for than equations), and as a result they often miss some solutions and require the fine tuning of convergence parameters and *a priori* knowledge of the modes that were missed; a problem amplified by the complex wavenumbers of leaky waves. At the same time, other formulations depend on appropriate choices of absorbing parameters to effectively absorb the exponentially growing fields of leaky waves without numerical reflections, or result in non-linear eigenvalue problems that require problem specific treatments; see Section 1.1.2 for a more detailed discussion on some common numerical challenges associated with leaky waves.

The work presented in this chapter overcomes the numerical challenges associated with the accurate identification of leaky waves and investigates leakage from elastic waveguides into fluid media. The work develops a SCM for the computation of dispersion curves of leaky Lamb waves propagating along a waveguide that is in contact with two different inviscid fluid half-spaces, a problem that would traditionally produce a non-linear eigenvalue problem

with a SCM discretisation. This new solution is applied and demonstrated using a specific example of a flat elastic plate with a different inviscid fluid half-space on each side, however, the proposed technique has a powerful generic potential and is applicable to more complex problems; cylindrical geometries and leakage into solid media will be investigated in subsequent chapters. It is worth noting that SAFE methods could have also been chosen here for the discretisation of the waveguide domain. That choice was not made as the simple geometry of the elastic waveguide does not require the spatial versatility of SAFE, while, on the other hand, it allows for the favourable spectral accuracy of spectral collocation to easily be exploited.

The closed waveguide domain is discretised with Chebyshev collocation points and polynomials, while to deal with the open fluid half-spaces and the inherent exponential growth of leaky waves, a new technique for the discretisation of the open domains, that is based on Rational Chebyshev polynomials and does not require the use of any absorbing boundaries, is proposed. A polynomial eigenvalue problem is then produced and solved using a companion matrix linearisation and conventional numerical solvers. Finally, the dispersion characteristics and displacement fields of leaky Lamb waves are computed. Without loss of generality of the proposed discretisation, the case presented here is one that the root-finding algorithm of DISPERSE can solve satisfactorily, allowing the verification of SCM results against those from DISPERSE and demonstrating in this way the ability of the method to produce accurate results.

This chapter is organised as follows – Section 2.2 presents a brief summary of the theory relevant to the solution of the leaky Lamb wave problem of a waveguide in contact with two different inviscid fluid half-spaces. This is followed by a description of the discretisation method in Section 2, and a discussion of results in Section 2.4.

The discussion and results presented in this chapter were published in [41].

2.2 Problem Statement

Consider a homogeneous, isotropic, linear-elastic waveguide of infinite extent in the x and z directions, and finite thickness, $2d$, which is immersed between two inviscid fluids. The fluids can be different above, and below, the waveguide and have densities ρ_{f_1}, ρ_{f_2} and wave speeds c_{f_1} and c_{f_2} respectively, while the waveguide has density ρ, longitudinal wave speed c_l and transverse wave speed c_t. A schematic of the cross-section of the waveguide, also showing the coordinate axes, is shown in Figure 2.1.

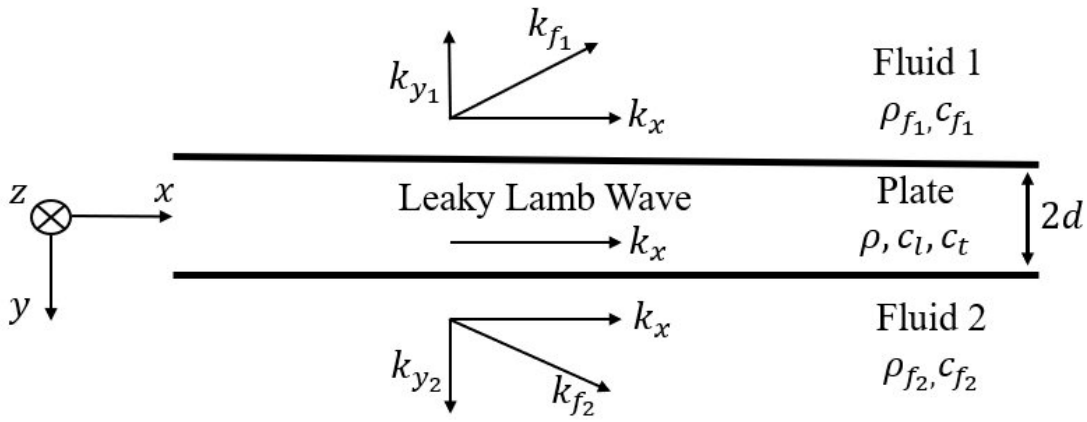

Figure 2.1: Schematic of an elastic waveguide of thickness $2d$, infinite extent in the x and z directions, density ρ, longitudinal wave speed c_l and transverse wave speed c_t, lying between two inviscid fluids of densities ρ_{f_1}, ρ_{f_2} and wave speeds c_{f_1} and c_{f_2} respectively.

The centreline of the waveguide is along $y = 0$, and the axis orientation has waves propagating in the positive x direction with wavenumber k_x. For an angular frequency, ω, the phase velocity is given by $c_{\text{ph}} = \omega/\Re(k_x)$ and the attenuation in the propagation direction is $\alpha_x = \Im(k_x)$, with $\Re(\cdot)$ and $\Im(\cdot)$ denoting real and imaginary components of a complex number. Waves

with displacements in the z direction decouple from those with displacements in the x and y directions [81]; the latter encompass the leaky Lamb waves of interest and hence only displacements in the x and y directions will be considered in the waveguide and the two fluids, say $\bar{u}_x, \bar{u}_{x_{f_1}}$ and $\bar{u}_{x_{f_2}}$ and $\bar{u}_y, \bar{u}_{y_{f_1}}$ and $\bar{u}_{y_{f_2}}$.

Snell's law requires that waves in all layers must share the same frequency and complex wavenumber in the x direction; this is depicted in Figure 2.1, where a common wavenumber, k_x, in the direction of propagation, is assumed for waves in all layers of the system. It follows that, assuming plane harmonic waves, all displacement and stress fields, in both fluids and the waveguide, contain the common exponential factor, $\exp[i(k_x x - \omega t)]$, which is henceforth assumed present in all fields and omitted for brevity. Following the discussion presented in Section 1.2, the displacement vector $\boldsymbol{u}_w = (u_x, u_y)$ of displacement in the isotropic solid, adheres to the two dimensional wave motion governed by the momentum equations, Eq. (1.19) and (1.20), for λ, μ the elastic Lamé parameters of the elastic material of the waveguide.

When it comes to the displacement fields in the two fluids, a similar approach is followed to derive the equation of motion in the two spaces. Let $\boldsymbol{u}_{f_1} = (u_{x_{f_1}}, u_{y_{f_1}})$, and $\boldsymbol{u}_{f_2} = (u_{x_{f_2}}, u_{y_{f_2}})$ be the vectors of displacements in the two fluids. By employing a Helmholtz decomposition [82], the two can be expressed in terms of two scalar wave potentials, ϕ_{f_1} and ϕ_{f_2}, as

$$\boldsymbol{u}_{f_1} = \begin{pmatrix} u_{x_{f_1}} \\ u_{y_{f_1}} \end{pmatrix} = \nabla\phi_{f_1}, \quad \boldsymbol{u}_{f_2} = \begin{pmatrix} u_{x_{f_2}} \\ u_{y_{f_2}} \end{pmatrix} = \nabla\phi_{f_2}. \tag{2.1}$$

The scalar wave potentials correspond to a partial wave representation of the radiated wave field, which, for leakage into inviscid fluids, can only have compressional polarisations. Thus, the scalar wave potentials ϕ_{f_1} and ϕ_{f_2}, correspond to longitudinal partial waves in the fluids. Expanding Eq. (2.1)

yields

$$u_{x_{f_n}} = ik_x\phi_{f_n}, \tag{2.2}$$

$$u_{y_{f_n}} = \frac{\partial\phi_{f_n}}{\partial y}, \tag{2.3}$$

with the subscripts $n = 1, 2$ corresponding to the fluids above and below the waveguide respectively.

Following the discussion of Nayfeh and Nagy [78], specialising their viscous fluid model to the inviscid fluids of this setup, the inviscid fluid spaces may be modelled as elastic spaces of zero shear component, i.e. solids with $\mu = 0$. The equations governing wave motion in the fluids, derived by replicating the discussion of Section 1.2 with $\mu = 0$, are

$$\rho_{f_n}\omega^2 u_{x_{f_n}} - \lambda_{f_n}k_x^2 u_{x_{f_n}} + \lambda_{f_n}ik_x\frac{\partial u_{y_{f_n}}}{\partial y} = 0, \tag{2.4}$$

$$\rho_{f_n}\omega^2 u_{y_{f_n}} + \lambda_{f_n}ik_x\frac{\partial u_{x_{f_n}}}{\partial y} + \lambda_{f_n}\frac{\partial^2 u_{y_{f_n}}}{\partial y^2} = 0, \tag{2.5}$$

with $\lambda_{f_n} = \rho_{f_n}c_{f_n}^2$ in each fluid. A substitution of Eqs. (2.2) and (2.3) into Eqs. (2.4) and (2.5) allow the equations of motion in the two fluids to be reduced into a single equation in the scalar wave potential ϕ_{f_n}, as

$$\rho_{f_n}\omega^2\phi_{f_n} - \lambda_{f_n}k_x^2\phi_{f_n} + \lambda_{f_n}\frac{\partial^2\phi_{f_n}}{\partial y^2} = 0. \tag{2.6}$$

To fully describe wave motion in the immersed waveguide system, in addition to equations of motion, interface conditions are required. For a two-sided fluid-loaded system, these are the continuity of normal stress and normal displacement, and the vanishing of shear stress at the two interfaces [52]

$$\sigma_{xy} = \sigma_{y_{f_n}} - \sigma_y = u_{y_{f_n}} - u_y = 0, \text{ at } y = \pm d, \tag{2.7}$$

with $\sigma_{y_{f_n}} = -\rho_{f_n}\omega^2\phi_{f_n}$ the normal stress in the two fluids [51]. A direct substitution of stresses and displacements in Eq. (2.7) allow interface conditions to explicitly be given by

$$\left[(\lambda + 2\mu)\frac{\partial u_y}{\partial y} + \lambda i k_x u_x + \rho_{f_n}\omega^2\phi_{f_n}\right]\Big|_{y=\pm d} = 0, \tag{2.8}$$

$$\left[ik_x u_y + \frac{\partial u_x}{\partial y}\right]\Big|_{y=\pm d} = 0, \tag{2.9}$$

$$\left[\frac{\partial \phi_{f_n}}{\partial y} - u_y\right]\Big|_{y=\pm d} = 0. \tag{2.10}$$

Wave propagation in the waveguide is captured by a single wavenumber, k_x, whereas the inhomogeneous bulk waves that propagate in the fluids, at an angle from the waveguide, see Figure 2.1, require additional wavenumbers; these represent the projection of outgoing waves in the transverse, y, direction. The aforementioned wavenumbers are denoted by k_{y_1} and k_{y_2} for the two fluids and similar to k_x, their real parts describe the speed of propagation in the y direction and their imaginary parts describe their attenuation or growth as they propagate along the same direction. It is common to define the propagation wave vectors of these inhomogeneous bulk waves as

$$\boldsymbol{k_{f_1}} := \begin{pmatrix} k_x \\ k_{y_1} \end{pmatrix} \text{ and } \boldsymbol{k_{f_2}} := \begin{pmatrix} k_x \\ k_{y_2} \end{pmatrix}, \tag{2.11}$$

which, for inviscid fluids, have real magnitudes given by [83]

$$|\boldsymbol{k_{f_n}}| = k_{f_n} = \frac{\omega}{c_{f_n}}, \text{ for } n = 1, 2, \tag{2.12}$$

and satisfy the trigonometric relation

$$k_{f_n}^2 = k_x^2 + k_{y_n}^2, \text{ for } n = 1, 2. \tag{2.13}$$

Consequently, one may write the longitudinal wave potentials, ϕ_{f_1} and ϕ_{f_2}, in the two fluid half-spaces, as [78, 84]

$$\phi_{f_1}(y) = A_1 \exp\left[-ik_{y_1}(y+d)\right], \tag{2.14}$$

$$\phi_{f_2}(y) = A_2 \exp\left[ik_{y_2}(y-d)\right], \tag{2.15}$$

where A_1, A_2 are unknown constants to be found.

It is important to highlight that Eq. (2.13) implies that $k_x^2 + k_{y_n}^2$ must be real valued, which in turn requires the imaginary components of k_x and k_{y_n} to have opposite signs when outgoing waves of positive phase velocities are considered, i.e. when both $\Re(k_x)$ and $\Re(k_{y_n})$ are positive. In particular, when leaky waves are propagating and attenuating along the positive x direction – a behaviour described by a complex wavenumber k_x of positive real and imaginary parts – it follows that $\Im(k_{y_n})$ must be negative and thus the wave fields described by Eqs. (2.14) and (2.15) in the two fluid spaces will exhibit exponential growth as a function of perpendicular distance from the waveguide; this forms the mathematical basis for the exponential growth of the leaky waves of interest in this study. For more details on the symmetries of the (k_x, k_{y_n}) spectrum and a classification of waves according to their complex wavenumbers see [85].

One approach to formulating the problem mathematically is to substitute Eqs. (2.14), (2.15) in Eqs. (2.6)-(2.10), discretise the waveguide and arrive at a non-linear eigenvalue problem [43], where the non-linearity of the problem is a result of the square root term arising from the use of Eqs. (2.12) and (2.13). For a single fluid, either on one side or on both sides, and leaky Lamb waves in a waveguide, Kiefer *et al.* [43] employ a SCM using Chebyshev polynomials to discretise the waveguide; a neat change of variables [86] reduces the algebraic non-linear eigenvalue problem to a polynomial one which is then solvable

with well-established methods. However, fluid coupling by two different fluids leads to a more complicated non-linear eigenvalue problem that appears not to reduce quite so pleasantly.

The aim of this work is a general approach for leaky waves in immersed waveguides or pipes. The solution method of choice is presented in the section to follow, where a spectral collocation discretisation of both the waveguide and of the two open spaces of inviscid fluids is proposed; the discretisation of the fluid spaces is key, as it is what deals with the exponential growth of leaky waves, and will be described in detail. This discretisation results in a polynomial eigenvalue problem with the complex wavenumber k_x as its eigenvalue and the wave displacements, complemented by the wave amplitudes of Eqs. (2.14) and (2.15), as the eigenvector; an eigenvalue problem solvable with standard methods.

2.3 Discretisation

The discretisation of both the waveguide and the open fluid domains is done using spectral collocation [55, 56]. For the problem of planar geometry discussed in this chapter, spectral collocation was advantageous and easy to implement, however, it is worth noting that the discretisation method to be presented here is not unique to spectral collocation.

Recall that, in brief, spectral collocation revolves around creating differentiation matrices and expressing an ODE or PDE as a matrix equation. When one wishes to differentiate a function that is defined over some known domain, spectral collocation approximates said derivative by generating differentiation matrices. Those differentiation matrices are generated based on a discretisation of the domain of the function with a set of collocation points and a choice of global interpolants. The operation of differentiating a function

then becomes a matrix multiplication between the differentiation matrix and a column vector of the function to be differentiated sampled at the set of collocation points; see Section 1.3 for more details.

The identification of the collocation points is thus key, and a common choice, when the function one is working with is smooth and the domain it is defined over, bounded, is that of the Gauss–Lobatto Chebyshev collocation points of Eq. (1.28), for which the Chebyshev differentiation matrices exhibit spectral accuracy [56,57]. This accuracy, together with their flexibility and established use in guided wave problems [24,27,43], motivates their use for approximating the derivatives of displacement fields in the bounded waveguide domain $[-d, d]$.

The treatment of the bounded waveguide domain follows that presented in [24]. A discretisation of the domain $[-d, d]$ and corresponding differentiation matrices defined over the same domain are desired. To start, the differentiation matrix suite of Weideman and Reddy [58] is employed to obtain the first and second order differentiation matrices, denoted by $D^{(1)}$ and $D^{(2)}$ respectively, for the N Gauss–Lobatto Chebyshev collocation points, $\{s_j\}_{j=1}^{N}$, defined in Eq. (1.28) over the interval $[-1, 1]$. The discretisation of the waveguide domain $[-d, d]$ with Chebyshev collocation points is simply achieved with

$$y_p^j = d s_j, \tag{2.16}$$

which produces a set of collocation points, $\{y_p^j\}_{j=1}^{N}$, spanning over the desired waveguide domain. Just like in Eq. (1.31), the corresponding first and second order differentiation matrices in $[-d, d]$ as

$$\begin{aligned} D_p^{(1)} &= \left(\frac{1}{d}\right) D^{(1)}, \\ D_p^{(2)} &= \left(\frac{1}{d}\right)^2 D^{(2)}. \end{aligned} \tag{2.17}$$

To treat the open spaces of fluid, $[-\infty, -d]$ and $[d, \infty]$, a generalisation of Chebyshev methods is used instead – specifically of Rational Chebyshev [57] approaches; these have been used for guided waves in optics, i.e. in the modal analysis of a multilayered optical waveguide [87]. Rational Chebyshev nodes arise from the mapping of Chebyshev collocation nodes, through rational maps, onto an open space, infinite or semi-infinite, and preserve the performance benefits of traditional Chebyshev differentiation matrices.

Start again from the N Chebyshev collocation points, $\{s_j\}_{j=1}^{N}$, defined over the interval $[-1, 1]$ and note that although the same starting point is assumed for the discretisation of both fluids for brevity, this needs not be the case in general; a different number of points and differentiation matrices may be used in each layer. Instead of the real valued rational maps of Rational Chebyshev methods, consider the complex coordinate transformations $h_{f_1} : [-1, 1] \longrightarrow \mathbb{C}$ and $h_{f_2} : [-1, 1] \longrightarrow \mathbb{C}$ given by

$$h_{f_1} : s \longrightarrow y = -d - \zeta_{f_1} \frac{1 - s}{1 + s}, \tag{2.18}$$

$$h_{f_2} : s \longrightarrow y = d + \zeta_{f_2} \frac{1 + s}{1 - s}, \tag{2.19}$$

with $\zeta_{f_1}, \zeta_{f_2} \in \mathbb{C}$; the choice of the two complex parameters ζ_{f_1} and ζ_{f_2} plays an important role in the discretisation of the fluid domains and is deserving of a detailed discussion.

A choice of positive real numbers ζ_{f_1} and ζ_{f_2}, such as the one made in previous work on optical waveguides [87], maps the collocation points of Eq. (1.28), through h_{f_1} and h_{f_2}, to $[-\infty, -d]$ and $[d, \infty]$ respectively. The implicit exponential growth of leaky waves prevents conventional eigenvalue solvers from reliably retrieving the solution and requires the use of PMLs, absorbing layers or outgoing wave boundary conditions at infinity which simply transfers the

numerical problems normally encountered to elsewhere in the problem. Note that, within such PMLs, a map to complex space, to appropriately adjust the leaky PML solutions to decay [48], allows leaky wave solutions.

A choice of complex ζ_{f_1} and ζ_{f_2} maps a real interval onto two semi-infinite intervals in complex space, denoted by $\mathbb{C}_{f_1}$ and $\mathbb{C}_{f_2}$. The complex intervals are exactly the complex lines adjoining $h_{f_n}(s_1)$ with $h_{f_n}(s_N)$. If, without loss of generality, one considers h_{f_1}, then depending on the choice of ζ_{f_1}, the complex interval $\mathbb{C}_{f_1}$ is the line adjoining $h_{f_1}(-1) = \pm\infty \pm i\infty$ to $h_{f_1}(1) = d$.

This choice of complex ζ_{f_1} and ζ_{f_2} is key in the proposed discretisation and will enable the solution of leaky waves. To understand how, one needs consider the leaky problem and the equations of motion Eq. (2.6), defined over the complex intervals $\mathbb{C}_{f_1}$ and $\mathbb{C}_{f_2}$. Even when defined over $\mathbb{C}_{f_n}$, Eq. (2.6) is still a wave equation of the same wavenumber, k_x, and consequently attains solutions of the form

$$\tilde{\phi}_{f_1}(y_{f_1}) = \tilde{A}_1 \exp[-ik_{y_1}(y_{f_1} + d)], \tag{2.20}$$

$$\tilde{\phi}_{f_{f_2}}(y_2) = \tilde{A}_2 \exp[ik_{y_2}(y_{f_2} - d)], \tag{2.21}$$

with $\tilde{A}_n$ unknown amplitudes and $y_{f_n} \in \mathbb{C}_{f_n}$.

The unknown amplitudes, $\tilde{A}_n$, just like A_n, are determined by imposing the interface conditions at the two solid-fluid interfaces. As the choice of mapping guarantees a collocation point on the real space of the two fluid-solid interfaces, interface conditions are applied at the collocation points located at the physical fluid-solid interfaces for both the physical problem and $\phi_{f_n}(y)$ with real y, and the complex problem and $\tilde{\phi}_{f_n}(y_{f_n})$ with complex y_{f_n}. From Eqs. (2.20), (2.21) and (2.14), (2.15), it is clear that $\phi_{f_n}(\pm d) = A_n$ and $\tilde{\phi}_{f_n}(\pm d) = \tilde{A}_n$, which implies that if they are to satisfy identical equations at the same collocation points, it must be that $A_n = \tilde{A}_n$. In fact the unknown

amplitudes A_n fully determine both $\tilde{\phi}_{f_n}$ and ϕ_{f_n}, with the two only different in their domains of definition; the $\tilde{\phi}_{f_n}$ are the analytic continuations of ϕ_{f_n}, with domains of definition the complex paths $\mathbb{C}_{f_n}$, and will henceforth be referred to as the complex wave potentials in the two fluids.

Crucially, introducing the maps h_{f_1} and h_{f_2} allows control over the behaviour of the complex wave potentials of Eqs. (2.20) and (2.21), which, under a careful choice of ζ_{f_n}, can be made to numerically decay. To illustrate how that may be achieved, consider the following: the leaky waves that are sought in this study are radiating from the waveguide and into the adjacent fluid spaces, and cause outgoing wave fields in the two fluid spaces that grow exponentially as a function of perpendicular distance from the waveguide. For that to be the case, the wave potentials of Eqs. (2.14) and (2.15) must correspond to outgoing and growing waves and, as previously discussed, the transverse wavenumbers k_{y_1} and k_{y_2} both have to lie in the 4^{th} complex quadrant. That is, they have positive real and negative imaginary parts and may be written as $k_{y_n} = \alpha + i\beta$, with $\alpha \in \mathbb{R}_{>0}$ and $\beta \in \mathbb{R}_{<0}$. If the complex wave potentials of Eqs. (2.20) and (2.21) are rewritten as

$$\tilde{\phi}_{f_n}(y_{f_n}) = A_n \exp(ik_{y_n}\zeta_{f_n}y_0), \tag{2.22}$$

with y_0 the real half line $[0, \infty)$ such that $y_{f_1} = -d - \zeta_{f_1}y_0$ and $y_{f_2} = d + \zeta_{f_2}y_0$, then a choice of $\zeta_{f_n} = \gamma + i\delta$, with $\gamma, \delta \in \mathbb{R}_{\geq 0}$, yields

$$\begin{aligned}
\tilde{\phi}_{f_n}(y_{f_n}) &= A_n \exp(ik_{y_n}\zeta_{f_n}y_0), \\
&= A_n \exp[i(\alpha + i\beta)(\gamma + i\delta)y_0], \\
&= A_n \exp[i(\alpha\gamma + i\alpha\delta + i\beta\gamma - \beta\delta)y_0], \\
&= A_n \exp[i(\alpha\gamma - \beta\delta)y_0] \exp[-y_0(\alpha\delta + \beta\gamma)].
\end{aligned} \tag{2.23}$$

It follows that the complex potentials $\tilde{\phi}_{f_n}(y_{f_n})$ numerically decay as $y_0 \to \infty$,

when

$$\begin{aligned} -y_0(\alpha\delta+\beta\gamma) &< 0, \\ \alpha\delta+\beta\gamma &> 0, \\ \delta &> -\gamma(\beta/\alpha), \text{ if } \alpha \neq 0. \end{aligned} \tag{2.24}$$

This means that due to the choice of complex maps, the Chebyshev collocation points, $\{s_j\}_{j=1}^N$, may be mapped to two complex intervals, $\mathbb{C}_{f_1}$ and $\mathbb{C}_{f_2}$, where importantly, both complex fluid wave potentials, $\tilde{\phi}_{f_n}$, are made to numerically decay while still satisfying the momentum equations of Eq. (2.6) and all six of the interface conditions of Eqs. (2.8)-(2.10), this way preserving all the essential characteristics of the original leaky wave solution, i.e. the $\tilde{\phi}_{f_n}$ numerically decay for the same wavenumber and amplitude of leaky waves. Thus, the proposed complex coordinate transformation allows for a numerically decaying problem to be solved instead of an exponentially growing one, without compromises on any of the underlying physics. It should be noted that the proposed complex rational maps of Eqs. (2.18)-(2.19) resemble the complex coordinate stretching used in the technique of PMLs; see Appendix A for more details and a discussion.

To obtain differentiation matrices in the complex fluid domains, $\mathbb{C}_{f_1}$ and $\mathbb{C}_{f_2}$, denote by $\boldsymbol{y}_{f_1} = \left\{y_{f_1}^j = h_{f_1}(s_j)\right\}_{j=1}^N$ the vector of collocation points in $\mathbb{C}_{f_1}$ and by $\boldsymbol{y}_{f_2} = \left\{y_{f_2}^j = h_{f_2}(s_j)\right\}_{j=1}^N$ the vector of collocation points in $\mathbb{C}_{f_2}$. A repeated use of the chain rule gives the differentiation matrices for the fluids in the two complex domains. The $N \times N$ differentiation matrices for the fluid at the

top of the waveguide are given by

$$D_{f_1}^{(1)} = \text{diag}\left(\frac{2\zeta_{f_1}}{[\zeta_{f_1} - (\boldsymbol{y}_{f_1} + \boldsymbol{d})]^2}\right) D^{(1)}, \tag{2.25}$$

$$\begin{aligned} D_{f_1}^{(2)} =& \text{diag}\left(\frac{4\zeta_{f_1}}{[\zeta_{f_1} - (\boldsymbol{y}_{f_1} + \boldsymbol{d})]^3}\right) D^{(1)} \\ &+ \text{diag}\left(\frac{4\zeta_{f_1}^2}{[\zeta_{f_1} - (\boldsymbol{y}_{f_1} + \boldsymbol{d})]^4}\right) D^{(2)}, \end{aligned} \tag{2.26}$$

and similarly the ones for the fluid at the bottom of the waveguide read

$$D_{f_2}^{(1)} = \text{diag}\left(\frac{2\zeta_{f_2}}{[\zeta_{f_2} + (\boldsymbol{y}_{f_2} - \boldsymbol{d})]^2}\right) D^{(1)}, \tag{2.27}$$

$$\begin{aligned} D_{f_2}^{(2)} =& \text{diag}\left(\frac{-4\zeta_{f_2}}{[\zeta_{f_2} + (\boldsymbol{y}_{f_2} - \boldsymbol{d})]^3}\right) D^{(1)} \\ &+ \text{diag}\left(\frac{4\zeta_{f_2}^2}{[\zeta_{f_2} + (\boldsymbol{y}_{f_2} - \boldsymbol{d})]^4}\right) D^{(2)}. \end{aligned} \tag{2.28}$$

Here, $\boldsymbol{d} = (d, \ldots, d)^T$ is a column vector of appropriate size, and likewise for $\boldsymbol{\zeta}_{f_1}$ and $\boldsymbol{\zeta}_{f_2}$. The diagonal matrices in Eqs. (2.25)-(2.28) are the matrices whose diagonals are the expressions in parenthesis, evaluated at each of the collocation points, and have zeros everywhere else.

Due to the choice of discretisation, a numerically decaying function is now extracted rather than an exponentially growing one. As a result, imposing Dirichlet zero boundary condition at the farthest collocation point in the complex space associated with a fluid domain is relevant only insofar as it ensures that the solution vanishes at infinity in that complex space. This is achieved by removing the rows and columns of differentiation matrices corresponding to that collocation point, as well as the collocation point itself. For the fluid space at the top of the waveguide, the first rows and columns

of $D_{f_1}^{(1)}$ and $D_{f_1}^{(2)}$ and $y_{f_1}^1$ are deleted, while for the fluid space at the bottom, the last rows and columns of $D_{f_2}^{(1)}$ and $D_{f_2}^{(2)}$ and the collocation point $y_{f_2}^N$ are deleted.

Having generated differentiation matrices for both the waveguide and complex fluid domains, the differential operators of Eqs. (1.19),(1.20) and (2.6) may be expressed as matrix operators by replacing first and second order derivatives in Eqs. (1.19),(1.20) and (2.6) with the appropriate differentiation matrices $D_p^{(m)}$ or $D_{f_n}^{(m)}$, for $n = 1, 2$ and $m = 1, 2$. Those read

$$L_p = k_x^2 L_{p_2} + k_x L_{p_1} + L_{p_0}, \tag{2.29}$$

$$L_{f_n} = k_x^2(-\lambda_{f_n} I) + \rho_{f_n}\omega^2 I + \lambda_{f_n} D_{f_n}^{(2)}, \tag{2.30}$$

with L_{p_k} given by

$$L_{p_2} = \begin{bmatrix} -(\lambda + 2\mu)I & 0 \\ 0 & -\mu I \end{bmatrix}, \tag{2.31}$$

$$L_{p_1} = \begin{bmatrix} 0 & i(\lambda + \mu)D_p^{(1)} \\ i(\lambda + \mu)D_p^{(1)} & 0 \end{bmatrix}, \tag{2.32}$$

$$L_{p_0} = \begin{bmatrix} \rho\omega^2 I + \mu D_p^{(2)} & 0 \\ 0 & \rho\omega^2 I + (\lambda + 2\mu)D_p^{(2)} \end{bmatrix}, \tag{2.33}$$

for $k = 1, 2, 3$ and I the identity matrix of appropriate size. In Eqs. (2.29)-(2.33), matrix operators were separated into k_x^2-dependent, k_x-dependent and constant components; this is convenient for the polynomial eigenvalue problem formulation presented later. These matrix operators allow the equations of motion of the immersed plate problem to be written as the eigenvalue problem

$$\tilde{L}\boldsymbol{u} = \mathbf{0}, \tag{2.34}$$

with

$$\tilde{L} = \begin{pmatrix} L_{f_1} & 0 & 0 \\ 0 & L_p & 0 \\ 0 & 0 & L_{f_2} \end{pmatrix}, \tag{2.35}$$

a $(4N-2)\times(4N-2)$ diagonal matrix operator and

$$\boldsymbol{u} = \begin{pmatrix} \tilde{\boldsymbol{\phi}}_{f_1} \\ \boldsymbol{u}_x \\ \boldsymbol{u}_y \\ \tilde{\boldsymbol{\phi}}_{f_2} \end{pmatrix}, \tag{2.36}$$

a column vector of $(4N-2)$ entries containing the displacement fields in the waveguide and complex fluid wave potentials evaluated on the collocation points discretising their respective domains of definition. Explicitly those are given by

$$\begin{aligned} \tilde{\boldsymbol{\phi}}_{f_1} &= \begin{pmatrix} \tilde{\phi}_{f_1}(y_{f_1}^2) \\ \vdots \\ \tilde{\phi}_{f_1}(y_{f_1}^N) \end{pmatrix}, \boldsymbol{u_x} = \begin{pmatrix} u_x(y_p^1) \\ \vdots \\ u_x(y_p^N) \end{pmatrix}, \\ \boldsymbol{u_x} &= \begin{pmatrix} u_y(y_p^1) \\ \vdots \\ u_y(y_p^N) \end{pmatrix}, \tilde{\boldsymbol{\phi}}_{f_2} = \begin{pmatrix} \tilde{\phi}_{f_1}(y_{f_2}^1) \\ \vdots \\ \tilde{\phi}_{f_2}(y_{f_2}^N) \end{pmatrix}. \end{aligned} \tag{2.37}$$

By separating the matrix operator $\tilde{L}$ into its k_x^2-dependent, k_x-dependent and constant constituent components, say $\tilde{L}_2, \tilde{L}_1$ and $\tilde{L}_0$ respectively, Eq. (2.34) may be rewritten as

$$\left(k_x^2\tilde{L}_2 + k_x\tilde{L}_1 + \tilde{L}_0\right)\boldsymbol{u} = 0. \tag{2.38}$$

To complete the discretisation of the problem with spectral collocation, the interface conditions Eqs. (2.8)-(2.10) must be incorporated in the matrix equation of Eq. (2.38). To achieve this, the differential operators of interface condition equations must first be discretised into row operators by replacing the derivatives of displacements and wave potentials with appropriate rows of differentiation matrices. For example, interface conditions at the top interface at $y = -d$, are discretised as

$$\begin{aligned}
&\left[\rho_{f_1}\omega^2 I\tilde{\boldsymbol{\phi}}_{f_1}\right]\big|_{y=-d} + \left[i\lambda k_x I\boldsymbol{u}_x\right]\big|_{y=-d} + \left[(\lambda+2\mu)D_p^{(1)}\boldsymbol{u}_y\right]\Big|_{y=-d} = 0,\\
&\left[D_p^{(1)}\boldsymbol{u}_x\right]\Big|_{y=-d} + \left[ik_x I\boldsymbol{u}_y\right]\big|_{y=-d} = 0,\\
&\left[D_{f_1}^{(1)}\tilde{\boldsymbol{\phi}}_{f_1}\right]\Big|_{y=-d} + \left[-I\boldsymbol{u}_y\right]\big|_{y=-d} = 0,
\end{aligned} \tag{2.39}$$

with the operation $[\cdot]|_{y=-d}$ interpreted as the discrete evaluation of the operator in square brackets at the top solid-fluid interface. This evaluation is equivalent to taking the row of the matrix operator in the square brackets that corresponds to the collocation point at $y = -d$. Due to the ordering of collocation points throughout the domain and the imposition of Dirichlet zero boundary conditions, the matrix operators acting on $\tilde{\boldsymbol{\phi}}_{f_1}$ are of size $(N-1)\times(N-1)$ and their last rows correspond to the collocation point at $y = -d$, while matrix operators acting on either $\boldsymbol{u}_x$ or $\boldsymbol{u}_y$ are of size $N \times N$ and their first rows correspond to the collocation point at the top interface.

The above may be combined into a discrete matrix equation of interface conditions at $y = -d$, as

$$IC_{(-d)}\boldsymbol{u} = \mathbf{0}, \tag{2.40}$$

with $IC_{(-d)}$ a matrix operator of size $3 \times (4N-2)$ explicitly given as

$$\begin{aligned} IC_{(-d)} = k_x & \begin{bmatrix} 0 & i\lambda I & 0 & 0 \\ 0 & 0 & iI & 0 \\ 0 & 0 & 0 & 0 \end{bmatrix} \Bigg\|_{y=-d} \\ + & \begin{bmatrix} \rho_{f_1}\omega^2 I & 0 & (\lambda+2\mu)D_p^{(1)} & 0 \\ 0 & D_p^{(1)} & 0 & 0 \\ D_{f_1}^{(1)} & 0 & -I & 0 \end{bmatrix} \Bigg\|_{y=-d} . \end{aligned} \tag{2.41}$$

In Eq. (2.41), $IC_{(-d)}$ is represented for simplicity by a 3×4 matrix whose elements are the row vectors representing the discrete evaluation of the differential operators of the interface conditions at the interface $y = -d$, i.e. the appropriate rows of the matrix operators of Eq. (2.39).

Similarly, the matrix of interface conditions at the bottom interface is obtained as

$$\begin{aligned} IC_{(d)} = & k_x \begin{bmatrix} 0 & i\lambda I & 0 & 0 \\ 0 & 0 & iI & 0 \\ 0 & 0 & 0 & 0 \end{bmatrix} \Bigg\|_{y=d} \\ + & \begin{bmatrix} 0 & 0 & (\lambda+2\mu)D_p^{(1)} & \rho_{f_2}\omega^2 I \\ 0 & D_p^{(1)} & 0 & 0 \\ 0 & 0 & -I & D_{f_2}^{(1)} \end{bmatrix} \Bigg\|_{y=d} , \end{aligned} \tag{2.42}$$

with the same convention for the evaluation of the differential operators used here. For evaluation at the interface $y = d$, the first row of the operators for the complex fluid potential of the fluid at the bottom of the waveguide and the N^{th} row of the operators of the waveguide displacements must be taken.

To incorporate those interface conditions, like with the example of Poisson's equation in Section 1.3, rows of $\tilde{L}$, or equivalently of $\tilde{L}_2, \tilde{L}_1$ and $\tilde{L}_0$, that correspond to the two interfaces must be replaced with rows from the interface condition matrices of Eqs. (2.41) and (2.42). Again, due to the discretisation and construction of $\tilde{L}$ from the matrix differential operators of Eqs. (2.29) and (2.30), the rows corresponding to the interface $y = -d$ are $N-1, N$ and $2N$, and each of those is replaced with a row from the interface condition matrix $IC_{(-d)}$. Similarly, the rows corresponding to the interface at $y = d$ are $2N-1, 3N-1$ and $3N$, and each of those is replaced with an appropriate row from $IC_{(d)}$. An illustration of this process is shown in Figure 2.2.

By imposing the discretised interface conditions on $\tilde{L}$, one arrives at a new matrix operator, L, with a decomposition analogous to the one of Eq. (2.38). The resulting polynomial eigenvalue problem is

$$\left(k_x^2 L_2 + k_x L_1 + L_0\right) \boldsymbol{u} = \mathbf{0}, \tag{2.43}$$

where for a given ω, k_x is the eigenvalue and $\boldsymbol{u}$ is the eigenvector.

To solve the polynomial eigenvalue problem and retrieve the dispersion curves and mode shapes of leaky waves, a companion matrix linearisation [88] is employed by setting $\boldsymbol{U} = [k_x \boldsymbol{u}, \boldsymbol{u}]^T$ and defining the square companion matrices

$$A = \begin{bmatrix} -L_1 & -L_0 \\ I & 0 \end{bmatrix} \text{ and } B = \begin{bmatrix} L_2 & 0 \\ 0 & I \end{bmatrix}, \tag{2.44}$$

with I the identity matrix of dimension $(4N-2) \times (4N-2)$. The polynomial eigenvalue problem of Eq. (2.43) is then equivalent to the generalised linear eigenvalue problem,

$$(A - k_x B)\boldsymbol{U} = \mathbf{0}, \tag{2.45}$$

that is solvable with conventional generalised eigenvalue problem solvers, with

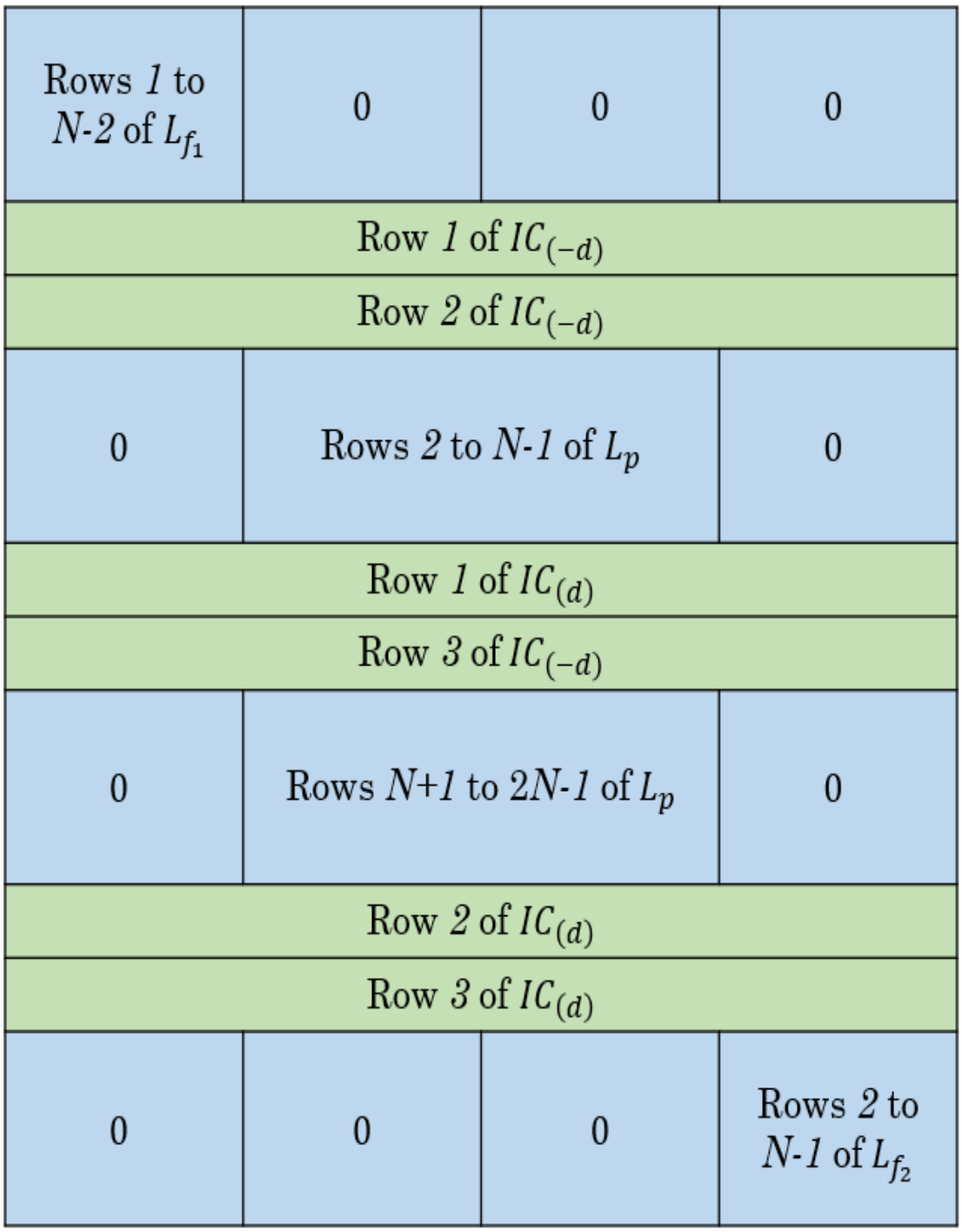

Figure 2.2: An illustration of imposing interface conditions by replacing rows $N-1, N$ and $2N$ with rows from $IC_{(-d)}$ and rows $2N-1, 3N-1$ and $3N$ with rows from $IC_{(d)}$.

eigenvalue k_x and eigenvector $\boldsymbol{U}$. By formulating and solving the eigenvalue problem of Eq. (2.45) for multiple real frequencies in a desired range, i.e. performing frequency sweeps, the full set of leaky wave dispersion curves is retrieved.

To summarise, using a spectral collocation discretisation, a polynomial eigenvalue problem that preserves the characteristics of leaky wave propagation in a waveguide immersed between two fluids of the same or different wave speeds was formulated and solved. The key idea of the method was to model wave propagation in carefully selected paths in the complex plane rather than the physical fluid domains. This allows the search for exponentially decaying numerical solutions that fully and accurately describe the exponentially growing physical ones, without the need of solving non-linear eigenvalue problems or absorbing boundaries at infinity. Additionally, the method does not itself introduce attenuation to the material, and thus delivers correct solutions for the wave fields in the exterior domain without attenuating them – this method could also be applied for viscous fluids, in which case there would be a physical attenuation due to viscosity which would be retained correctly in this representation. Finally, a very significant property of the proposed technique is that it is not unique to spectral collocation; the key principle would work with any other choice of discrete representation of the waveguide, e.g. SAFE methods, to accurately obtain solutions to problems where energy leakage in infinite media is observed.

2.4 Results & Discussion

The presented spectral collocation discretisation is employed here to compute the dispersion curves and displacement fields, as eigenvalues and eigenvectors of Eq. (2.43), for leaky modes radiating from an elastic waveguide with

different inviscid fluids either side. The well-established software DISPERSE [16] provides a good basis for comparison with the proposed SCM as its reliability has been demonstrated in multiple scenarios [35, 89–92].

Consider the typical example of a 1 mm thick brass plate (ρ = 8.4 g/cm^3, c_t = 2.2 m/ms, c_l = 4.4 m/ms) loaded on the top side by water (ρ_{f_1} = 1 g/cm^3, c_{f_1} = 1.5 m/ms) and at the bottom side by diesel oil (ρ_{f_2} = 0.8 g/cm^3, c_{f_2} = 1.25 m/ms). Recall that to compute the dispersion curves of leaky waves in the system, a choice of complex parameters ζ_{f_n} that ensures the convergence of the complex wave potentials $\tilde{\phi}_{f_n}$ of Eq. (2.22) needs to be made. The convergence study of Eq. (2.24) suggested that when a complex wavenumber solution, k_x, and corresponding transverse wavenumbers, k_{y_n}, are to be solved for, a choice of ζ_{f_n} ought to be made such that $\Re(k_{y_n})\Im(\zeta_{f_n}) + \Re(\zeta_{f_n})\Im(k_{y_n}) > 0$. For the leaky modes ($\Re(k_{y_n}) > 0$ and $\Im(k_{y_n}) < 0$) of concern in this study, one may assume, without loss of generality, $\Re(\zeta_{f_j}) = 1$ and maintain in this way the span of the Gauss–Lobatto Chebyshev collocation points of Eq. (1.28), along the complex paths $\mathbb{C}_{f_n}$; further choosing $\Im(\zeta_{f_n}) > -\Im(k_{y_n})/\Re(k_{y_n})$ ensures the condition of Eq. (2.24) is satisfied.

The choice may be automated through the following rule-of-thumb: solve for the same waveguide immersed in two identical inviscid fluids twice, say with the SCM of [43], each time taking the inviscid fluids to be one of the two distinct fluids of the current setup, and record the maximum value of the ratio $-\Im(k_y)/\Re(k_y)$ for leaky wave solutions in the frequency range of interest. These maximum ratios provide initial guesses for the ratios $-\Im(k_{y_n})/\Re(k_{y_n})$. For the problem at hand, leaky waves in a brass waveguide fully immersed in water and then in oil were solved for; in the angular frequency range 0-20 MHz, the recorded maximum ratios were found to be less than 1.

In light of this, for the computation of dispersion curves with SCM, the

conservative choice of $\zeta_{f_j} = 1 + 10i$ was made, satisfying in this way Eq. (2.24). As this translates to a rapidly decaying solution, a sufficient number of collocation points was also chosen to capture this decay. A conservative choice is $N = 30$, which yields a convergent solution. The stability of the algorithm regarding the choices of ζ_{f_n} and the number of collocation points was briefly investigated and the scheme was found to be very robust to the choices taken in the frequency range studied. Despite that fact, it must be recognised that a more thorough investigation of these combinations is required to confidently and accurately obtain the full set of leaky wave solutions for all frequencies and every possible combination of solids and external fluids. The computation at 200 frequency points took a total of 40.36 seconds on a personal computer with a 32GB Random Access Memory (RAM) and an Intel i7-10700 Central Processing Unit (CPU).

The SCM results are compared with those from DISPERSE in Figure 2.3 with pleasing agreement for both the phase velocity and attenuation. There are infinitely many possible modes that can propagate through the waveguide and filtering prior to plotting was performed so that those leaky modes of most physical interest are illustrated. The filtering comprises a positively propagating wave requirement with $\Re(k_x) > 0$ and attenuation with $\Im(k_x) > 0$ and $|k_x| \neq \infty$. Also, for plotting purposes, an arbitrary choice of cut-off attenuation at 1 Np/mm was made. It should be noted that only leaky modes that radiate in both fluid spaces are depicted on Figure 2.3 – those are the traditionally more complex solutions to obtain due to the exponential growth of amplitude in both half-spaces of fluids. The full set of solutions, that is modes that only leak in one of the fluids or modes trapped in the waveguide and do not leak at all, can also be attained with an appropriate choice of complex parameters ζ_{f_n} – this will be demonstrated in the next chapter.

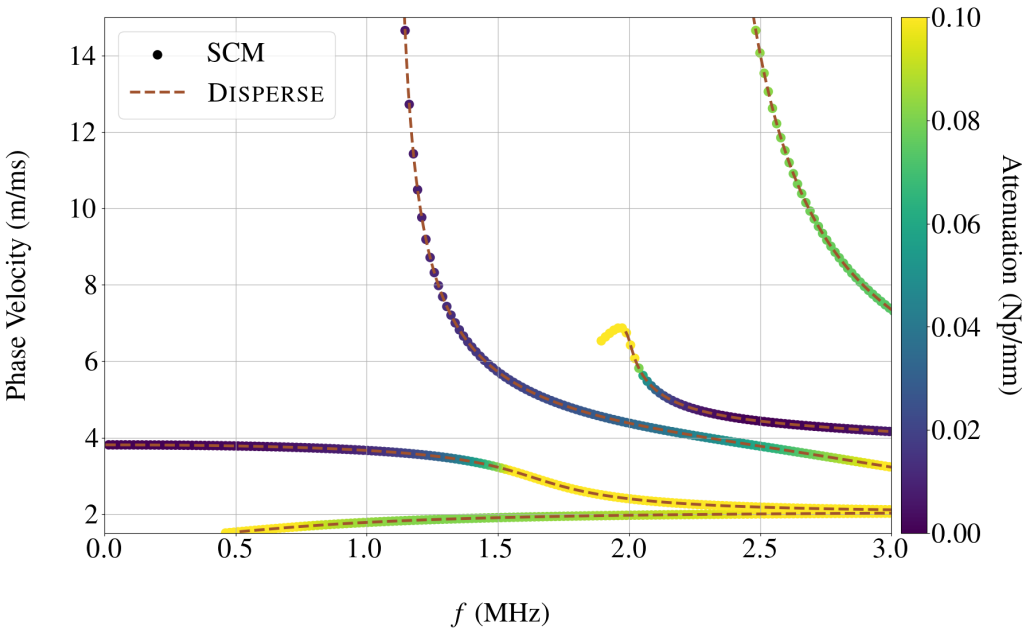

(a)

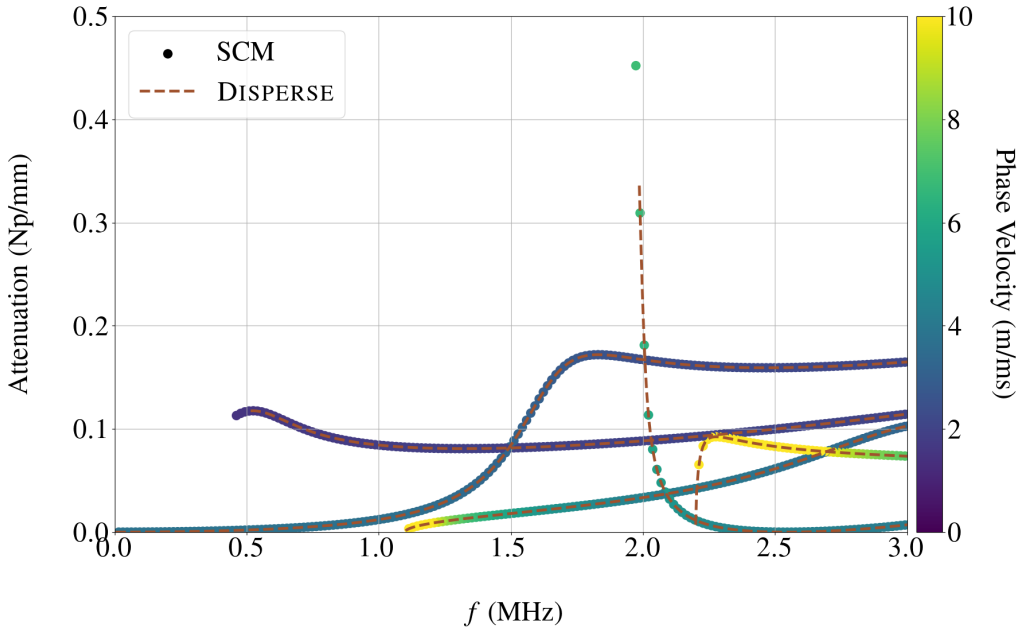

(b)

Figure 2.3: Comparison of dispersion curves obtained from the SCM model and from DISPERSE, for a 1 mm thick brass plate, loaded on one side by water and on the other by diesel oil. Figure 2.3(a) plots phase velocity against frequency, with SCM results coloured according to their value of attenuation, while Figure 2.3(b) plots attenuation against frequency, with SCM results coloured according to their value of phase velocity.

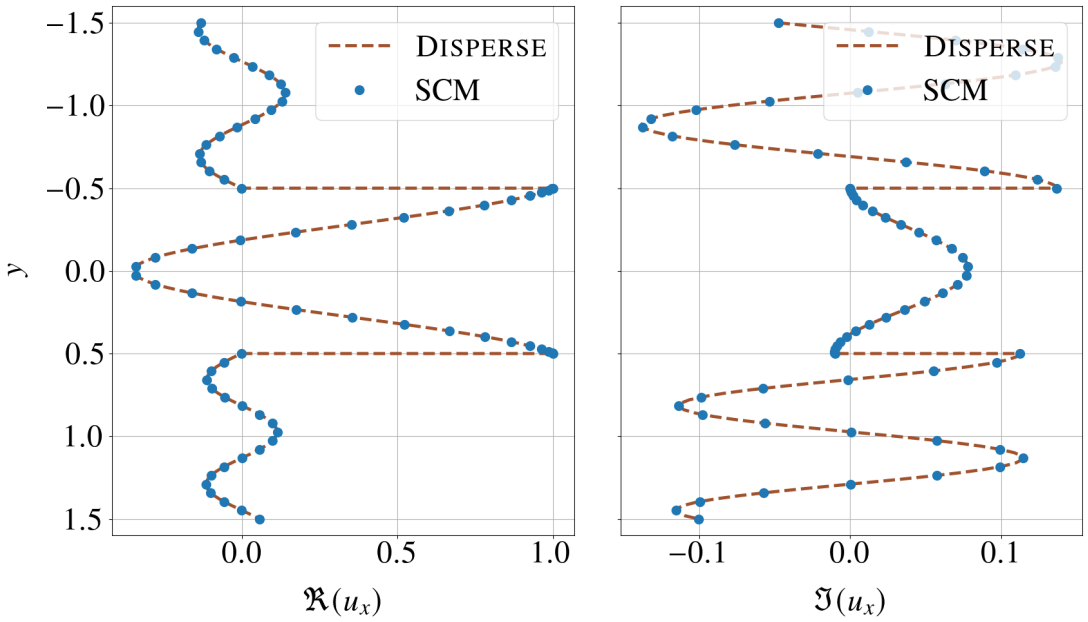

(a)

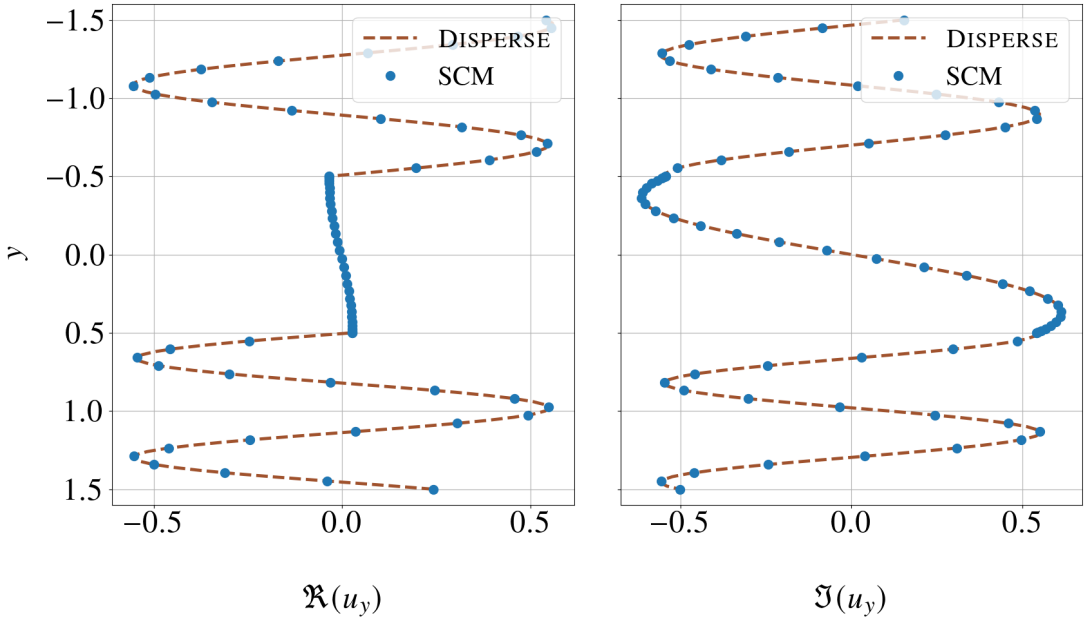

(b)

Figure 2.4: Mode shapes for a 1 mm thick brass plate loaded on one side by water and on the other by diesel oil, for the frequency-phase velocity pair $(f, c_{\text{ph}}) \approx (2 \text{ MHz}, 6.2 \text{ m/ms})$. Figure 2.4(a) plots the real and imaginary parts of u_x and Figure 2.4(b) plots the real and imaginary parts of u_y. The scale is chosen such that $u_x = 1$ for both SCM and DISPERSE results.

In addition to dispersion curves, the SCM conveniently retrieves the values of the amplitudes of the fluid potential and the displacements in the solid from the eigenvector through $\boldsymbol{U}$; as these fully describe the acoustic fields in the fluids and the solid, the whole of the wave field is obtained without any extra effort. Using those amplitudes, the displacements in the fluids are computed through the Helmholtz decomposition equations of displacements in the fluid, Eq. (2.1), and the wave potentials in Eqs. (2.14) and (2.15).

For the water-brass-oil system of Figure 2.3, a comparison of the y-dependent components of displacement, in both the direction of propagation and the normal direction, between the SCM displacements and the corresponding DISPERSE solution is made in Figure 2.4. Note that because SCM displacements are obtained as an eigenvector of a polynomial eigenvalue problem, any scalar multiple of these remains a valid eigenvector; the same fact is true for the mode shapes of DISPERSE [16]. Thus, to fix upon a solution and for the two fields to be comparable, the same u_x displacement at the interface $y = -d$ was imposed to both SCM and DISPERSE solutions ($u_x = 1$). The displacements of Figure 2.4, for an arbitrarily selected frequency-phase velocity pair $(f, c_{\text{ph}}) \approx (2 \text{ MHz}, 6.2 \text{ m/ms})$ from Figure 2.3, again show a good match between the two methods.

2.5 Conclusion

The leaky Lamb wave problem for a plate loaded on both sides by two different fluids is an exemplar of leaky waves and exhibits the key difficulty of studying such systems; the non-linear eigenvalue problem is difficult to solve, a neat change of variables to transform it is not easily available, the exponential growth poses a numerical challenge to the retrieval of accurate solutions. To overcome this inherent difficulty, a mapping of the fluid domains onto

paths in complex domains was performed. This map built in the exponential growth of leaky waves, and allowed the problem to be reformulated as a polynomial eigenvalue problem and be solved using standard solvers thence obtaining the complete physical solution robustly, accurately and without the need of user intervention; each of which attributes, or a combination of them, is a potential challenge to other existing methods. The use of spectral collocation, based on Chebyshev approaches, for the discretisation of both the open and closed domains of the system provides the method with speed, accuracy and robustness whilst keeping the eigenvalue systems compact. The formulation leads to systems amenable to standard eigensolvers and enables the retrieval of all the complex wavenumbers and displacement fields of leaky Lamb waves for any given frequency.

The complex mapping and the treatment of the exponential growth of the leaky waves of the system presented here is very importantly not unique to the planar elastic waveguiding problem: the introduced methodology can be extended to multilayered elastic systems of plain or cylindrical geometries. The underlying SCM technique is also general and can be extended to more complicated geometries and guiding structures, and also to more general media i.e. anisotropic or viscoelastic guides [80] and attenuating (e.g. viscous) fluids, and thereby together with the leaky wave SCM provides a methodology for all wave systems of this generic type.

Chapter 3

Leaky Wave Radiation from Buried Waveguides

3.1 Introduction

So far, the leakage of acoustic energy from a waveguide into a surrounding space of inviscid fluid, in planar geometries, has been investigated; this is but the simplest case where leaky waves manifest. Leaky waves feature prominently, not only in immersed waveguides but also in buried ones. In the context of NDE inspections, a structure under inspection often comprises an elastic waveguide in contact with dissimilar spaces of elastic media; elastic waves are then radiated from the waveguide into the surrounding media, with the amplitude of the leaked energy often displaying exponential growth with distance in the adjacent elastic medium and leaky guided waves propagating and attenuating along the structure with complex wavenumbers. This behaviour is common in a wide range of settings, some of which extend beyond NDE and structural integrity, including reinforced concrete structures [30], seismology [31], adhesive joints and fibre composites [32,33], buried pipes [14,34–37]

and biological structures such as bones surrounded by tissue [38–40]. Consequently, understanding the dispersion and attenuation characteristics of leaky systems, and in particular leaky Lamb waves [41, 43, 54, 65], for waveguides in contact with spaces of different elastic materials is of recurrent and broad interest.

When energy is radiated from a buried waveguide into adjacent spaces of solid media, the elastodynamic waves propagating in the exterior elastic spaces have both compressive and shear polarisations. Thus, unlike leakage from fluid coupled waveguide where a single compressive wave fully describes the radiated field in an adjacent fluid space, radiated waves in elasticity are described as the superposition of two partial waves, one longitudinal and one shear; this is a step-change in complexity from fluid loading cases, as either one or both longitudinal/shear waves can exponentially grow for leaky waves in elasticity. Consequently the existence of possibly multiple exponentially growing fields in the computational domain further complicates matters when attempting to model or accurately identify the dispersion and attenuation characteristics of leaky waves.

Recent contributions in the field have overcome some of the inherent computational challenges associated with the computation of leaky wave dispersion curves by formulating and solving non-linear eigenvalue problems. Notable contributions include those of Kiefer *et al.* [43], Tang *et al.* [93], and Gravenkamp *et al.* [44], where spatial discretisations – with SCM or SAFE – of straight waveguides coupled to unbounded fluid [43, 93] or isotropic solid [44] media were used to formulate non-linear eigenvalue problems that were subsequently linearised by a neat change of variables in the case of [43], by moving to a higher dimensional state space in [93], or by exploiting multiparameter eigenvalue problems in [44]. Despite their success, these methods are limited by their ability to linearise non-linear problems: it would be a major chal-

lenge to attempt to implement the aforementioned methods for the solution of the non-linear eigenvalue problems that emerge from cylindrical geometries or elasticity when different anisotropic media surround a waveguide.

The SCM introduced in the previous chapter for the computation of leaky waves radiating from fluid loaded waveguides, bypassed non-linear eigenvalue problems altogether. Instead, due to imposing mappings of the discretised fluid domains to complex paths, in which the numerical solution decayed while also maintaining the physics of wave propagation in the physical space, linear eigenvalue problems were formulated and solved with conventional solvers. In this chapter, the method is taken a step further and is extended to waveguides in contact with elastic half-spaces. The key contribution of this work is the development of a methodology that accounts for the presence of two distinct partial waves within each exterior elastic domain and solves the challenging problem of leakage into solids – a problem of practical relevance to the NDE community. A SCM will be demonstrated, in which the discretisation of the exterior elastic domains is determined by the nature of the solution to be found, and that delivers complete spectra of leaky wave dispersion curves and their mode shapes, with high accuracy, and as "black-box" solutions: there is no need for priori knowledge of the nature of the solutions nor of the tuning of parameters to approach the solution.

To validate the approach quantitatively, results will firstly be compared with those obtained using the commercially available PWRF software DISPERSE [16]. The validation will then be strengthened by comparing SCM predictions with FE modelling results. As FE simulations are agnostic to the modal concepts introduced by the proposed method and only result in a weighted superposition of modes [61], the comparison with the SCM will further enhance the credibility of the findings of the method and will instil confidence in the robustness of the approach, particularly in regions where

DISPERSE may not yield viable solutions.

This chapter is organised as follows – Section 3.2 presents a summary of the underlying theory of leaky Lamb waves radiating from a waveguide in contact with two different isotropic elastic half-spaces. Following that, Section 3.3 presents the discretisation method and FE model, while a discussion and the validation of results are found in Section 3.4.

The discussion and results presented in this chapter were published in [94].

3.2 Problem Statement

Consider an isotropic, linear-elastic waveguide, of finite thickness, $2d$, and infinite extent in both the x and z directions, now embedded between two half-spaces of different isotropic and linear-elastic media. Assume that both the elastic waveguide and half-spaces are homogeneous with densities ρ, ρ_1 and ρ_2, longitudinal wave speeds c_l, c_{l_1} and c_{l_2} and transverse wave speeds c_t, c_{t_1} and c_{t_2} respectively. A pictorial representation of the cross-section of the setup together with the axis configuration is shown in Figure 3.1. Consistent with the physical interpretation of the classical definition of Auld [51] for a free plate, refer to those modes of non-zero energy flux as propagating modes; the investigation presented in this chapter will focus on propagating modes of positive phase velocities.

Energy radiation into the adjacent half-spaces is expressed mathematically in terms of a common complex wavenumber of propagation, denoted by k_x, with again its real part revealing information about the velocity of propagation and its imaginary part corresponding to the attenuation of propagated waves. Because the spaces on either side of the elastic waveguide are now made of elastic materials, unlike the fluid spaces considered in Chapter 2, the exterior spaces can now support waves of both compressional and shear

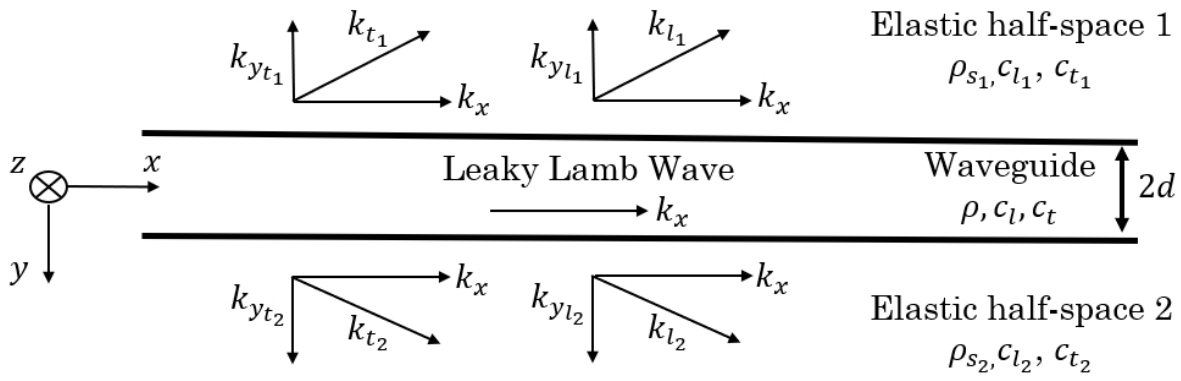

Figure 3.1: Schematic of an elastic waveguide between two elastic half-spaces of thickness $2d$ and infinite extent in the x and z directions. The densities of the elastic media of the setup are ρ, ρ_1 and ρ_2, their longitudinal wave speeds are c_l, c_{l_1} and c_{l_2} and their transverse wave speeds are c_t, c_{t_1} and c_{t_2} respectively.

waves. Thus, in each of the solid half-spaces, the radiated waves are regarded as the superposition of two partial waves, one longitudinal and one shear, whose complex wavenumbers along the y direction are $k_{y_{l_n}}$ and $k_{y_{t_n}}$ respectively, with $n = 1, 2$ for each of the two elastic half-spaces. For a given angular frequency, ω, the wave vectors of each of the partial waves depicted in Figure 3.1 are denoted with

$$\boldsymbol{k}_{l_n} := \begin{pmatrix} k_x \\ k_{y_{l_n}} \end{pmatrix} \text{ and } \boldsymbol{k}_{t_n} := \begin{pmatrix} k_x \\ k_{y_{t_n}} \end{pmatrix}, \tag{3.1}$$

and have real-valued magnitudes

$$|\boldsymbol{k}_{l_n}| = k_{l_n} = \frac{\omega}{c_{l_n}}, \tag{3.2}$$

$$|\boldsymbol{k}_{t_n}| = k_{t_n} = \frac{\omega}{c_{t_n}}. \tag{3.3}$$

Under this notation the following identities hold [78]:

$$\begin{aligned} k_{l_n}^2 &= k_{y_{l_n}}^2 + k_x^2, \\ k_{t_n}^2 &= k_{y_{t_n}}^2 + k_x^2. \end{aligned} \tag{3.4}$$

The leaky Lamb waves of interest are assumed to be propagating along the elastic waveguide and radiating energy into the adjacent elastic media while also causing material displacement in only the x and y directions. To represent displacement fields, denote by $\bar{\boldsymbol{u}}_w$ the displacement vector in the waveguide and by $\bar{\boldsymbol{u}}_1$ and $\bar{\boldsymbol{u}}_2$ the vectors of displacements in the two elastic half-spaces. Those are explicitly written as

$$\bar{\boldsymbol{u}}_w = \begin{pmatrix} \bar{u}_x \\ \bar{u}_y \\ 0 \end{pmatrix} \text{ and } \bar{\boldsymbol{u}}_{\boldsymbol{n}} = \begin{pmatrix} \bar{u}_{x_n} \\ \bar{u}_{y_n} \\ 0 \end{pmatrix}, \tag{3.5}$$

whereby $\bar{u}_x, \bar{u}_{x_n}$ and $\bar{u}_y, \bar{u}_{y_n}$ are the respective displacements along the direction of propagation and the transverse direction, in the waveguide and the two media. It will be convenient to decompose the displacement fields in the two elastic half-spaces through a Helmholtz decomposition [82], expressing the two displacement vectors, $\bar{\boldsymbol{u}}_1$ and $\bar{\boldsymbol{u}}_2$, as

$$\bar{\boldsymbol{u}}_n = \begin{pmatrix} \bar{u}_{x_n} \\ \bar{u}_{y_n} \\ 0 \end{pmatrix} = \boldsymbol{\nabla}\bar{\phi}_n + \boldsymbol{\nabla} \times \begin{pmatrix} 0 \\ 0 \\ \bar{\Psi}_n \end{pmatrix}, \tag{3.6}$$

where $\boldsymbol{\nabla} = (\partial/\partial x, \partial/\partial y, \partial/\partial z)$ is the three dimensional gradient operator, $\bar{\phi}_n$ are the longitudinal wave potentials in the spaces while $\bar{\Psi}_n$ designates the $z-$component of their transverse vector wave potentials, which is henceforth referred to as their transverse wave potentials.

Assuming time and space harmonic waves, the exponential factor $\exp\left[i(k_x x - \omega t)\right]$, in terms of the wavenumber k_x and frequency ω, describes the spatial and temporal dependence of waves of the system and is common in all displacement and stress fields. The common exponential term will henceforth be assumed and omitted for brevity; the notation $\bar{\cdot}$ is dropped throughout.

By expanding Eq. (3.6) and differentiating with respect to x, the $y-$dependent components of the x and y displacements in the two half-spaces are explicitly given by

$$u_{x_n} = ik_x\phi_n + \frac{\partial \Psi_n}{\partial y}, \tag{3.7}$$

$$u_{y_n} = \frac{\partial \phi_n}{\partial y} - ik_x\Psi_n. \tag{3.8}$$

Taking λ and μ the Lamé parameters of the linear elastic material of the waveguide and $\boldsymbol{u}_w = (u_x, u_y)$ the vector of $y-$dependent displacements in the waveguide, the normal and shear stresses and governing equations of motion in the waveguide are identical to those of the immersed waveguide of the previous chapter, given in Eqs. (1.16)-(1.18) and (1.19),(1.20).

Stresses and governing equations in the two elastic media of the exterior can be similarly derived. Following the discussion presented in Section 1.2, the normal and shear stresses in the two elastic media are given by

$$\sigma_{y_n} = (\lambda_n + 2\mu_n)\frac{\partial u_{y_n}}{\partial y} + \lambda i k_x u_{x_n}, \tag{3.9}$$

$$\sigma_{xy_n} = \mu_n\left(ik_x u_{y_n} + \frac{\partial u_{x_n}}{\partial y}\right), \tag{3.10}$$

while the governing momentum equations are

$$\rho_n\omega^2 u_{x_n} - (\lambda_n + 2\mu_n)k_x^2 u_{x_n} + (\lambda_n + \mu_n)ik_x\frac{\partial u_{y_n}}{\partial y} + \mu_n\frac{\partial^2 u_{x_n}}{\partial y^2} = 0, \tag{3.11}$$

$$\rho_n\omega^2 u_{y_n} - \mu_n k_x^2 u_{y_n} + (\lambda_n + \mu_n)ik_x\frac{\partial u_{x_n}}{\partial y} + (\lambda_n + 2\mu_n)\frac{\partial^2 u_{y_n}}{\partial y^2} = 0. \tag{3.12}$$

In the above, λ_n and μ_n are the Lamé parameters of the elastic materials making up the two exterior half-spaces. Substituting Eqs. (3.7) and (3.8) into Eqs. (3.9)-(3.12) allows the stresses in the two spaces to be expressed in terms of the scalar potentials ϕ_n and Ψ_n as

$$\sigma_{y_n} = -\lambda_n k_x^2\phi_n + (\lambda_n + 2\mu_n)\frac{\partial^2\phi_n}{\partial y^2} + 2\mu_n ik_x\frac{\partial\Psi_n}{\partial y}, \tag{3.13}$$

$$\sigma_{xy_n} = \mu_n\left(2ik_x\frac{\partial\phi_n}{\partial y} - k_x^2\Psi_n - \frac{\partial^2\Psi_n}{\partial y^2}\right), \tag{3.14}$$

and the governing equations of motion to decouple into

$$\rho_n\omega^2\phi_n - k_x^2(\lambda_n + 2\mu_n)\phi_n + (\lambda_n + 2\mu_n)\frac{\partial^2\phi_n}{\partial y^2} = 0, \tag{3.15}$$

$$\rho_n\omega^2\Psi_n - k_x^2\mu_n\Psi_n + \mu_n\frac{\partial^2\Psi_n}{\partial y^2} = 0. \tag{3.16}$$

The physics of the problem require the continuity of tractions and displacements at the two interfaces [82]. That is to say,

$$\begin{aligned} &\sigma_y - \sigma_{y_n} = \sigma_{xy} - \sigma_{xy_n} = 0, \text{ at } y = \pm d, \\ &u_x - u_{x_n} = u_y - u_{y_n} = 0, \text{ at } y = \pm d. \end{aligned} \tag{3.17}$$

Substituting stresses and displacements into Eq. (3.17), the continuity of normal and shear stresses at the two interfaces is explicitly given in terms of wave potentials in the elastic half-spaces as

$$\left[(\lambda+2\mu)\frac{\partial u_y}{\partial y}+\lambda i k_x u_x+\lambda_n k_x^2\phi_n-(\lambda_n+2\mu_n)\frac{\partial^2\phi_n}{\partial y^2}\right.$$
$$\left.-2\mu_n i k_x\frac{\partial \Psi_n}{\partial y}\right]\Big|_{y=\pm d}=0, \tag{3.18}$$

$$\left[\mu\left(ik_x u_y+\frac{\partial u_x}{\partial y}\right)-\mu_n\left(2ik_x\frac{\partial\phi_n}{\partial y}-k_x^2\Psi_n-\frac{\partial^2\Psi_n}{\partial y^2}\right)\right]\Big|_{y=\pm d}=0, \tag{3.19}$$

and the continuity of displacements along the directions parallel and normal to the waveguide is given by

$$\left[u_x-ik_x\phi_n+\frac{\partial\Psi_n}{\partial y}\right]\Big|_{y=\pm d}=0, \tag{3.20}$$

$$\left[u_y-\frac{\partial\phi_n}{\partial y}-ik_x\Psi_n\right]\Big|_{y=\pm d}=0. \tag{3.21}$$

Finally, the equations of motion in the exterior domains admit wave potential solutions of the form [78]

$$\phi_1=A_{\phi_1}\exp[ik_{y_{l_1}}(y-d)], \tag{3.22}$$

$$\Psi_1=A_{\Psi_1}\exp[ik_{y_{t_1}}(y-d)], \tag{3.23}$$

$$\phi_2=A_{\phi_2}\exp[-ik_{y_{l_1}}(y+d)], \tag{3.24}$$

$$\Psi_2=A_{\Psi_2}\exp[-ik_{y_{l_1}}(y+d)], \tag{3.25}$$

with the $A_{\phi_1}, A_{\Psi_1}, A_{\phi_2}, A_{\Psi_2}$ unknown wave potential amplitudes determined by the interface conditions Eqs. (3.18)-(3.21).

3.3 Method

3.3.1 Discretisation

The numerical issues associated with the exponential growth of leaky wave solutions for the simpler case of fluid exteriors have already been discussed and a method was introduced to counter the numerical instabilities inherent to the growth in Chapter 2; leakage into adjacent solid media is a step-change in complexity due to the existence now of both longitudinal and shear waves in the exterior spaces that, for leaky waves, may both exponentially grow simultaneously. In this section a solution scheme is proposed that allows the methods presented in Section 2.3 to handle leakage into solids.

Wave solutions of the setup described in the previous section are generally split into two types – non-leaky (also known as trapped [48,85,95]) and leaky modes. Here, the waveguide is in contact with solids; hence the media surrounding the waveguide support shearing as well as compressive motion. For that reason, in addition to the non-leaky evanescent, wave solutions, leaky mode solutions can further be split in two cases – those that have purely shear (shear-leaky) or shear and compressive (fully-leaky) polarisations. For these cases, the exponential growth of the amplitude of leaky waves is attributed to the exponential growth of some or all of the partial waves depicted in Figure 3.1. In particular, when shear-leaky waves are to be considered in an elastic half-space, the shear partial wave and corresponding transverse wave potential of that space, Ψ_n, exponentially grow in amplitude, while the longitudinal partial wave and corresponding wave potential, ϕ_n, are evanescent. In the fully-leaky case, both partial waves and their wave potentials in the solid exhibit exponential growth.

Consider again the structure of Figure 3.1, and assume without loss of generality $c_{l_1} \geq c_{l_2} > c_{t_1} \geq c_{t_2}$. The classical model of sound radiation from

vibrating surfaces suggests that in the region where the phase velocity of the propagating wave, c_{ph} is less than c_{t_2}, evanescent waves in both solids are expected, while when it is between c_{t_1} and c_{t_2}, shear-leaky waves in the bottom solid and evanescent at the top are expected. When c_{ph} is between c_{l_2} and c_{t_1}, shear-leaky waves in both spaces are expected, while when it is between c_{l_1} and c_{l_2}, the leaky waves of the bottom solid are now expected to be fully-leaky. Finally, when c_{ph} is greater than c_{l_1}, fully-leaky waves are expected to be radiating in both elastic half-spaces. An analogous analysis can be deduced for other combinations of longitudinal and shear bulk wave speeds. An illustration of this is shown in Figure 3.2. It should be noted that some exceptions of this rule, namely of subsonic radiation, have been recorded in the literature [43, 85, 96, 97]. Such examples are still obtainable by the method to be presented, however they are not considered here.

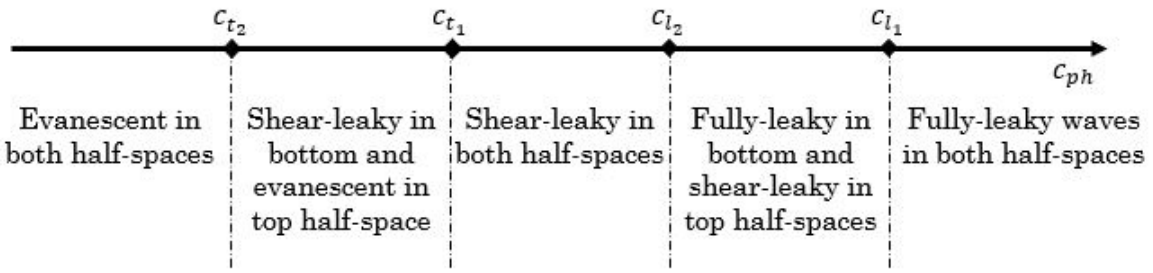

Figure 3.2: Illustration of the different radiation cases with an increase in phase velocity for the example case of $c_{l_1} \geq c_{l_2} > c_{t_1} \geq c_{t_2}$.

As shown in Figure 3.2, with elastic half-spaces adjacent to a waveguide and all media having both shear and longitudinal wave speeds, an exponential growth of the solution is prominent in most but not all cases, and a discretisation catering to this growth is necessary. Here, each of the cases described above are solved separately, every time considering whether the partial waves of the solution exponentially grows in one or both elastic spaces. When this

is the case, a discretisation analogous to the one described in Section 2.3 is judiciously implemented for each of Eqs. (3.15) and (3.16), provided that the corresponding wave potential exponentially grows, allowing for a numerically decaying problem to always be solved instead. It is important to comment that this separation into several solutions does not indicate a necessity to know the nature of the guided modes *a priori*; all that is done here is composing the full solution from the several contributions of solutions for these cases. The nature of the unknown guided wave modes then determines when they emerge as solutions as the calculations of the different cases are carried forward.

The discretisation of the closed waveguide domain and the two open elastic half-spaces is presented next. Both the waveguide and the open spaces of the elastic solids are again discretised via spectral collocation and specifically Chebyshev differentiation matrices resulting from Chebyshev polynomials and the N Gauss-Lobatto Chebyshev collocation points of Eq. (1.28). Start by utilising the differentiation matrix suite of Weideman and Reddy [58], and produce the N collocation points of Eq. (1.28) defined over the bounded interval $[-1, 1]$, and the corresponding first and second order differentiation matrices, $D^{(1)}$ and $D^{(2)}$, based on Chebyshev polynomials.

A discretisation of the domains of definition of the displacements and wave potentials of the problem and corresponding differentiation matrices in those domains is desired. Said domains are the waveguide domain $[-d, d]$ for the displacements u_x and u_y, and the elastic half-spaces at $[-\infty, -d]$ and $[d, \infty]$ for the potentials ϕ_1 and Ψ_1 and ϕ_2 and Ψ_2 respectively. To achieve the desired discretisation and corresponding differentiation matrices, mappings that relate the collocation points $\{s_j\}_{j=1}^{N}$ of $[-1, 1]$ to collocation points within those domains are employed; the corresponding differentiation matrices are then the result of the application of the chain rule.

The waveguide domain is treated first. A linear map, that is, a multiplication by d, maps the collocation points from $[-1, 1]$ to $[-d, d]$. The map that yields the discretisation of the waveguide domain here was originally introduced in Eq. (2.16) alongside the resulting differentiation matrices in the closed domain of the waveguide in Eq. (2.17).

To discretise the domains of definition of the wave potentials inside the two elastic half-spaces, the rational maps

$$h_{\phi_1} : s \longrightarrow y = -d - \zeta_{\phi_1} \frac{1 - s}{1 + s}, \tag{3.26}$$

$$h_{\Psi_1} : s \longrightarrow y = -d - \zeta_{\Psi_1} \frac{1 - s}{1 + s}, \tag{3.27}$$

with $\zeta_{\phi_1}, \zeta_{\Psi_1} \in \mathbb{R}^+$, map the collocation points from $[-1, 1]$ to points in $[-\infty, -d]$, while the rational maps

$$h_{\phi_2} : s \longrightarrow y = d + \zeta_{\phi_2} \frac{1 + s}{1 - s}, \tag{3.28}$$

$$h_{\Psi_2} : s \longrightarrow y = d + \zeta_{\Psi_2} \frac{1 + s}{1 - s}, \tag{3.29}$$

with $\zeta_{\phi_2}, \zeta_{\Psi_2} \in \mathbb{R}^+$, map the collocation points from $[-1, 1]$ to points in $[d, \infty]$.

By applying the chain rule for first and second order derivatives, the resulting differentiation matrices for functions defined over the two open spaces of the elastic media are explicitly given in terms of $D^{(1)}$ and $D^{(2)}$ as

$$D_{X_1}^{(1)} = \text{diag}\left(\frac{2\boldsymbol{\zeta}_{X_1}}{[\boldsymbol{\zeta}_{X_1} - (\boldsymbol{y}_{X_1} + \boldsymbol{d})]^2}\right) D^{(1)}, \tag{3.30}$$

$$\begin{aligned} D_{X_1}^{(2)} =& \text{diag}\left(\frac{4\boldsymbol{\zeta}_{X_1}}{[\boldsymbol{\zeta}_{X_1} - (\boldsymbol{y}_{X_1} + \boldsymbol{d})]^3}\right) D^{(1)} \\ &+ \text{diag}\left(\frac{4\boldsymbol{\zeta}_{X_1}^2}{[\boldsymbol{\zeta}_{X_1} - (\boldsymbol{y}_{X_1} + \boldsymbol{d})]^4}\right) D^{(2)}. \end{aligned} \tag{3.31}$$

for $[-\infty, d]$ and as

$$D_{X_2}^{(1)} = \text{diag}\left(\frac{2\boldsymbol{\zeta}_{X_2}}{[\boldsymbol{\zeta}_{X_2} + (\boldsymbol{y}_{X_2} - \boldsymbol{d})]^2}\right) D^{(1)}, \tag{3.32}$$

$$\begin{aligned} D_{X_2}^{(2)} =& \text{diag}\left(\frac{-4\boldsymbol{\zeta}_{X_2}}{[\boldsymbol{\zeta}_{X_2} + (\boldsymbol{y}_{X_2} - \boldsymbol{d})]^3}\right) D^{(1)} \\ &+ \text{diag}\left(\frac{4\boldsymbol{\zeta}_{X_2}^2}{[\boldsymbol{\zeta}_{X_2} + (\boldsymbol{y}_{X_2} - \boldsymbol{d})]^4}\right) D^{(2)}, \end{aligned} \tag{3.33}$$

for $[d, \infty]$. In the above, $X = \phi$ or Ψ, $\boldsymbol{\zeta}_{X_n} = [\zeta_{X_n}, \ldots, \zeta_{X_n}]^T$ and $\boldsymbol{d} = [d, \ldots, d]^T$ are constant vectors of N entries, and $\boldsymbol{y}_{X_n} = \left\{ y_{X_n}^j = h_{X_n}(s_j) \right\}_{j=1}^{N}$ is the vector of collocation points in the open spaces, resulting from each of the mappings of Eqs. (3.26)-(3.29).

These maps and resulting differentiation matrices, give a suitable discretisation of both elastic half-spaces, provided that the solution one is after is that of non-leaky waves where all four partial waves are evanescent in the two spaces, i.e. all wave potentials in the exterior domains exponentially decay. However, as was discussed earlier, special care and a modification of the maps of Eqs. (3.26)-(3.29), needs to be carried out when solving for the cases of Figure 3.2, where some or all of the partial waves and corresponding wave potentials exponentially grow. When a wave potential is exponentially growing, say X_n, a complex rational map is to be used instead by allowing

ζ_{X_n} in the map h_{X_n}, i.e. the map that corresponds to X_n, to take complex values. As a result, collocation points from $[-1, 1]$ are assigned to a path in the complex plane and, as discussed in the previous chapter, a careful choice of the map enables the exponentially growing potential to be turned into a numerically decaying function without any compromises to the underlying physics.

For clarity, the process of modifying maps and discretising the domains is demonstrated with an example. Suppose that one is interested in waves that radiate as shear-leaky waves in one of the half-spaces, say the bottom one, and are evanescent in the other. In this case, only the transverse wave potential within the lower solid, Ψ_2, demonstrates exponential growth. As such, attention is directed towards modifying the mapping associated with this specific potential, given in Eq. (3.29). Allowing ζ_{Ψ_2} to take on complex values results in the discretisation of a complex path, say $\mathbb{C}_{\Psi_2}$, similarly to those defined in the previous chapter, with one of the collocation points located on the interface at $y = d$.

The discussion presented in Section 2.3 holds true here: when considered over the complex interval $\mathbb{C}_{\Psi_2}$, the equation of motion for the transverse wave potential in the bottom fluid, Eq. (3.16), admits a solution of the form

$$\tilde{\Psi}(y_{\Psi_2}) = A_{\Psi_2} \exp[ik_{y_{t_2}}(y_{\Psi_2} - d)], \tag{3.34}$$

with $y_{\Psi_2} \in \mathbb{C}_{\Psi_2}$, given by $y_{\Psi_2} = \zeta_{\Psi_2}(y - d) + d$ for $y \in [d, \infty]$, and A_{Ψ_2} the amplitude of the original, exponentially growing, wave potential of Eq. (3.25). Additionally, for the outgoing partial waves corresponding to the exponentially growing transverse wave potential Ψ_2, the wavenumber $k_{y_{t_2}}$ must have $\Re(k_{y_{t_2}}) > 0$ and $\Im(k_{y_{t_2}}) < 0$, and the choice of ζ_{Ψ_2} allows control over the

exponent of Eq. (3.34). Choosing ζ_{Ψ_2} such that

$$\Re(k_{y_n})\Im(\zeta_{f_n}) + \Re(\zeta_{f_n})\Im(k_{y_n}) > 0, \tag{3.35}$$

makes the exponential term, and $\tilde{\Psi}_2$ numerically decay. This newly constructed, numerically decaying, function is the analytical continuation of the transverse potential Ψ_2 over the complex path defined by Eq. (3.29), and just like Ψ_2, it is fully determined by its value at the interface.

Thus, to summarise, due to the choice of mapping, which maintains one collocation point at the physical interface of the waveguide and the bottom solid, Ψ_2 and $\tilde{\Psi}_2$ attain the same value at that interface, A_{Ψ_2}, while, $\tilde{\Psi}_2$ also numerically decays and satisfies the governing Eq. (3.16) for the same wavenumber k_x. As a result, by discretising a complex path as opposed to the physical half-space of the elastic solid, one is able to solve Eq. (3.16) for the numerically stable and decaying function, $\tilde{\Psi}_2$, and the same complex wavenumber k_x, and then reconstruct the physical, exponentially growing, solution of Ψ_2 from its value at the interface (the amplitude A_{Ψ_2}).

For the rest of the evanescent partial waves and their decaying wave potentials, the rational maps of Eqs. (3.26)-(3.27) can be used. This time, as there is no need to impose further decay to the already decaying potentials of evanescent waves, real valued parameters are used for the maps, and analogous discretisations of the domains are obtained.

Having now discretised the domain, while also ensuring the numerical decay of all functions of interest, the differential operators of the equations of motion in the waveguide and the elastic half-spaces can be discretised with differentiation matrices. The matrix operators of the equations of motion in the waveguide are given by L_p and Eqs. (2.29) and (2.31)-(2.33) of the previous chapter, while those in the two exterior solids are explicitly given

by

$$L_{\phi_n} = -k_x^2(\lambda_n + 2\mu_n)I + \rho_n\omega^2 I + (\lambda_n + 2\mu_n)D^{(2)}_{\phi_n}, \tag{3.36}$$

$$L_{\Psi_n} = -k_x^2\mu_n I + \rho_n\omega^2 I + 2\mu_n D^{(2)}_{\Psi_n}. \tag{3.37}$$

Merging all matrix operators together, the discrete problem may be expressed as an eigenvalue problem

$$\tilde{L}\boldsymbol{u} = \mathbf{0}, \tag{3.38}$$

with $\tilde{L}$ a $6N \times 6N$ diagonal matrix operator and $\boldsymbol{u}$ a column vector of $6N$ entries explicitly given by

$$\tilde{L} = \begin{pmatrix} L_{\phi_1} & 0 & 0 & 0 & 0 \\ 0 & L_{\Psi_1} & 0 & 0 & 0 \\ 0 & 0 & L_p & 0 & 0 \\ 0 & 0 & 0 & L_{\phi_2} & 0 \\ 0 & 0 & 0 & 0 & L_{\Psi_2} \end{pmatrix} \text{ and } \boldsymbol{u} = \begin{pmatrix} \boldsymbol{\phi}_1 \\ \boldsymbol{\Psi}_1 \\ \boldsymbol{u}_x \\ \boldsymbol{u}_y \\ \boldsymbol{\phi}_2 \\ \tilde{\boldsymbol{\Psi}}_2 \end{pmatrix}. \tag{3.39}$$

In the above, $\boldsymbol{u}$ contains the displacement fields in the waveguide and the wave potentials evaluated on the collocation points discretising their respective domains of definition; $\tilde{\boldsymbol{\Psi}}_2$ is the only complex wave potential here and it is evaluated on collocation points located on the complex line $\mathbb{C}_{\Psi_2}$.

To complete the discretisation, interface conditions must be incorporated; a procedure analogous to that of Chapter 2 is followed. The discretised interface conditions are expressed as two $4 \times 6N$ matrices, one for each interface. The matrix of interface conditions for the interface at the top of the waveguide is explicitly given by

$$
\begin{aligned}
IC_{(-d)} = {} & k_x^2 \begin{bmatrix} \lambda_1 I & 0 & 0 & 0 & 0 & 0 \\ 0 & \mu_1 I & 0 & 0 & 0 & 0 \\ 0 & 0 & 0 & 0 & 0 & 0 \\ 0 & 0 & 0 & 0 & 0 & 0 \end{bmatrix} \Bigg\|_{y=-d} \\
& + k_x \begin{bmatrix} 0 & -2i\mu_1 D^{(1)}_{\Psi_1} & i\lambda I & 0 & 0 & 0 \\ -2i\mu_1 D^{(1)}_{\phi_1} & 0 & 0 & i\mu I & 0 & 0 \\ -iI & 0 & 0 & 0 & 0 & 0 \\ 0 & -iI & 0 & 0 & 0 & 0 \end{bmatrix} \Bigg\|_{y=-d} \\
& + \begin{bmatrix} -(\lambda_1 + 2\mu_1) D^{(2)}_{\phi_1} & 0 & 0 & (\lambda + 2\mu) D^{(1)}_{p} & 0 & 0 \\ 0 & \mu_1 D^{(2)}_{\Psi_1} & \mu D^{(1)}_{p} & 0 & 0 & 0 \\ 0 & D^{(1)}_{\Psi_1} & I & 0 & 0 & 0 \\ -D^{(1)}_{\phi_1} & 0 & 0 & I & 0 & 0 \end{bmatrix} \Bigg\|_{y=-d} .
\end{aligned}
\tag{3.40}
$$

Similarly the matrix of interface conditions at the bottom interface reads

$$
\begin{aligned}
IC_{(d)} = {} & k_x^2 \begin{bmatrix} 0 & 0 & 0 & 0 & \lambda_2 I & 0 \\ 0 & 0 & 0 & 0 & 0 & \mu_2 I \\ 0 & 0 & 0 & 0 & 0 & 0 \\ 0 & 0 & 0 & 0 & 0 & 0 \end{bmatrix} \Bigg\|_{y=d} \\
& + k_x \begin{bmatrix} 0 & 0 & i\lambda I & 0 & 0 & -2i\mu_2 D^{(1)}_{\Psi_2} \\ 0 & 0 & 0 & i\mu I & -2i\mu_2 D^{(1)}_{\phi_2} & 0 \\ 0 & 0 & 0 & 0 & -iI & 0 \\ 0 & 0 & 0 & 0 & 0 & -iI \end{bmatrix} \Bigg\|_{y=d} \\
& + \begin{bmatrix} 0 & 0 & 0 & (\lambda + 2\mu) D^{(1)}_{p} & -(\lambda_2 + 2\mu_2) D^{(2)}_{\phi_2} & 0 \\ 0 & 0 & \mu D^{(1)}_{p} & 0 & 0 & \mu_2 D^{(2)}_{\Psi_2} \\ 0 & 0 & I & 0 & 0 & D^{(1)}_{\Psi_2} \\ 0 & 0 & 0 & I & -D^{(1)}_{\phi_2} & 0 \end{bmatrix} \Bigg\|_{y=d} .
\end{aligned}
\tag{3.41}
$$

For interface conditions to be incorporated into the discretised problem, appropriate rows of the matrix operator $\tilde{L}$ are to be replaced with rows of the

interface conditions matrices of Eqs. (3.40) and (3.41) and Dirichlet zero boundary conditions at the collocation point at infinity. Specifically rows N, $2N$, $2N+1, 3N+1$ correspond to collocation points at the top interface and are replaced with rows from the interface condition matrix $IC_{(-d)}$, while $3N, 4N, 4N+1, 5N+1$ correspond to collocation points at the bottom interface and are replaced with rows from the interface condition matrix $IC_{(d)}$. Dirichlet zero boundary conditions are imposed at the collocation points at infinity, i.e. rows $1, N+1, 5N$ and $6N$. An illustration of this procedure is shown in Figure 3.3

Finally, separating the resulting operator into its k_x^2, k_x and constant term constituents results in a polynomial eigenvalue problem of the form

$$(k_x^2 L_2 + k_x L_1 + L_0)\boldsymbol{u} = 0, \tag{3.42}$$

which is solved with the companion matrix linearisation of Eqs. (2.44) and (2.45) and conventional eigenvalue problem solvers.

Due to the choice of complex transformation, the polynomial eigenvalue problem of Eq. (3.42) only admits pairs of positive and negative phase velocity outgoing wave solutions while, for completeness, the corresponding incoming wave solutions are also attainable via the same method with a choice of the conjugate complex parameters.

The other cases of Figure 3.2 are treated in the same manner: pick a case from Figure 3.2 to solve; consider which partial waves exponentially grow in that particular case; discretise complex paths that accommodate for the exponential growth of the partial waves that grow in the case under consideration; discretise the equations of motion and incorporate interface conditions; solve the resulting polynomial eigenvalue problem with a companion matrix linearisation.

<table>
<tr><td colspan="6">Dirichlet Zero Boundary Condition</td></tr>
<tr><td>Rows 2 to N-1 of L_{φ_1}</td><td>0</td><td>0</td><td>0</td><td>0</td><td>0</td></tr>
<tr><td colspan="6">Row 1 of $IC_{(-d)}$</td></tr>
<tr><td colspan="6">Dirichlet Zero Boundary Condition</td></tr>
<tr><td>0</td><td>Rows 2 to N-1 of L_{Ψ_1}</td><td>0</td><td>0</td><td>0</td><td>0</td></tr>
<tr><td colspan="6">Row 2 of $IC_{(-d)}$</td></tr>
<tr><td colspan="6">Row 3 of $IC_{(-d)}$</td></tr>
<tr><td>0</td><td>0</td><td colspan="2">Rows 2 to N-1 of L_p</td><td>0</td><td>0</td></tr>
<tr><td></td><td colspan="3">Row 1 of $IC_{(d)}$</td><td></td><td></td></tr>
<tr><td></td><td colspan="3">Row 4 of $IC_{(-d)}$</td><td></td><td></td></tr>
<tr><td>0</td><td>0</td><td colspan="2">Rows N+1 to 2N-1 of L_p</td><td>0</td><td>0</td></tr>
<tr><td></td><td colspan="3">Row 2 of $IC_{(d)}$</td><td></td><td></td></tr>
<tr><td></td><td colspan="3">Row 3 of $IC_{(d)}$</td><td></td><td></td></tr>
<tr><td>0</td><td>0</td><td>0</td><td>0</td><td>Rows 2 to N-1 of L_{φ_2}</td><td>0</td></tr>
<tr><td colspan="6">Dirichlet Zero Boundary Condition</td></tr>
<tr><td colspan="6">Row 4 of $IC_{(d)}$</td></tr>
<tr><td>0</td><td>0</td><td>0</td><td>0</td><td>0</td><td>Rows 2 to N-1 of L_{Ψ_2}</td></tr>
<tr><td colspan="6">Dirichlet Zero Boundary Condition</td></tr>
</table>

Figure 3.3: Illustration of imposing interface conditions by replacing rows N, $2N$, $2N+1, 3N+1$ with rows from $IC_{(-d)}$, rows $3N, 4N, 4N+1, 5N+1$ with rows from $IC_{(d)}$, and rows $1, N+1, 5N, 6N$ with Dirichlet zero boundary conditions.

3.3.2 Finite Element Modelling

The problem of leaky waves in the waveguide of finite thickness adjacent to two elastic half-spaces shown schematically in Figure 3.1, is one that DISPERSE cannot satisfactorily solve (dispersion curves are often incomplete). For that reason, as an additional verification tool, FE modelling was employed to model wave propagation in such embedded structures, with the FE model serving as a spot-checking tool, specifically applied at selected locations along the predicted dispersion curves. Details of the FE model used for further validation of SCM results are presented in this section.

The FE tool of choice was the GPU-based FE solver POGO [59], that discretises the equation of motion from elasticity theory in space and time. Discretisation in time is achieved by the finite-difference method [61] and in this way displacement values at a given time step are retrieved as a function of displacement values at the two time steps preceding it. The FE modelling approach described here follows the FE models applied in other elastic wave propagation studies [62–64, 98].

For the FE modelling of leaky wave propagation in a waveguide coupled to two elastic half-spaces, a rectangular domain was used – a schematic of the cross-sectional area of the domain is shown in Figure 3.4. Each element of the domain is assigned with the material properties of the space it is a part of (Young's modulus, density, Poisson's ratio), while linear, square elements of four nodes each were used. To ensure sufficient convergence of the solution [99], for a given frequency, the mesh element size was set to approximately $dx = \lambda_f/30$. Here, λ_f is the smallest wavelength of bulk waves possible amongst the three materials, calculated at the frequency of the simulation, f. Stiffness-reducing absorbing layers [45] were defined around the domain to accommodate for its unbounded nature, with thickness equal to four times the longest bulk wavelength. In the absorbing layers region, damping pro-

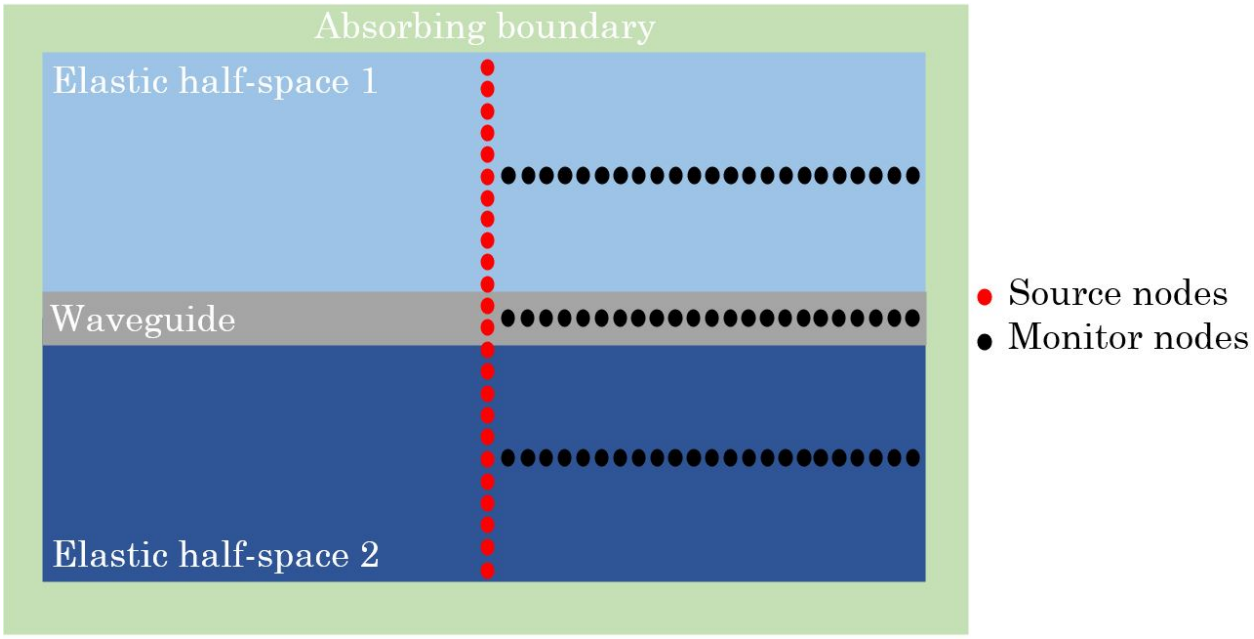

Figure 3.4: A schematic of a FE domain used to model elastic wave propagation and retrieve the dispersion curves of guided modes in a waveguide adjacent to two elastic half-spaces. In the figure, source nodes are shown in red and monitor nodes in black. Absorbing layers around the domain are shown in green while different colours denote the different materials within the domain.

portional to the stiffness is gradually introduced into the system throughout the thickness of the region, resulting in the attenuation of outgoing waves and minimal reflections.

A source line, comprised of multiple source nodes, was defined in the middle of the domain – a predefined displacement of the source nodes acts as the initial boundary condition of the FE model and excites propagating waves. Source nodes were displaced in the x and y directions, in accordance to two Hann-windowed tonebursts; an example of such a toneburst is depicted in Figure 1.2.

In this study, the excitation of multiple modes at once, validating the existence of multiple of the modes predicted by the SCM simultaneously, as well as the excitation of a single mode, enabling the selective validation of modes and their mode shapes, were both desired. Depending on the nature of the desired excitation, multi-modal or single-mode excitation, the amplitude and relative phase of the tonebursts at each source node were determined. For a multi-modal excitation, all source nodes were excited in phase with the same broadband (single-cycled) toneburst in both directions. For single-mode excitation, the method discussed in [65] was followed; first, the eigenvectors of Eq. 3.38 were computed and the partial wave potential amplitudes of a mode of interest were recorded. The displacement fields of the desired mode, (its mode shapes), were then computed through Eqs. (3.7) and (3.8) as a function of perpendicular distance, y. To preferentially excite a desired mode, the FFT of x and y excitation signals imposed at the source node located a distance y from the centreline of the waveguide were modulated in accordance to the amplitudes and phases of the predicted u_x and u_y mode shapes at that same distance y. Signals were modulated based on the "centre mode shapes" excitation technique [65] by appropriately multiplying the FFT of the signals with the predicted mode shape value as in Eq. (1.41); see Section 1.4.2 for

more details.

It is worth noting that the "centre mode shapes" technique which excites the desired mode at the central frequency is used in this thesis despite it, as discussed in Section 1.4.2, also resulting in non-pure excitations. That is because in this thesis only results at a chosen frequency in the frequency domain will be looked at, meaning that the excitation only needs to be correct at that one frequency; a pure-mode excitation [100] was therefore not pursued further. For an analysis of the modal basis of such systems and the orthogonality of eigenfunctions for pure-mode excitations, see [72, 85, 100–102] and references therein.

A monitor line, comprised of multiple monitor nodes, was placed horizontally, to the right of the source line, along the length of the domain, as shown in Figure 3.4 – a monitor node is a node whose displacement profile is recorded and stored for post-processing. The placement of the monitor line is dependent on the nature of the desired mode to be observed. Leaky modes attenuate as they propagate along the waveguide, with most of their energy observable in the exterior solids, requiring a monitor line that is placed close to the source line and in the exterior elastic solids. Contrary to that, non-leaky modes remain trapped in the waveguide and can propagate longer distances; thus a monitor line in the middle of the waveguide is more suitable for their observation. In post-processing, a two-dimensional fast Fourier transform (2D-FFT) [103], that is a FFT of signals in both space and time, is applied to the collection of the stored monitor signals of interest. The results of the 2D-FFT were then normalised to the maximum amplitude of all the modes recorded to obtain the dispersion curves of the excited modes in a normalised amplitude scale.

A typical model size is of the order of 1×10^7 degrees of freedom. The models were solved using an Nvidia (Santa Clara, California) 2080 Ti graphics card

with 8GB of memory. The solution time was approximately forty seconds. More details about the excitation, the size of the domain and the material properties will be given in the following section as they are specific to the example presented there.

3.4 Results & Discussion

In this section the SCM described for leaky waves radiating in elastic media is utilised to retrieve the dispersion and attenuation curves of leaky and non-leaky modes in an elastic waveguide in contact with two elastic half-spaces. The obtained dispersion and attenuation plots are then verified against the commercially-available software DISPERSE while the dispersion curves are also validated against FE simulations of elastic wave propagation using POGO.

Without loss of generality, the method is illustrated on the example case of adhesive joints of two aluminium alloys, studied in [104] to demonstrate ways of determining the material properties and thickness of the adhesive layer and assess the quality of the joint – an example inspired by real NDE applications. An epoxy adhesive is modelled as a waveguide of finite half-thickness d = 0.5 mm, density ρ_{ep} = 1.17 g/cm^3, longitudinal wave speed $c_{l_{\text{ep}}}$ = 2.61 m/ms and transverse wave speed $c_{t_{\text{ep}}}$ = 1.1 m/ms. The spaces of the aluminium components are modelled as linear elastic half-spaces of isotropic media, both with density ρ_{al} = 2.82 g/cm^3, longitudinal wave speed $c_{l_{\text{al}}}$ = 6.33 m/ms and transverse wave speed $c_{t_{\text{al}}}$ = 3.12 m/ms.

For the retrieval of the solution, the phase velocity domain was split up in three regions in accordance with Figure 3.2 and the wave speeds of the adjacent aluminium half-spaces. For each region, an angular frequency sweep of 150 frequency steps, up to ω = 30 MHz, was performed, with the com-

plex parameter pairs $(\zeta_{\phi_n}, \zeta_{\Psi_n})$ being chosen to accommodate the radiation characteristics of the solutions to be found within that particular region and remaining constant for all frequencies of the sweep.

In line with the example of shear-leaky waves discussed in the previous section, the pairs are appropriately chosen for each region to distribute the collocation points across real and complex paths and ensure the numerical decay of all the wave potentials to be found. For the retrieval of non-leaky solutions, $\left(\zeta_{\phi_n}, \zeta_{\Psi_n}\right) = (10, 10)$ was chosen, while $\left(\zeta_{\phi_n}, \zeta_{\Psi_n}\right) = (10, 10i)$ were chosen for shear-leaky and $\left(\zeta_{\phi_n}, \zeta_{\Psi_n}\right) = (10i, 10i)$ for fully-leaky ones. In each domain, 50 collocation points were used. The results of the SCM were found to be stable to the choices of complex parameters and number of collocation points.

Subsequently, the numerical solutions obtained underwent a comprehensive filtering process; only modes of finite attenuation and positive phase velocity were kept. In terms of the wavenumber, k_x, that is achieved by requiring $\Re(k_x) > 0$, which ensures a mode of non-negative and finite phase velocity, and $|k_x| < \infty$, which results in non-zero phase velocity and finite attenuation modes. Highly attenuating modes were further filtered out by requiring a non-negative attenuation of less than 15 Np/mm. Lastly, spurious, non-converged and bulk wave solutions were discarded by requiring that the mode complies with interface conditions of Eqs. (3.18)-(3.21) (up to 3 decimal places), under the assumption that the wave potentials of the outgoing waves in the two elastic half-spaces assume the general forms of Eqs. (3.22)-(3.25), subject to the choice of positive or negative square root for $k_{y_{l_n}}$ and $k_{y_{t_n}}$, for which the complex wave potentials, $\tilde{\phi}_n$ and $\tilde{\Psi}_n$, correspond to the solution found by the SCM. The computation took a total of approximately 18 minutes on a personal computer with 32GB RAM and an Intel i7-10700 CPU.

A comparison of the SCM results with those from a FE simulation of a

multi-modal excitation of the adhesive joint domain was possible from the excitation of all source nodes in phase and with the same broadband toneburst in both the x and y directions. The excitation toneburst used at each source node was the sum of sixteen single-cycled Hann-windowed tonebursts, each with a central frequency varying from $0.25 - 4$ MHz at 0.25 MHz increments. In this case, wavelengths and element size, dx, were calculated at 4 MHz. Employing a toneburst excitation composed of the cumulative energy from 16 distinct broadband tonebursts is equivalent to exciting each of these 16 tonebursts independently and subsequently combining their excited fields. This ensures that at each frequency increment, modes are excited with more intensity than they would have been excited with, say, a single-cycled toneburst centred at the middle of the frequency range of interest, thereby promoting stronger mode excitation throughout the desired frequency range. The domain, excluding absorbing layers, was 11 mm thick, 1 mm of epoxy in the middle of the domain and 5 mm of aluminium each side of the waveguide, and 100 mm in length. The monitor line used for post-processing was placed at $y = 2$ mm. Normalised results of the described FE model are shown in Figure 3.5.

As shown in Figure 3.5, there is good agreement between all three methods for the modes that the chosen excitation in the FE model was able to produce. There were, however, instances where DISPERSE was not able to fully retrieve a mode, or missed it altogether, highlighting the merits of using the proposed SCM instead of root-finding techniques.

Additionally, a comparison of the attenuation values obtained by the SCM against those of DISPERSE is shown in Figure 3.6(a). For visualisation purposes, solutions with high attenuation, $\Im(k_x) > 10$ Np/mm, are not displayed here. A detail of the region of up to 1 Np/mm is shown in Figure 3.6(b). The attenuation values obtained by the SCM match those obtained by DISPERSE,

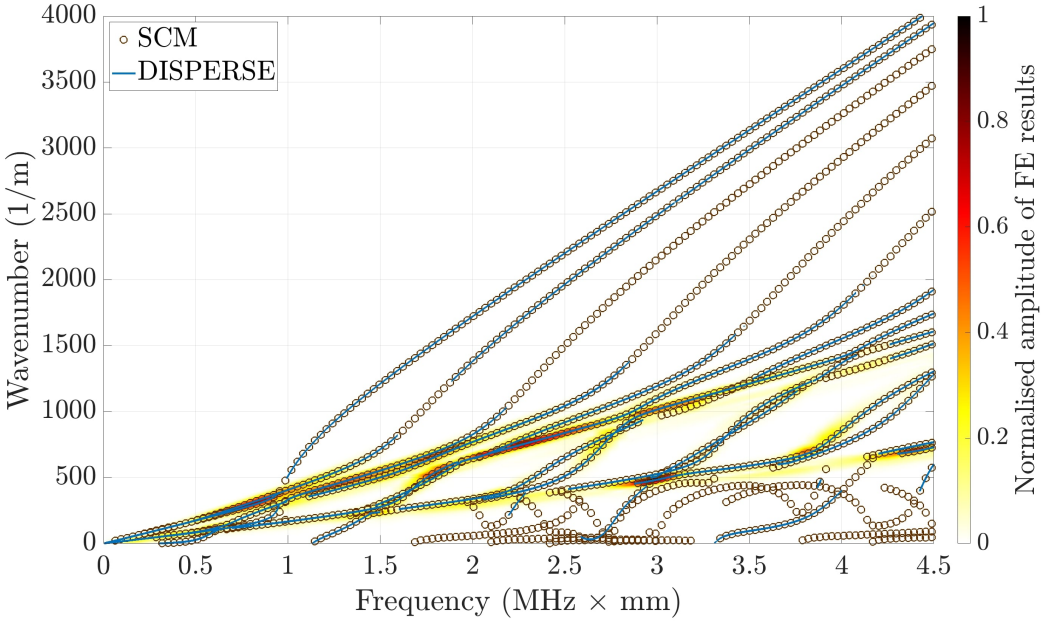

Figure 3.5: Dispersion curves of an epoxy waveguide in contact with an aluminium half-space on each side, obtained by the SCM (denoted by ∘), by DISPERSE (denoted by –) and by FE modelling (normalised intensity in colour).

demonstrating in this way the ability of the SCM to accurately capture the complex wavenumber solutions of the leaky modes of the system.

Following these initial validations of the SCM results, two cases of single-mode excitation are presented next – one where both DISPERSE and SCM were able to retrieve the mode to be excited, and one where only SCM was able to obtain the relevant mode. In each case, the excitation tonebursts were set to the same central frequency, and for the purposes of a narrowband excitation, the number of cycles in the excitation signal was increased to eleven. The size of the absorbing layers, and dx were calculated accordingly at the central frequency.

Figure 3.7(a) shows the results from the independent excitation of a leaky mode using FE modelling, at f = 1.03 MHz and c_{ph} = 5.98 m/ms, which both

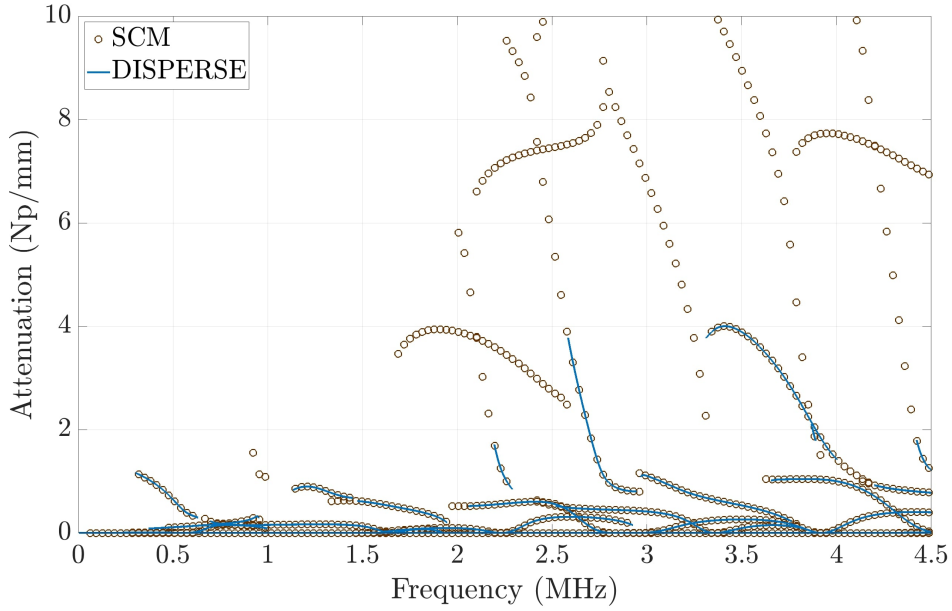

(a)

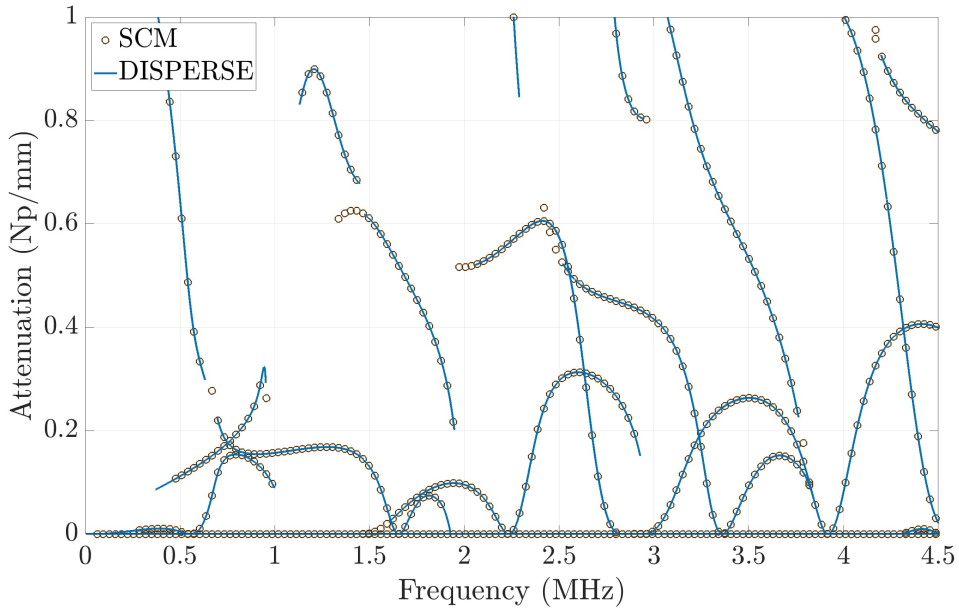

(b)

Figure 3.6: Comparison of attenuation values obtained by the SCM (denoted by ∘) and by DISPERSE (denoted by –) for waves in an epoxy waveguide in contact with an aluminium half-space on each side 3.6(a). A detail of the region with attenuation of up to 1 Np/mm 3.6(b).

DISPERSE and SCM were able to retrieve. The FE results shown are from the post-processing of monitor signals from a monitor line placed horizontally at $y = 5$ mm. As the phase velocity of the mode is between the transverse and longitudinal bulk wave speeds of the exterior aluminium spaces, from Figure 3.2, this is in fact a shear-leaky mode, radiating energy in both exterior domains purely in the form of shear waves. To achieve this excitation and validate the proposed SCM, mode shapes from the SCM were used and are displayed in Figure 3.7(b), where they can be seen to exponentially grow away from the waveguide. Alongside them, mode shapes from DISPERSE are also shown, demonstrating a pleasing concordance between the two methods in computing the mode shapes of the shear-leaky mode.

Figure 3.8(a) shows the results from the excitation of a non-leaky mode, at $f = 3.53$ MHz and $c_{\text{ph}} = 1.50$ m/ms, which only the SCM was able to retrieve, alongside the relevant FE result. As the energy of such modes is confined within the boundaries of the waveguide, the monitor line of the FE model is now placed horizontally in the middle of the waveguide. The mode shapes used for this excitation, decaying away from the waveguide, are shown in Figure 3.8(b) as obtained from the SCM.

It is important to note that any input to the FE model will inherently result in a weighted superposition of its modal responses [61]. Consequently, the agreement between the FE model and the results obtained from SCM and DISPERSE in the figures above is regarded as a robust validation of both methods. This validation, in particular, emphasises the reliability of SCM in scenarios where a DISPERSE solution is not readily available.

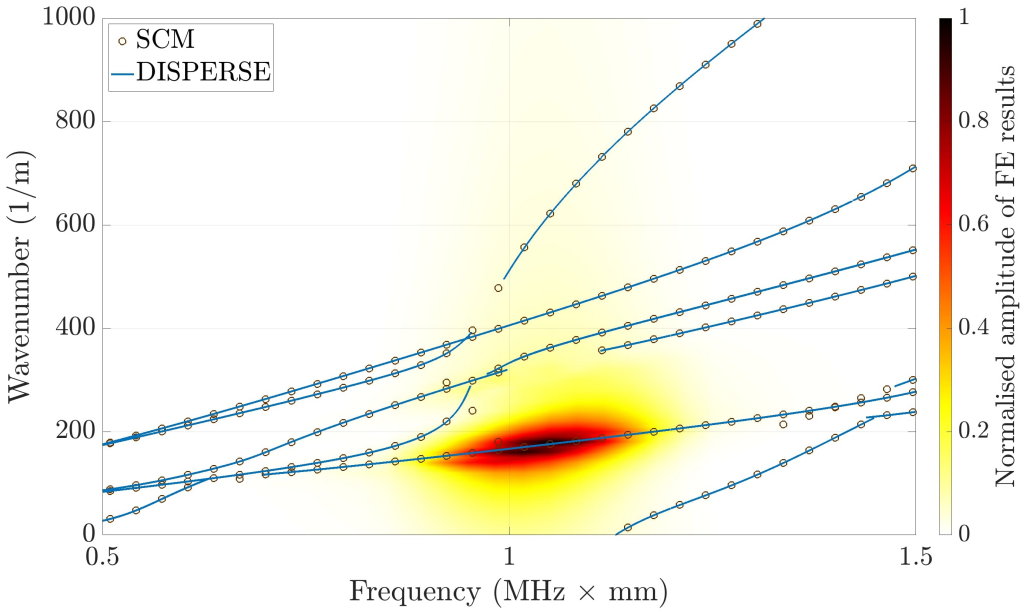

(a)

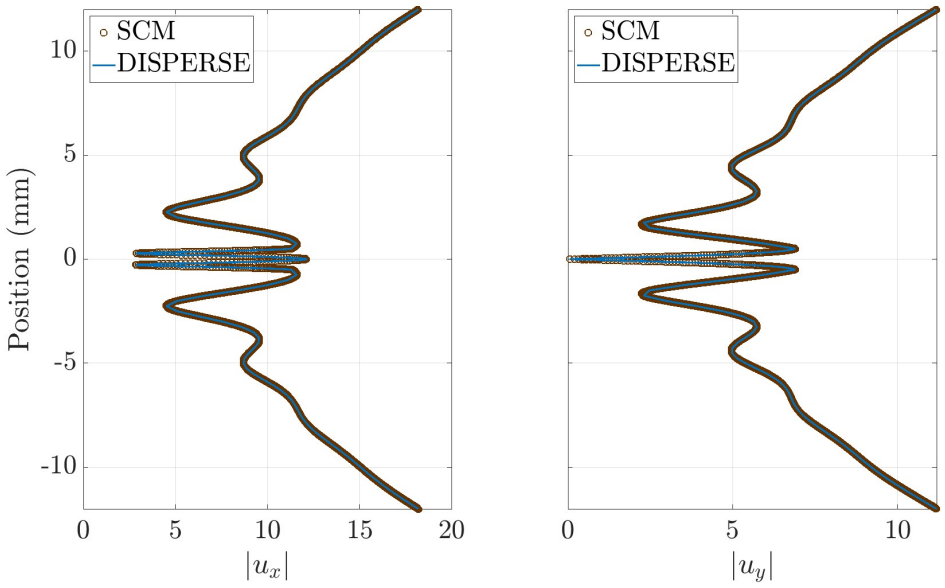

(b)

Figure 3.7: Dispersion curves showing the intensity and dispersion of the shear-leaky mode excited at f = 1.03 MHz and c_{ph} = 5.98 m/ms with a single-mode excitation, validated against SCM and DISPERSE 3.7(a). The exponentially growing mode shapes from the SCM that were used for the excitation are validated against those obtained by DISPERSE 3.7(b).

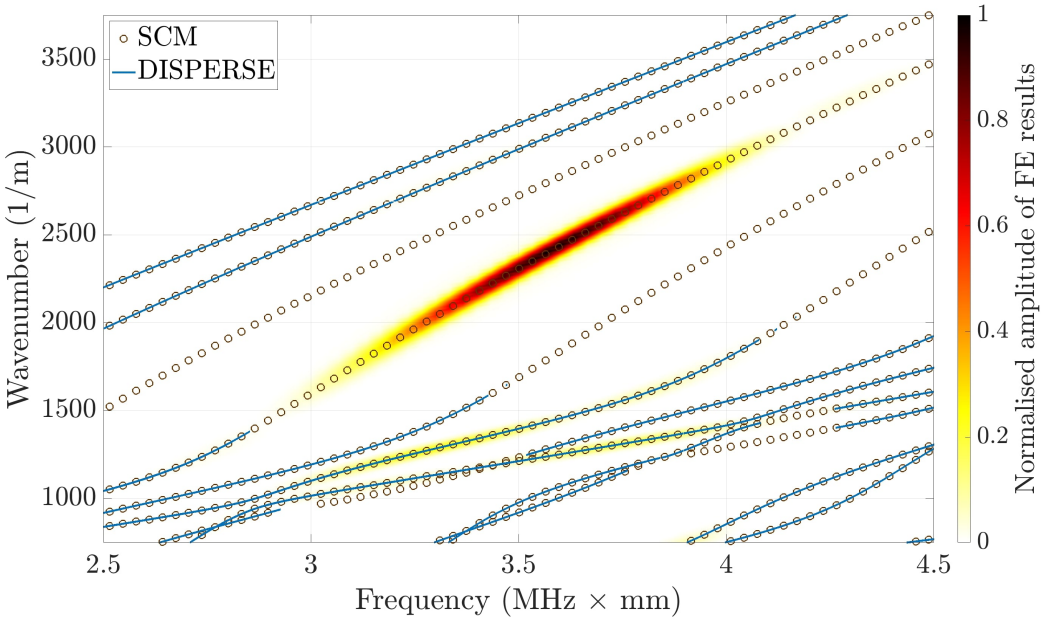

(a)

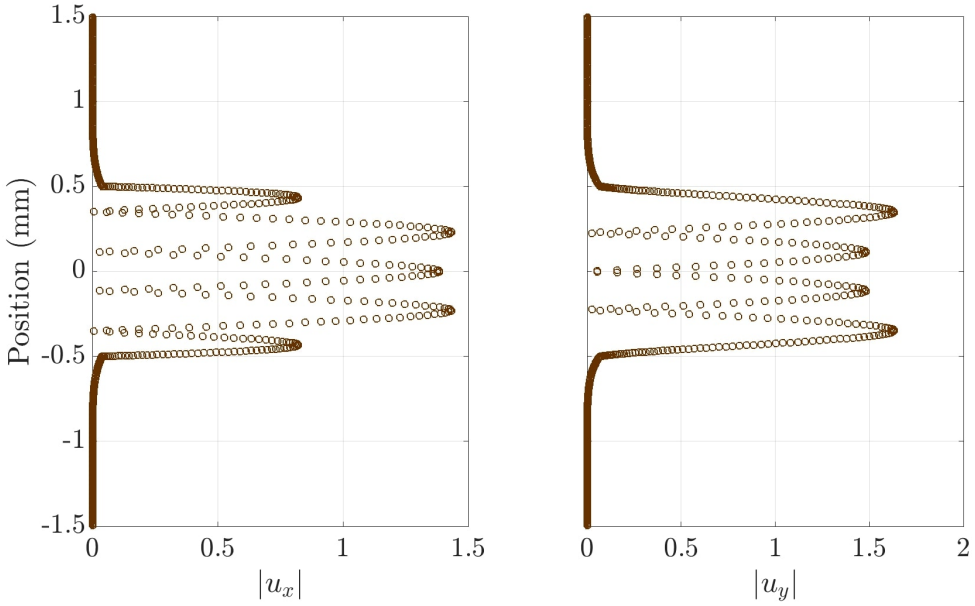

(b)

Figure 3.8: Dispersion curves showing the normalised intensity and dispersion of the non-leaky mode, found only by SCM, and excited at f = 3.53 MHz and c_{ph} = 1.50 m/ms with a single-mode excitation 3.8(a). The decaying mode shapes from the SCM that were used for the excitation are in Figure 3.8(b).

3.5 Conclusion

In this chapter, leaky Lamb wave propagation in a waveguide that is in contact with elastic half-spaces has been considered; these wave modes are often characterised by a complex wavenumber, a subsequent exponential growth in amplitude far into the surrounding elastic media and a highly attenuative nature along the waveguide, making their retrieval by traditional numerical solvers challenging. These obstacles were overcome here by formulating a theoretical framework for the problem, discretising it using an SCM that also accommodated the exponentially growing nature of the problem, and finally solving the resulting polynomial eigenvalue problem for the retrieval of the wave mode solutions of interest. The framework introduced was developed for the general case of a waveguide between two possibly different elastic half-spaces, however it can be simplified to handle other cases of loading by elastic half-spaces or inviscid fluids, like waveguides loaded only on one side by a solid or one with a solid and a fluid half-space each side of the waveguide.

The results of the SCM have been verified against DISPERSE, and FE modelling in places where a DISPERSE solution was not readily available. The SCM approach is accurate, versatile, it readily identifies all leaky modes in elasticity without requiring knowledge of the modes or any tuning *a priori* and is easy to code; the key point is to remove the exponential growth from the numerical scheme via judiciously applying mappings to complex paths that reduce the leaky problem to a standard form for numerical implementation, whilst also preserving all the important physics of the original problem.

Chapter 4

Leaky Circumferential Waves in Submerged Hollow Cylinders

4.1 Introduction

Thus far, the propagation and leakage of Lamb waves in planar geometries has been examined and a SCM was proposed for the accurate identification of leaky waves in waveguides coupled to infinite fluid or elastic media. In this chapter, attention is directed towards understanding leaky waves in cylindrical geometries and developing a SCM for the accurate computation of their dispersion curves.

A circumferential guided wave in a cylindrical waveguide is one that is propagating in the circumferential direction, and has its direction guided by the curved walls of the structure. Because of their ability to propagate around curved surfaces, circumferential guided waves are sensitive to features prominent in the radial direction, making them a popular choice for the detection and sizing of defects within NDE; see for example [105–107].

Quite often, as was the case for planar geometries and straight waveguides, one is interested in inspecting structure submerged in fluid, e.g. pipes in water. In that case, circumferential guided waves become leaky; their energy radiates into the surrounding space of fluid, causing the attenuation of the guided wave. Just like any other guided wave inspection, understanding the physics underlying this leaky behaviour and the different modes that exist in a structure become essential information when one is selecting which mode to use for an effective inspection to take place.

For that reason, the study of circumferential guided waves received much attention over the years. Contributions to the field date back to the work of Sezawa [108] and the study of propagation of circumferential Rayleigh and Love waves on the surface of the earth. Therein the ansatz $e^{i\nu\theta}$ was first introduced for integer angular wavenumbers, ν. Later, Viktorov [109] formulated equations for Rayleigh waves on concave and convex cylinders, also generalising to non-periodic real wavenumbers and Lamb-type waves [110]. Around the same time, Grace and Goodman [111] introduced complex wavenumbers in their investigation of the attenuation of circumferential waves in a submerged elastic cylinder. Several years later, numerical results of the computation of dispersion curves for circumferential guided waves in structures in vacuum were presented by Liu and Qu [112] for waves in an isotropic annulus, by Valle *et al.* [113] for waves in multilayered cylinders and by Towfighi *et al.* [114] for waves in cylinders of anisotropic material. Some of the effects of fluid or solid loading on pipes was reported by Fong [115] and Fong and Lowe [116].

In the aforementioned studies, extracting the dispersion relations of a system often involved formulating the problem as a matrix equation of Bessel functions and computing dispersion curves as the zeros of the determinant of the matrix. When it comes to complex structures, like immersed or embedded

annuli of multiple layers of anisotropic and viscoelastic materials, matrices become increasingly difficult to formulate, while the inaccurate evaluations of Bessel functions of large – and possibly complex – orders and arguments [117] render matrices numerically unstable. Moreover, such matrix methods are heavily dependent on root-finding algorithms which, as was already discussed in previous chapters, are known to struggle [17] when complex wavenumbers, like those of leaky waves, are sought.

Consequently, in recent years, researchers have turned their attention to alternative numerical schemes in search of a numerically stable, accurate and automated way of modelling circumferential guided waves and computing their dispersion curves. Such alternatives include the use of high frequency approximations of Bessel functions [117], the SAFE methods [118], the spectral element methods [119]or spectral collocation which has proven to be very effective in computing the dispersion curves of circumferential waves in annuli of multiple layers of viscoelastic or anisotropic materials [24].

The work already presented in this thesis demonstrated a SCM for the computation of leaky wave dispersion curves for waves radiating from straight waveguides in contact with possibly dissimilar spaces of fluid or elastic media; immersed or embedded plates. Therein, judiciously applying complex coordinate transformations of the infinite fluid or solid space, allowed for the exponentially growing leaky wave problem to be transformed into a numerically decaying one and for the dispersion curves of the structure to be robustly and accurately retrieved by solving generalised eigenvalue problems. This chapter extends those ideas to cylindrical geometries and investigates leaky circumferential guided waves in an immersed cylindrical structure with an annular cross-section. A SCM and accompanying complex coordinate transformations are proposed here and enable the computation of leaky circumferential wave dispersion curves of two types: dispersion curves of real

frequency against complex wavenumber or real wavenumber against complex frequency. Following its introduction, results and validations of the method against commercially available software and analytic formulations will be presented.

The chapter is organised as follows: equations of motion and an analytical formulation of the problem of leaky circumferential waves propagating around a submerged hollow cylinder are introduced in Section 4.2, followed by the development of a SCM for the computation of the complex wavenumber or frequency dispersion curves of the structure, described in Section 4.3, and a discussion of results and validation presented in Section 4.4.

4.2 Problem Statement

Consider an isotropic, linearly elastic hollow cylinder, of inner radius a and outer radius b, immersed in an inviscid fluid. The geometry and annular cross-section of the cylinder are depicted in Figure 4.1. The elastic annu-

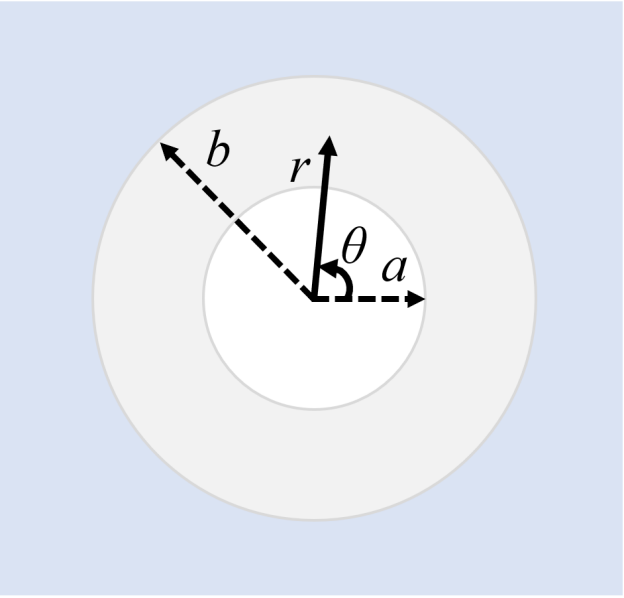

Figure 4.1: The annular cross-section of a hollow cylinder of inner radius a and outer radius b, immersed in fluid.

lus material is taken to have a longitudinal wave speed c_l and a transverse wave speed c_t, while bulk waves in the surrounding fluid are taken to have speed c_f. Two-dimensional, time-harmonic leaky Lamb-like waves are assumed propagating circumferentially around the annulus, in the θ-direction with deformations in the (r,θ)-plane, and radiating into the surrounding fluid space. The displacement field caused by the waves of interest in the annulus, under plain-strain assumptions, is denoted by $\boldsymbol{u}_c = (u, v, 0)$ in cylindrical polar coordinates.

The in-plane displacements, u and v, are independent of the axial direction for Lamb waves and, due to the time and space harmonic nature of the circumferential waves, they are characterised by the common exponential $\exp[i(\nu\theta - \omega t)]$, where ν and ω are the angular wavenumber and frequency respectively. This allows for the in-plane displacements u and v, to be explicitly expressed as

$$\begin{aligned} u &= u_r(r)\exp[i(\nu\theta - \omega t)], \\ v &= u_\theta(r)\exp[i(\nu\theta - \omega t)], \end{aligned} \tag{4.1}$$

with u_r, u_θ the r-dependent components of the in-plane displacements.

A Helmholtz decomposition [82] of the displacement fields in the annulus yields

$$\boldsymbol{u}_c = \nabla_c\Phi + \nabla_c \times \begin{pmatrix} 0 \\ 0 \\ \Psi \end{pmatrix}, \tag{4.2}$$

with $\nabla_c = [\partial/\partial r, (1/r)\partial/\partial\theta, \partial/\partial z]$ the gradient operator in cylindrical polars and Φ and Ψ two scalar potentials corresponding respectively to longitudinal and shear waves in the annulus. For the time harmonic waves under

consideration, write

$$\begin{aligned}\Phi &= \phi(r)\exp[i(\nu\theta - \omega t)],\\ \Psi &= i\psi(r)\exp[i(\nu\theta - \omega t)],\end{aligned} \tag{4.3}$$

with, ϕ and ψ the r-dependent components of the two wave potentials. Under this decomposition, u_r, u_θ may be expressed as

$$\begin{aligned}u_r &= \frac{\partial\phi}{\partial r} - \frac{\nu}{r}\psi,\\ u_\theta &= \frac{i\nu}{r}\phi - i\frac{\partial\psi}{\partial r},\end{aligned} \tag{4.4}$$

in terms of the potential components ϕ and ψ.

A similar decomposition, like that of Eq. (2.1), is possible of the displacement field in the surrounding fluid, $\boldsymbol{u_f} = (u_f, v_f, 0)$, which may be expressed in terms of a scalar longitudinal wave potential $\Phi_f = \phi_f(r)\exp[i(\nu\theta - \omega t)]$ as

$$\boldsymbol{u}_f = \begin{pmatrix} u_f \\ v_f \\ 0 \end{pmatrix} = \nabla_c \Phi_f. \tag{4.5}$$

Expanding on Eq. (4.5) and explicitly differentiating with respect to θ yields

$$u_{r_f} = \frac{\partial\phi_f}{\partial r}, \quad u_{\theta_f} = \frac{i\nu}{r}\phi_f, \tag{4.6}$$

with u_{r_f} and u_{θ_f} the r-dependent components of u_f and v_f respectively.

In the absence of body forces and henceforth omitting the common $\exp[i(\nu\theta - \omega t)]$, the governing momentum equations in polar coordinates by means of

general tensor calculus [24, 82] are

$$\left(\frac{\partial^2}{\partial r^2}+\frac{1}{r}\frac{\partial}{\partial r}-\frac{\nu^2}{r^2}\right)\phi=-\frac{\omega^2}{c_l^2}\phi, \tag{4.7}$$

$$\left(\frac{\partial^2}{\partial r^2}+\frac{1}{r}\frac{\partial}{\partial r}-\frac{\nu^2}{r^2}\right)\psi=-\frac{\omega^2}{c_t^2}\psi, \tag{4.8}$$

for motion in the elastic annulus, and

$$\left(\frac{\partial^2}{\partial r^2}+\frac{1}{r}\frac{\partial}{\partial r}-\frac{\nu^2}{r^2}\right)\phi_f=-\frac{\omega^2}{c_f^2}\phi_f. \tag{4.9}$$

for motion in the surrounding fluid.

To couple the solid and fluid wave motion of Eqs. (4.7)-(4.9), boundary and interface conditions are imposed at $r = a, b$. The inner surface of the annulus at $r = a$ is taken to be stress free, while the solid-fluid interface at $r = b$, requires the continuity of radial stresses and displacements, and the vanishing of shear stresses. That is

$$\sigma_r = \sigma_{r\theta} = 0, \text{ at } r = a, \tag{4.10}$$

$$\sigma_{r\theta} = \sigma_r - \sigma_{r_f} = u_r - u_{r_f} = 0, \text{ at } r = b, \tag{4.11}$$

with $\sigma_r, \sigma_{r\theta}$ the radial and shear stresses in the annulus and σ_{r_f} the normal stress in the fluid.

From Hooke's law for linear elastic materials, the pertinent stress components

corresponding to the displacements u_r and u_θ in the annulus are [112]

$$\sigma_r = \lambda\left(\frac{\partial u_r}{\partial r} + \frac{u_r}{r} + \frac{i\nu}{r}u_\theta\right) + 2\mu\frac{\partial u_r}{\partial r}, \tag{4.12}$$

$$\sigma_\theta = \lambda\left(\frac{\partial u_r}{\partial r} + \frac{u_r}{r} + \frac{i\nu}{r}u_\theta\right) + 2\mu\left(\frac{u_r}{r} + \frac{i\nu}{r}u_\theta\right), \tag{4.13}$$

$$\sigma_{r\theta} = \mu\left(\frac{\partial u_\theta}{\partial r} - \frac{u_\theta}{r} + \frac{i\nu}{r}u_r\right), \tag{4.14}$$

where λ and μ are the Lamé parameters of the elastic material of the annulus. After some algebraic manipulation, the radial and shear stresses in the annulus satisfy the following

$$\frac{\sigma_r}{\mu} = \left[\kappa^2\frac{\partial^2}{\partial r^2} + (\kappa^2 - 2)\left(\frac{1}{r}\frac{\partial}{\partial r} - \frac{\nu^2}{r^2}\right)\right]\phi + 2\nu\left(\frac{1}{r^2} - \frac{1}{r}\frac{\partial}{\partial r}\right)\psi, \tag{4.15}$$

$$\frac{i\sigma_{r\theta}}{\mu} = 2\nu\left(\frac{1}{r^2} - \frac{1}{r}\frac{\partial}{\partial r}\right)\phi + \left(\frac{\partial^2}{\partial r^2} - \frac{1}{r}\frac{\partial}{\partial r} + \frac{\nu^2}{r^2}\right)\psi, \tag{4.16}$$

in terms of the two scalar potentials ϕ and ψ and with $\kappa = c_l/c_t$ in the above. In an analogous way, the radial stress in the surrounding fluid medium reads

$$\sigma_{r_f} = \lambda_f\left(\frac{\partial^2}{\partial r^2} + \frac{1}{r}\frac{\partial}{\partial r} - \frac{\nu^2}{r^2}\right)\phi_f, \tag{4.17}$$

with λ_f the Lamé parameter of the surrounding fluid.

Substituting Eqs. (4.4), (4.6) and (4.15)-(4.17) in Eqs. (4.10) and (4.11) and rearranging, the traction free boundary conditions at the inner surface of the

annulus at $r = a$ are satisfied when

$$\left\{\left[\kappa^2\frac{\partial^2}{\partial r^2} + (\kappa^2 - 2)\left(\frac{1}{r}\frac{\partial}{\partial r} - \frac{\nu^2}{r^2}\right)\right]\phi + 2\nu\left(\frac{1}{r^2} - \frac{1}{r}\frac{\partial}{\partial r}\right)\psi\right\}\Bigg|_{r=a} = 0, \tag{4.18}$$

$$\left[2\nu\left(\frac{1}{r^2} - \frac{1}{r}\frac{\partial}{\partial r}\right)\phi + \left(\frac{\partial^2}{\partial r^2} - \frac{1}{r}\frac{\partial}{\partial r} + \frac{\nu^2}{r^2}\right)\psi\right]\Bigg|_{r=a} = 0, \tag{4.19}$$

and the interface conditions at the fluid-solid interface at the outer surface, at $r = b$, of the annulus, are satisfied when

$$\left[2\nu\left(\frac{1}{r^2} - \frac{1}{r}\frac{\partial}{\partial r}\right)\phi + \left(\frac{\partial^2}{\partial r^2} - \frac{1}{r}\frac{\partial}{\partial r} + \frac{\nu^2}{r^2}\right)\psi\right]\Bigg|_{r=b} = 0, \tag{4.20}$$

$$\left\{\left[\kappa^2\frac{\partial^2}{\partial r^2} + (\kappa^2 - 2)\left(\frac{1}{r}\frac{\partial}{\partial r} - \frac{\nu^2}{r^2}\right)\right]\phi + 2\nu\left(\frac{1}{r^2} - \frac{1}{r}\frac{\partial}{\partial r}\right)\psi - \frac{\lambda_f}{\mu}\left(\frac{\partial^2}{\partial r^2} + \frac{1}{r}\frac{\partial}{\partial r} - \frac{\nu^2}{r^2}\right)\phi_f\right\}\Bigg|_{r=b} = 0, \tag{4.21}$$

$$\left[\frac{\partial\phi}{\partial r} - \frac{\nu}{r}\psi - \frac{\partial\phi_f}{\partial r}\right]\Bigg|_{r=b} = 0. \tag{4.22}$$

The equations of motion in cylindrical coordinates, Eqs. (4.7)-(4.8), are Bessel equations and merit Bessel function solutions of the form [120,121]

$$\phi(r) = AJ_\nu(k_l r) + BY_\nu(k_l r), \tag{4.23}$$

$$\psi(r) = CJ_\nu(k_t r) + DY_\nu(k_t r), \tag{4.24}$$

$$\phi_f(r) = EH_\nu(kr), \tag{4.25}$$

where $k_l = \omega/c_l$, $k_t = \omega/c_t$, $k = \omega/c_f$, J_ν and Y_ν are, the Bessel functions of first and second kind and order ν, $H_\nu = J_\nu + iY_\nu$ is the Hankel function of first kind and order ν and A, B, C, D, E are unknown wave amplitudes. Note that the choice of Hankel function in Eq. (4.25) is made to ensure that the solution adheres to the Sommerfeld radiation condition [122].

A direct substitution of the solutions of Eq. (4.23)-(4.25) in the five boundary and interface conditions of Eqs. (4.18)-(4.22), allows one to express the problem in matrix form, in terms of the unknown wave amplitudes $\boldsymbol{A} = [A, B, C, D, E]^T$, as

$$\boldsymbol{D}(\omega, \nu)\boldsymbol{A} = \boldsymbol{0}. \tag{4.26}$$

$\boldsymbol{D}(\omega, \nu)$ is a 5×5 matrix of Bessel functions and its entries are given in Appendix B. Eq. (4.26) is the characteristic equation of the problem and its non-trivial solutions, i.e. pairs (ω, ν) such that $\det[\boldsymbol{D}(\omega, \nu)] = 0$, define the dispersion relations of the system, while the corresponding wave amplitudes in $\boldsymbol{A}$ fully determine the displacement fields everywhere in the annulus and the surrounding fluid space.

There are two routes one may take when solving Eq. (4.26) – sweep through real ω and find ν or sweep through real ν and find ω. In both cases the unknown one seeks to find is, in general, complex valued, with the two, as evident by the common exponential factor $\exp[i(\nu\theta - \omega t)]$, representing problems of distinct physical interpretations. For complex wavenumbers, waves are propagating in the circumferential direction, with their amplitudes varying with distance of propagation, i.e. with the angle θ. On the other hand, amplitudes vary with time when complex frequencies are considered.

In this chapter both problems are solved and validated. It is important to note that the problem of leaky circumferential waves is one that DISPERSE, the primary tool used for validations in this thesis, cannot solve. Its capabilities in cylindrical geometries are limited to non-attenuating systems and real wavenumbers, such as waves in isotropic cylinders in vacuum. Nonetheless, some limiting cases of the system's materials and geometry will enable initial validations through comparisons with DISPERSE, while the general case of leaky circumferential waves will be validated against the analytical formulation of Eq. (4.26).

4.3 Discretisation

In this section, the problem of leaky circumferential waves in an immersed hollow cylinder, described in Section 4.2, is discretised and solved algebraically. The spectral collocation discretisation of previous chapters is adapted here to cylindrical geometries, enabling the spatial discretisation of the differential operators of the problem.

In Eqs. (4.7)-(4.9), the differentiation of the elastic wave potentials ϕ and ψ in the bounded annulus interval $[a, b]$, and of ϕ_f in the open space of fluid $[b, \infty]$ is sought. Following Chapters 2 and 3, a spectral collocation discretisation of both $[a, b]$ and $[b, \infty]$ will allow the calculation of approximate derivatives in those domains with differentiation matrices.

The starting point for both discretisations will again be the N Gauss-Lobatto Chebyshev collocation points of Eq. (1.28), defined over $[-1, 1]$, and the corresponding $N \times N$ Chebyshev differentiation matrices, $D^{(1)}$ and $D^{(2)}$. By defining coordinate maps, from $[-1, 1]$ to $[a, b]$ and from $[-1, 1]$ to $[b, \infty]$, mapping the Chebyshev collocation points to collocation points in each of the two domains, the desired discretisation of both domains will effectively be achieved.

For the annulus and $[a, b]$, the coordinate transformation

$$r_{a_j} = \frac{hs_j + a + b}{2}, \tag{4.27}$$

with $h = b - a$ the thickness of the annulus, yields the desired discretisation. Directly applying the chain rule on Eq. (4.27), it follows that the m^{th} derivative operator with respect to $r \in [a, b]$ relates to the m^{th} derivative operator

with respect to $s \in [-1, 1]$ via

$$\frac{\partial^m}{\partial r^m} = \left(\frac{2}{h}\right)^m \frac{\partial^m}{\partial s^m}. \tag{4.28}$$

As a result, differentiation matrices in the annulus are given by

$$D_a^{(m)} = \left(\frac{2}{h}\right)^m D^{(m)}. \tag{4.29}$$

For the surrounding fluid and $[b, \infty]$, the complex coordinate transformation

$$r_{f_j} = b + \zeta_f \frac{1 + s_j}{1 - s_j}, \tag{4.30}$$

with $\zeta_f \in \mathbb{C}$, is used instead. The resulting differentiation matrices, from the chain rule, are

$$D_f^{(1)} = \text{diag}\left(\frac{2\boldsymbol{\zeta}_f}{[\boldsymbol{\zeta}_f + (\boldsymbol{r}_f - \boldsymbol{b})]^2}\right) D^{(1)}, \tag{4.31}$$

$$\begin{aligned} D_f^{(2)} = &\text{diag}\left(\frac{-4\boldsymbol{\zeta}_f}{[\boldsymbol{\zeta}_f + (\boldsymbol{r}_f - \boldsymbol{b})]^3}\right) D^{(1)} \\ &+ \text{diag}\left(\frac{4\boldsymbol{\zeta}_f^2}{[\boldsymbol{\zeta}_f + (\boldsymbol{r}_f - \boldsymbol{b})]^4}\right) D^{(2)}, \end{aligned} \tag{4.32}$$

with $\boldsymbol{\zeta}_f = [\zeta_f, \ldots, \zeta_f]^T$, and $\boldsymbol{b} = [b, \ldots, b]^T$, column vectors of N entries and $\boldsymbol{r}_f$ a column vector of collocation points $\{r_{f_j}\}_{j=1}^N$.

The complex coordinate transformation of Eq. (4.30), like those of Eqs. (2.18) and (2.19) from previous work, maps the Chebyshev collocation points from $[-1, 1]$ to a line in the complex plane, which only coincides with the physical fluid space $[b, \infty]$ when ζ_f is a positive real number; denote this space by $\mathbb{C}_f$.

To interpret the effects of the map, a discussion analogous to those of previous

chapters is made here: the equation of motion in the fluid, Eq. (4.9), for complex valued $\tilde{r} \in \mathbb{C}_f$, is a Bessel equation for the same wavenumber ν and frequency ω and thus admits a solution of the form of Eq. (4.25), say

$$\tilde{\phi}_f(\tilde{r}) = \tilde{E} H_\nu(k\tilde{r}), \tag{4.33}$$

where $\tilde{E}$ is an unknown amplitude determined by interface conditions. Like in previous chapters, due to the choice of complex map, which always guarantees a collocation point on the physical interface between the annulus and the surrounding fluid at $r = b$, where interface conditions are imposed, it follows that the two wave potentials $\tilde{\phi}_f$ and ϕ_f attain the same value at the collocation point at $r = \tilde{r} = b$ and thus $\tilde{E} = E$; $\tilde{\phi}_f$ is the analytical continuation of ϕ_f defined in $\mathbb{C}_f$.

As the complex coordinate $\tilde{r} \in \mathbb{C}_f$, appears in the argument of the Hankel function of Eq. (4.33), the choice of map allows control over the rate of decay (or growth) of the complex wave potential $\tilde{\phi}_f$. To appreciate how, consider the following discussion on the behaviour of Hankel functions of complex orders and arguments.

A Hankel function is single-valued and entire with respect to its order ν [123]. When computing its behaviour for large orders or arguments, the asymptotic formulas used to represent it are expressed in terms of complex functions that are multiple-valued and require carefully selected branch cuts. The branch cut of an asymptotic representation gives rise to a line in the complex ν plane, known as a Stokes line [124], which determines the asymptotic behaviour of the Hankel function for large order and argument. This behaviour changes as the order of the function moves from one side of the Stokes line to the other [125], with the line consequently playing a central role in the definition of various types of waves. This was demonstrated in [126] for waves in

electromagnetism, where it was shown that the Stokes line acted as a boundary between improper (growing) and proper (decaying) behaviour of modes near the surface of a dielectric coated hollow cylinder in air. Specifically, surface waves in the cylinder, for which ν was on the left of a Stokes line, locally decayed with distance from the cylinder, while leaky waves, for which ν was on the right of a Stokes line, were shown to locally grow. This local behaviour ultimately turned into decay for both wave types due to the cylindrical geometry of the problem.

Importantly, in the same contribution the relation between circumferential waves in the cylinder and waves in a flat dielectric coated slab (straight waveguide coupled with air on one side) was established. It was demonstrated that the wavenumbers of waves in the cylinder approached those of waves in the flat slab when the size of the cylinder increased. In the limit, $b \to \infty$, the local decay or growth of the various wave types turned into global behaviour, meaning that surface waves became evanescent waves in the surrounding medium and leaky waves turned into inhomogeneous, exponentially growing, waves in the exterior. This was a direct consequence of the asymptotic behaviour of Hankel functions, which behave like exponentials for large orders, and agrees with what was physically expected – a large cylinder of finite thickness is effectively a flat waveguide; see the Appendix of [126] for more details on that large cylinder limit. As this relation is entirely associated to the behaviour of Hankel functions, it will be exploited here in the context of acoustic waves and will enable comparisons between results from the proposed SCM (large finite thickness annuli in fluid) and DISPERSE (straight waveguides in contact with fluid) to be made.

Asymptotic formulas for Hankel functions were proposed by Debye [127], Watson [128] and Olver [129]. For a Hankel function of order ν and argument ξ, with $|\arg(\xi)| < \pi/2$ and $\arg(\xi)$ the principal argument of the complex

number ξ with values in $(-\pi, \pi]$, the Debye approximation is thought to be valid when $|\nu - \xi| \gg |\nu|^{1/3}$, and the Watson approximation when $|\nu| \approx |\xi|$. In contrast, Olver's representation is uniformly valid for all ν and ξ, provided that ξ is large enough, and it reduces to the Debye approximation when ν and ξ are far apart, and to the Watson approximation when the two are close together. An exposition on the utility of the various asymptotic representations of Hankel functions can be found in [125].

Recall that for the circumferential waves of this thesis, from Eq. (4.25), the Hankel function of interest has the wavenumber of circumferential waves as its order and $\xi = kr$ as its argument. Assuming finite orders $|\nu| \neq \infty$, which is equivalent to cylinders of finite sizes [112, 126], and restricting to $|\arg(\xi)| < \pi/2$, the large argument form of the Hankel function [130],

$$H_\nu(\xi) \approx \sqrt{\frac{2}{\pi\xi}} \exp\left[i\left(\xi - \frac{1}{2}\nu\pi - \frac{1}{4}\pi\right)\right], \tag{4.34}$$

for $|\xi| \gg |\nu|$ applies. As $r \to \infty$, the wave potential in the fluid, ϕ_f of Eq. (4.25), may be approximated by

$$\phi_f(r) \approx E\sqrt{\frac{2}{\pi kr}} \exp\left[i\left(kr - \frac{1}{2}\nu\pi - \frac{1}{4}\pi\right)\right], \tag{4.35}$$

where ξ was substituted with kr in the above.

If one is interested in real frequencies and complex wavenumbers, the quantity kr is real valued and, in the limit, it follows from Eq. (4.35) that the wave potential in the fluid ϕ_f decays like $1/\sqrt{r}$ as $r \to \infty$. That is true of both leaky and non-leaky circumferential waves and agrees with the observations of [126] in electromagnetism.

If, on the other hand, one is interested in real wavenumbers and complex

frequencies, then kr is complex valued and for $|\arg(kr)| < \pi/2$, ϕ_f can both exponentially grow, e.g. when $\Re(\omega) > 0$ and $\Im(\omega) < 0$, or decay, e.g. when $\Re(\omega) > 0$ and $\Im(\omega) > 0$.

When the proposed complex map is applied, provided that $|\arg(k\tilde{r})| < \pi/2$, the complex wave potential $\tilde{\phi}_r$, for $|\tilde{r}| \to \infty$ takes the form

$$\tilde{\phi}_f(\tilde{r}) \approx E\sqrt{\frac{2}{\pi k\tilde{r}}}\exp\left[i\left(k\tilde{r} - \frac{1}{2}\nu\pi - \frac{1}{4}\pi\right)\right]. \tag{4.36}$$

Consequently, depending on the value of $k\tilde{r}$, for either complex wavenumbers or complex frequencies, Eq. (4.36) can be made to exponentially numerically decay, even for physical solutions where it was growing. In this study, complex wavenumbers with $\Re(\nu) > 0$ and $\Im(\nu) \geq 0$, and complex frequencies with $\Re(\omega) > 0$ and $\Im(\omega) \leq 0$, will be of interest; a choice of $\zeta_f = \alpha i$, with $\alpha \in \mathbb{R}_+$ allows for the retrieval of both. Thus, to summarise, instead of discretising the real line $[b, \infty]$ and the fluid space, a complex line, $\mathbb{C}_f$, defined by the transformation of Eq. (4.30), will be discretised instead, allowing for the solution of an exponentially decaying wave field which preserves all the important physics (wavenumber/frequency and amplitude) of the original problem.

Having now established the effects of the complex map and having obtained differentiation matrices, the differential operators acting on ϕ, ψ and ϕ_f in Eqs. (4.7)-(4.9) may be discretised with spectral collocation. The differential operators are

$$\mathcal{L}_\chi = \left(\frac{\partial^2}{\partial r^2} + \frac{1}{r}\frac{\partial}{\partial r} - \frac{\nu^2}{r^2}\right) + \frac{\omega^2}{c_\chi^2}, \tag{4.37}$$

with $\chi = \phi, \psi, \phi_f$, and by replacing derivatives in the radial direction with the appropriate differentiation matrices, the $N \times N$ matrix differential oper-

ators

$$L_\phi = \nu^2 \mathrm{diag}\left(-\frac{1}{\boldsymbol{r}_a^2}\right) + \left[D_a^{(2)} + \mathrm{diag}\left(\frac{1}{\boldsymbol{r}_a}\right) D_a^{(1)}\right] + \frac{\omega^2}{c_l^2} I, \tag{4.38}$$

$$L_\Psi = \nu^2 \mathrm{diag}\left(-\frac{1}{\boldsymbol{r}_a^2}\right) + \left[D_a^{(2)} + \mathrm{diag}\left(\frac{1}{\boldsymbol{r}_a}\right) D_a^{(1)}\right] + \frac{\omega^2}{c_t^2} I, \tag{4.39}$$

$$L_{\phi_f} = \nu^2 \mathrm{diag}\left(-\frac{1}{\boldsymbol{r}_f^2}\right) + \left[D_f^{(2)} + \mathrm{diag}\left(\frac{1}{\boldsymbol{r}_f}\right) D_f^{(1)}\right] + \frac{\omega^2}{c_f^2} I, \tag{4.40}$$

are obtained, with $\boldsymbol{r}_a$ the column vector of collocation points in the annulus, $\{r_{a_j}\}_{j=1}^N$, and I the $N \times N$ identity matrix.

Merging all matrix operators together, the discrete problem may be expressed as an eigenvalue problem

$$\tilde{L}\boldsymbol{u} = \begin{pmatrix} L_\phi & 0 & 0 \\ 0 & L_\Psi & 0 \\ 0 & 0 & L_{\phi_f} \end{pmatrix} \begin{pmatrix} \boldsymbol{\phi} \\ \boldsymbol{\Psi} \\ \tilde{\boldsymbol{\phi}}_f \end{pmatrix} = \mathbf{0}, \tag{4.41}$$

with $\tilde{L}$ a $3N \times 3N$ matrix operator and $\boldsymbol{u}$ a column vector of length $3N$, containing the wave potentials in the annulus and the complex wave potential in the fluid, each evaluated on the collocation points discretising their respective domains of definition.

As was done in previous work, to conclude the discretisation, the differential operators of the boundary and interface conditions of Eqs. (4.18)-(4.22) are discretised and represented by two boundary and interface condition matrices. Explicitly, the boundary condition matrix is a $2 \times 3N$ matrix given by

$$
\begin{aligned}
BC = \nu^2 &\begin{bmatrix} \mathrm{diag}\left(\frac{2-\kappa^2}{\boldsymbol{r}_a^2}\right) & 0 & 0 \\ 0 & \mathrm{diag}\left(\frac{1}{\boldsymbol{r}_a^2}\right) & 0 \end{bmatrix}\Bigg|_{r=a} \\
+ \nu &\begin{bmatrix} 0 & \mathrm{diag}\left(\frac{2}{\boldsymbol{r}_a^2}\right) - \mathrm{diag}\left(\frac{2}{\boldsymbol{r}_a}\right) D_a^{(1)} & 0 \\ \mathrm{diag}\left(\frac{2}{\boldsymbol{r}_a^2}\right) - \mathrm{diag}\left(\frac{2}{\boldsymbol{r}_a}\right) D_a^{(1)} & 0 & 0 \end{bmatrix}\Bigg|_{r=a} \\
+ &\begin{bmatrix} \kappa^2 D_a^{(2)} + \mathrm{diag}\left(\frac{\kappa^2-2}{\boldsymbol{r}_a}\right) D_a^{(1)} & 0 & 0 \\ 0 & D_a^{(2)} - \mathrm{diag}\left(\frac{1}{\boldsymbol{r}_a}\right) D_a^{(1)} & 0 \end{bmatrix}\Bigg|_{r=a},
\end{aligned}
\tag{4.42}
$$

while the interface condition matrix is a $3 \times 3N$ matrix given by

$$
\begin{aligned}
IC = \nu^2 &\begin{bmatrix} 0 & \mathrm{diag}\left(\frac{1}{\boldsymbol{r}_a^2}\right) & 0 \\ \mathrm{diag}\left(\frac{2-\kappa^2}{\boldsymbol{r}_a^2}\right) & 0 & \mathrm{diag}\left(\frac{\lambda_f}{\mu \boldsymbol{r}_f^2}\right) \\ 0 & 0 & 0 \end{bmatrix}\Bigg|_{r=b} \\
+ \nu &\begin{bmatrix} \mathrm{diag}\left(\frac{2}{\boldsymbol{r}_a^2}\right) - \mathrm{diag}\left(\frac{2}{\boldsymbol{r}_a}\right) D_a^{(1)} & 0 & 0 \\ 0 & \mathrm{diag}\left(\frac{2}{\boldsymbol{r}_a^2}\right) - \mathrm{diag}\left(\frac{2}{\boldsymbol{r}_a}\right) D_a^{(1)} & 0 \\ 0 & -\mathrm{diag}\left(\frac{1}{\boldsymbol{r}_a}\right) & 0 \end{bmatrix}\Bigg|_{r=b} \\
+ &\begin{bmatrix} 0 & D_a^{(2)} - \mathrm{diag}\left(\frac{1}{\boldsymbol{r}_a}\right) D_a^{(1)} & 0 \\ \kappa^2 D_a^{(2)} + \mathrm{diag}\left(\frac{\kappa^2-2}{\boldsymbol{r}_a}\right) D_a^{(1)} & 0 & -\frac{\lambda_f}{\mu}\left(D_f^{(2)} + \mathrm{diag}\left(\frac{1}{\boldsymbol{r}_f}\right) D_f^{(1)}\right) \\ D_a^{(1)} & 0 & -D_f^{(1)} \end{bmatrix}\Bigg|_{r=b}.
\end{aligned}
\tag{4.43}
$$

By replacing rows $1, N+1$ and $N, 2N, 2N+1$ of the operator $\tilde{L}$, which correspond to collocation points at $r = a$ and $r = b$, with the two rows of BC and the three rows of IC respectively, boundary and interface conditions are introduced into the discretised problem. In addition to those and to ensure the vanishing of the wave field, Dirichlet zero boundary conditions are imposed at infinity by replacing row $3N$ of $\tilde{L}$ with the last row of the $3N \times 3N$ identify matrix. After incorporating boundary and interface conditions into the matrix operator $\tilde{L}$ and separating into ν^2, ν, ω^2 and constant components,

the eigenvalue problem

$$\left(\nu^2 L_2 + \nu L_1 + L_0\right) \boldsymbol{u} = \omega^2 \mathcal{M} \boldsymbol{u}, \tag{4.44}$$

is reached.

Recall the two problems discussed in Section 4.2 – complex wavenumbers and spatially varying amplitudes versus complex frequencies and temporally varying amplitudes. It is important to note that the formulation of Eq. (4.44) allows for the solution of both problems, under the same SCM. Indeed, Eq. (4.44) presents a polynomial eigenvalue problem in complex wavenumber, solvable via a companion matrix linearisation [88], or a generalised eigenvalue problem in ω^2, solvable with conventional eigenvalue problem solvers. Thus, by performing frequency or wavenumber sweeps, it is possible to compute dispersion curves of both types.

4.4 Results & Validation

4.4.1 Complex Wavenumber

In this section, SCM results of the computation of the complex wavenumber dispersion curves of leaky circumferential guided waves propagating around a submerged hollow cylinder are presented. As an initial validating step, and due to the capability limits of DISPERSE, two limiting cases of the materials and geometry of the system are investigated: a hollow cylinder immersed in a fluid of low acoustic impedance, henceforth referred to as a "weak" fluid, and a submerged hollow cylinder of small curvature (the large cylinder limit of [126]). In the limit, the former converges to the case of a cylinder in vacuum, while the latter approximates a straight waveguide adjacent to a space of fluid; both limits are systems for which dispersion curves are available

from DISPERSE [16]. Following initial validations, the performance of the SCM for the general case is validated against analytic formulations.

Before proceeding to results, it is important to address what is meant by the phase velocity and attenuation of circumferential waves in an annulus. For a given solution pair (ν, ω), the phase velocity and attenuation of circumferential waves are constant along radial lines and vary linearly with radial distance [112]. That is, all particles located a distance r from the centre of the annulus of Figure 4.1 have the same phase velocity given by [115]

$$c(r) = r\frac{\omega}{\Re(\nu)}, \tag{4.45}$$

and attenuation

$$\alpha(r) = \Im(\nu)/r. \tag{4.46}$$

The phase velocity and attenuation of Eqs. (4.45) and (4.46), in all results presented in this work, will be calculated for the same radial distance, $r_c = (a+b)/2$, at the centreline of the annulus, and will be denoted by c_{r_c} and α_{r_c} respectively.

4.4.1.1 Cylinder Immersed in Weak Fluid

Consider a hollow cylinder, made of steel, immersed in a weak fluid first. The annular cross-section is taken to have inner radius $a = 18$ mm, outer radius $b = 20$ mm, density $\rho = 7.932$ g/cm^3, longitudinal wave speed $c_l = 5.960$ m/ms and shear wave speed $c_t = 3.260$ m/ms. The weak fluid surrounding the cylinder is taken to have density $\rho_f = 0.01$ g/cm^3 and wave speed $c_f = 0.01$ m/ms. Note that because, as discussed in the previous section, both non-leaky and leaky modes decay for complex wavenumbers, the same treatment and complex mapping of the fluid domain allows for the exponential decay of both types of modes at the same time. Thus, to obtain the dispersion curves of

interest, a single frequency sweep of 200 steps was performed for angular frequencies between $0 - 20$ MHz, and the choice of $\zeta_f = 10i$, found to produce excellent results for leaky waves in planar geometries, is made here for all frequencies. The domain of the annulus was discretised with $N_a = 30$ Chebyshev collocation points, while $N_f = 150$ points discretise the fluid (or more accurately the complex path $\mathbb{C}_f$).

To distinguish between physical solutions and numerical artifacts, filters were applied. The model was run twice, with the number of collocation points in the fluid halved in the second run. Only eigenvalues that remained unchanged, up to the fifth decimal place, were kept. Additionally, solutions of negative or high attenuation(≥ 10 Np/mm) and negative phase velocity were discarded. All calculations in Section 4.4.1, unless stated otherwise, were performed for the same frequency range, complex parameters and filtering, with computations at each frequency step of the sweep taking approximately 0.6 seconds on a personal computer with 32GB RAM and an Intel i7-10700 CPU.

SCM dispersion curves of circumferential guided waves propagating around a steel annulus immersed in weak fluid, are presented in Figure 4.2, as plots of phase velocity against frequency. Dispersion curves from DISPERSE for the same steel annulus in vacuum, overlay the SCM results. A good agreement between the two methods is demonstrated in Figure 4.2, for both phase velocity predictions and the zero attenuation values of circumferential guided waves in lossless media in vacuum.

4.4.1.2 Cylinder of Small Curvature

Moving now onto the second limiting case, that of an immersed cylinder of small curvature, consider again a cylinder made of steel. To achieve small curvature, the inner and outer radii of the cross-section are increased by

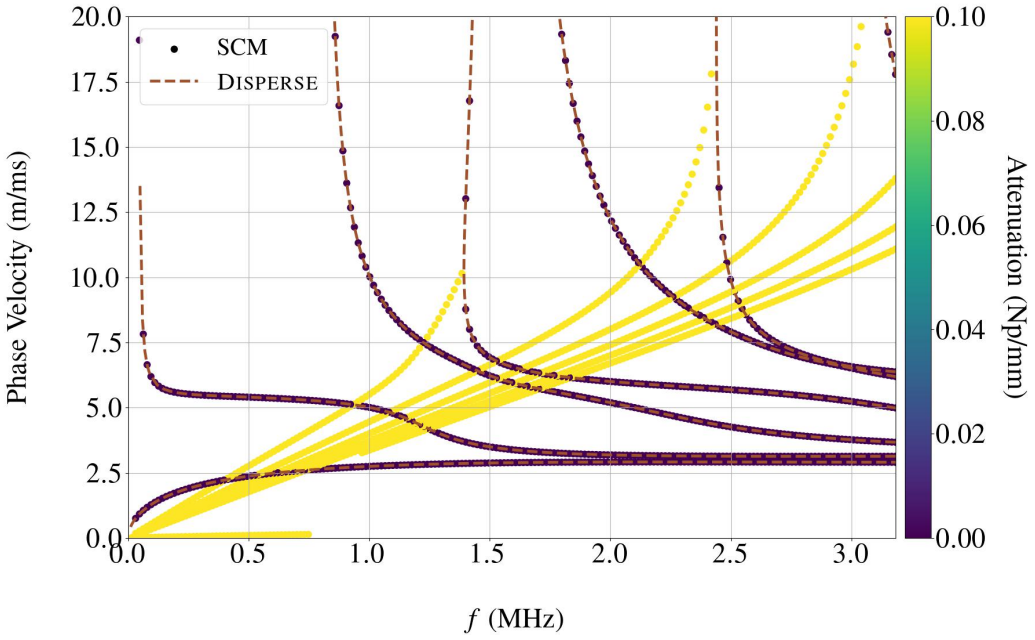

Figure 4.2: Phase velocity dispersion curves for a steel annulus immersed in a weak fluid, calculated by the SCM and coloured according to their value of attenuation. Overlaid are the dispersion curves of the same annulus in vacuum calculated with DISPERSE.

several orders of magnitude, to a = 10018 mm and b = 10020 mm, while keeping the thickness of the annulus, h = 2 mm, constant. The cylinder is assumed submerged in water of density ρ_f = 1 g/cm^3 and wave speed c_f = 1.5 m/ms. Figure 4.3 presents SCM phase velocity and attenuation results against dispersion curves from DISPERSE for a straight waveguide of the same thickness and material properties as the cylinder, in contact with water on one side. Again, good agreement can be seen for both phase velocity and attenuation values, up to a linear frequency of f = 2.5 MHz. Discrepancies observed beyond that point and for higher frequencies are attributed to the curvature of the annulus not being small enough for the two problems to be comparable.

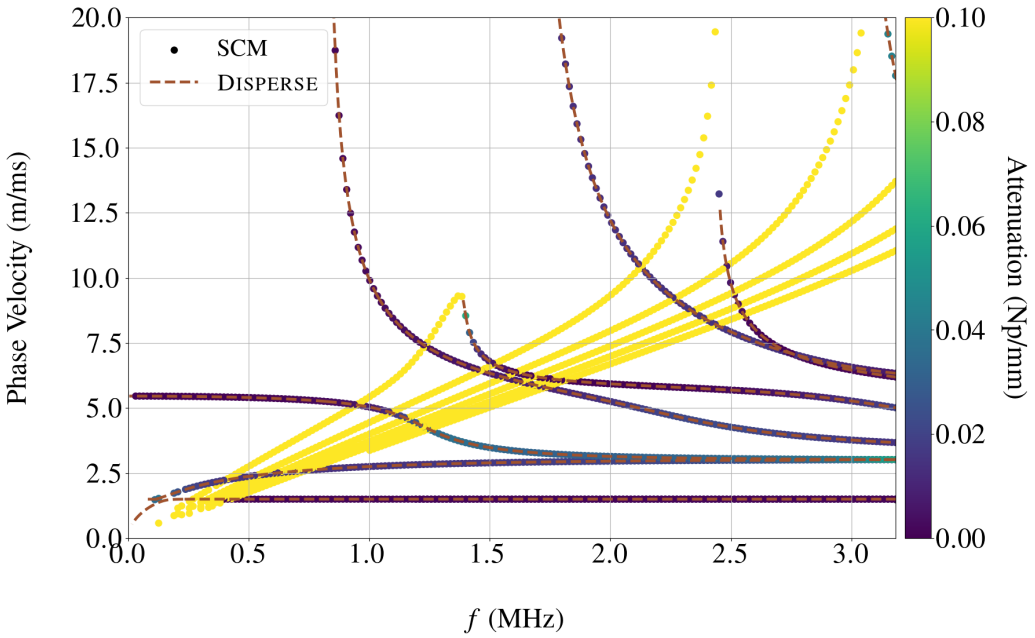

(a)

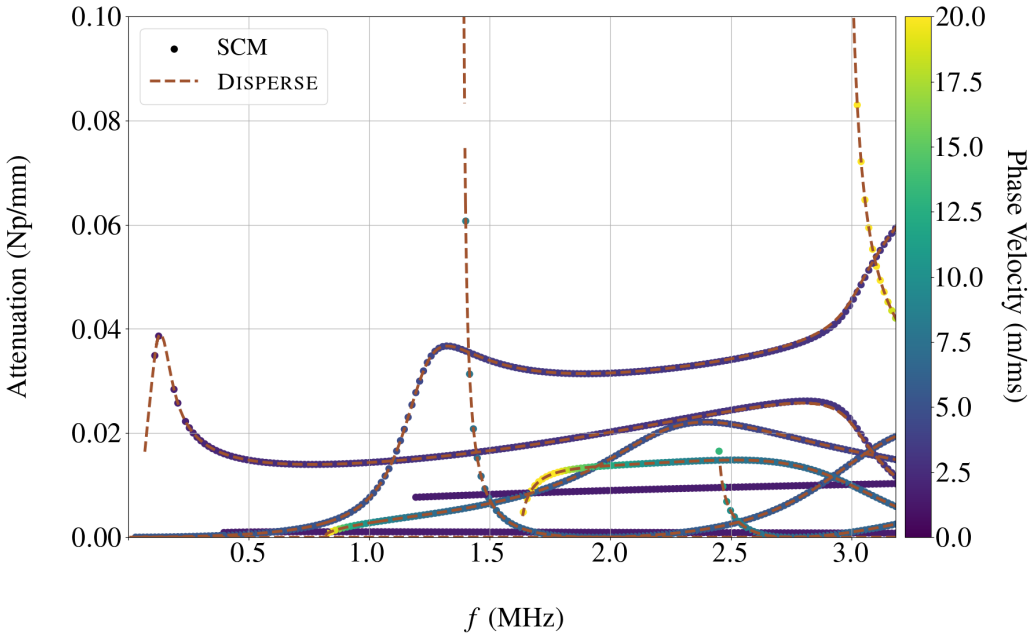

(b)

Figure 4.3: SCM phase velocity 4.3(a) and attenuation 4.3(b) curves for a steel annulus of small curvature immersed in fluid, respectively coloured based on their values of attenuation and phase velocity. Both are overlaid with curves from DISPERSE for a straight waveguide in contact with water on one side.

4.4.1.3 General Case

Having established confidence in the results of the method, the general case of leaky circumferential waves propagating around a submerged hollow cylinder is investigated next. Because DISPERSE results are not available for the general case, as a validation, consider the following approach: suppose that for a given frequency ω, one wishes to validate that a predicted wavenumber ν is a valid circumferential wave solution and recall that from Eq. (4.26), any valid solution pair (ω, ν) satisfies $\det[\boldsymbol{D}(\omega, \nu)] = 0$. To validate the prediction, a grid of points neighbouring ν is generated by slightly varying both its real and imaginary parts, and the value of $|\det[\boldsymbol{D}(\omega, \nu)]|$ is evaluated for all points on the grid. On a logarithmic scale, the surface obtained will diverge towards $-\infty$ if a zero of $\det[\boldsymbol{D}(\omega, \nu)]$ is close by. A contour plot representation of the surface will reveal whether a predicted solution is valid by whether or not it lies in such a divergent region.

In Figure 4.4, predicted SCM dispersion curves of leaky circumferential waves are presented alongside contour plot validations, for a steel cylinder of inner radius $a = 18$ mm, and outer radius $b = 20$ mm that is submerged in water. Dispersion curves were calculated on 100 frequency points in the angular frequency range $0 - 20$ MHz, with the computation taking approximately 1 minute in total.

The complete dispersion diagram is shown in Figure 4.4(a) and a detail of the linear frequency range $0 - 1.5$ MHz in Figure 4.4(b). In the zoomed-in region several leaky modes are observed converging towards the fluid wave speed, assumed 1.5 mm/ms. These modes arise due to the cylindrical geometry of the annulus, and even though, theoretically an infinity of them exists, only four are displayed here. The reason is that modes may not have fully converged, requiring additional collocation points for proper recovery, modes are highly attenuating and for that reason have been filtered out, or they

have cut-off frequencies beyond the frequency range displayed here. It is worth noting that at the flat waveguide limit of a cylinder of small curvature, these leaky modes vanish and only the surface Scholte mode persists.

Contour plots of the logarithm of $|\det[\boldsymbol{D}(\omega,\nu)]|$, evaluated in the vicinity of points marked in red boxes in Figures 4.4(a) and 4.4(b), are displayed in Figure 4.4(c) and Figure 4.4(d). Grids for both plots were generated by varying real and imaginary parts of wavenumber in 5×10^{-2} increments. In both instances, multiple SCM results can be seen to lie in divergent regions of the plot, indicating that they are indeed zeros of $\det[\boldsymbol{D}(\omega,\nu)]$, and thus valid solutions.

To illustrate the nature of complex wavenumber solutions for leaky circumferential waves, whose wave amplitudes vary with the transverse direction, θ, their fields are computed through Eqs. (4.4) and (4.6) and propagated around the annulus according to $e^{i\nu\theta}$. Figure 4.5 displays the field of two modes, annotated with black arrows in Figures 4.4(a) and 4.4(b). In Figure 4.5(a), the field of radial displacements of the mode at $(\omega, c_{r_c}) \approx (8.8\ \text{MHz}, 8.6\ \text{m/ms})$ are displayed as $\Re(u_r e^{i\nu\theta})$, while the field of azimuthal displacements of the mode at $(\omega, c_{r_c}) \approx (1.2\ \text{MHz}, 1.34\ \text{m/ms})$ are displayed in Figure 4.5(b) as $\Re(u_\theta e^{i\nu\theta})$. The scale of both fields is chosen to ensure unit radial displacements at the solid-fluid interface, i.e. $u_r(b) = 1$.

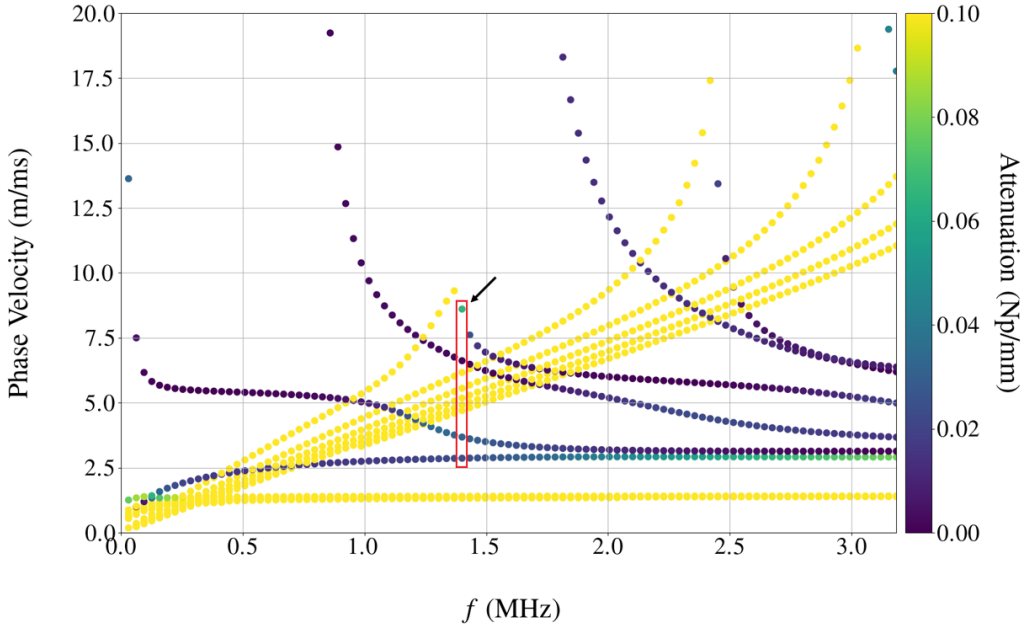
Phase Velocity (m/ms)
20.0
17.5
15.0
12.5
10.0
7.5
5.0
2.5
0.0
0.0
0.5
1.0
1.5
2.0
2.5
3.0
f (MHz)
Attenuation (Np/mm)
0.10
0.08
0.06
0.04
0.02
0.00

(a)

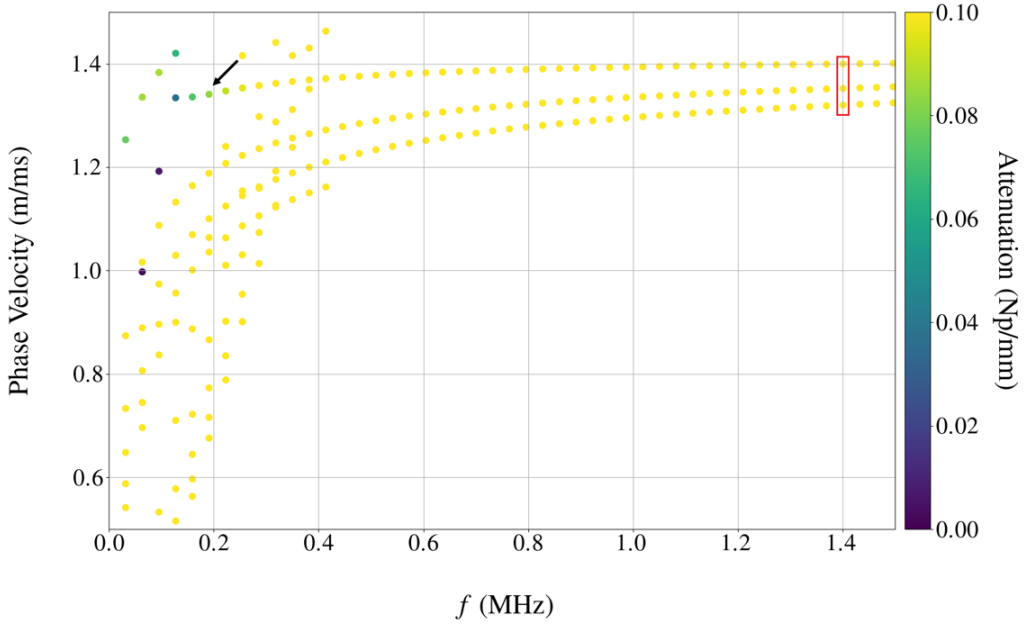
Phase Velocity (m/ms)
1.4
1.2
1.0
0.8
0.6
0.0
0.2
0.4
0.6
0.8
1.0
1.2
1.4
f (MHz)
Attenuation (Np/mm)
0.10
0.08
0.06
0.04
0.02
0.00

(b)

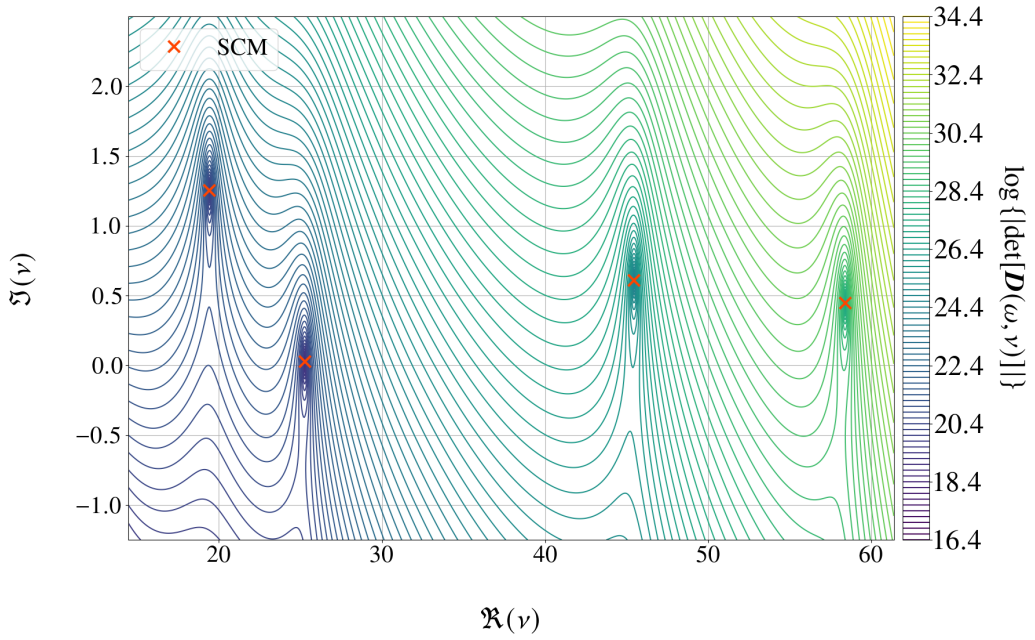

(c)

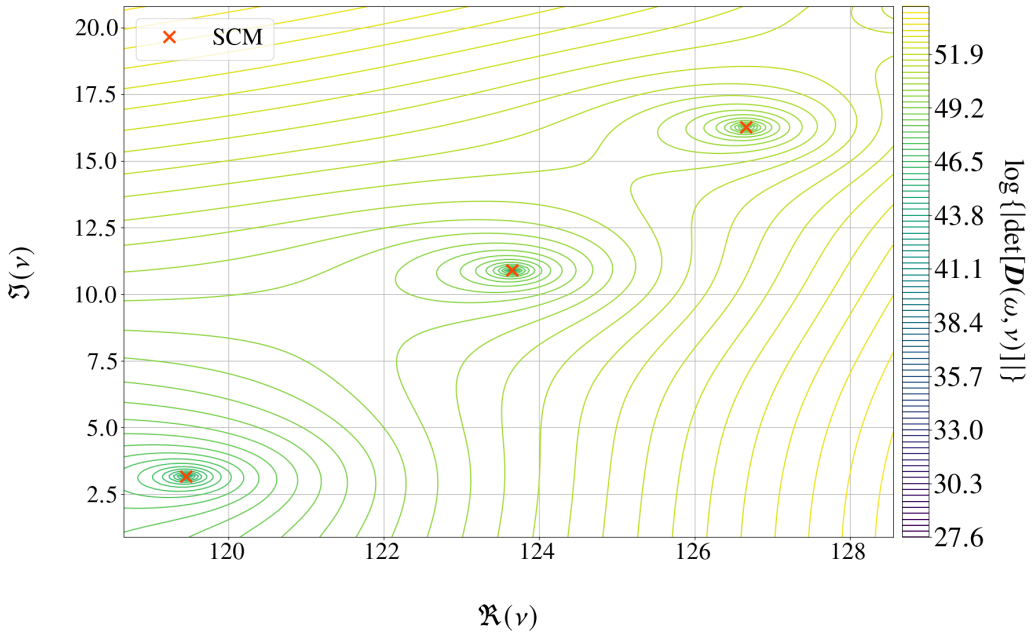

(d)

Figure 4.4: Phase velocity dispersion curves of circumferential waves in a steel annulus immersed in water 4.4(a), and a detail of the frequency region 0 – 1.5 MHz 4.4(b). Figures 4.4(c) and 4.4(d) present contour plots of the vicinity of predicted solutions marked in red boxes in 4.4(a) and 4.4(b) respectively.

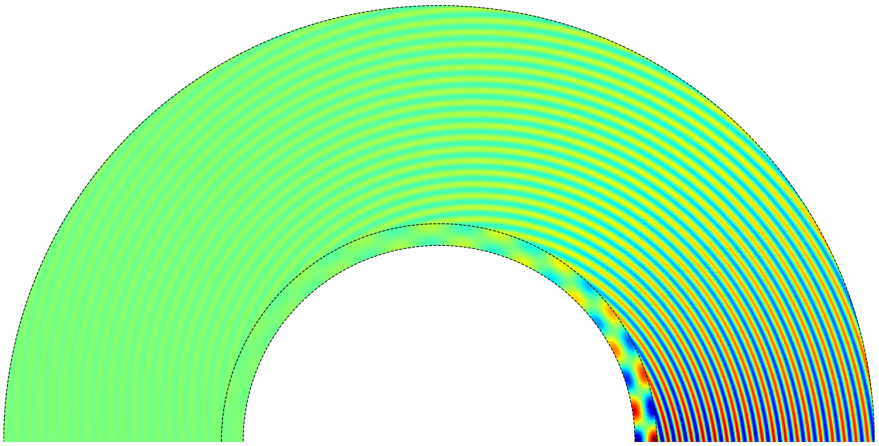

(a) $\omega = 8.8$ MHz, $c_{r_c} = 8.6$ m/ms

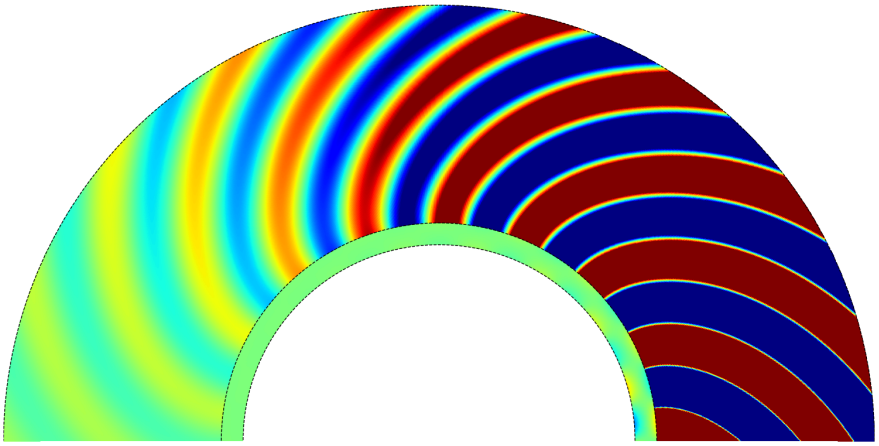

(b) $\omega = 1.2$ MHz, $c_{r_c} = 1.34$ m/ms

Figure 4.5: The field of leaky circumferential modes of complex wavenumbers for the solution pairs $(\omega, c_{r_c}) \approx (8.8 \text{ MHz}, 8.6 \text{ m/ms})$ in 4.5(a) and $(\omega, c_{r_c}) \approx (1.2 \text{ MHz}, 1.34 \text{ m/ms})$ in 4.5(b).

4.4.2 Complex Frequency

Having successfully computed complex wavenumber spectra of leaky circumferential waves, the proposed SCM is now employed for the computation of the real-wavenumber-versus-complex-frequency dispersion curves for the same steel hollow cylinder submerged in water from before. Computations are presented as dispersion curves of wavenumber against non-dimensional frequency, kb, and are again validated with contour plots of $|\det[\boldsymbol{D}(\omega,\nu)]|$.

When the wavenumber, ν is known, Eq. (4.44) is a generalised eigenvalue problem in ω^2, expressed as

$$L\boldsymbol{u} = \omega^2 \mathcal{M}\boldsymbol{u}, \tag{4.47}$$

where $L = \nu^2 L_2 + \nu L_1 + L_0$.

To retrieve the full set of dispersion curves, a wavenumber sweep, of positive integer wavenumbers up to $\nu = 100$, is performed, and the generalised eigenvalue problem of Eq. (4.47) is solved for ω, for each wavenumber of the sweep. The complex parameter, ζ_f, and number of collocation points in the two domains remain unchanged from the complex wavenumber problem of the previous section. To eliminate numerical artifacts, the model was, again, run twice, for N_f and $N_f/2$ collocation points in the fluid, and solutions were discarded if the non-dimensional frequency, kb, differed at the fifth decimal place between the two runs. Finally, only modes of $\Re(kb) \geq 0$ and $\Im(kb) \leq 0$ were kept. The dispersion curves presented in this section took approximately 8 seconds to compute (≈ 80 ms for each wavenumber).

Figure 4.6 presents the SCM dispersion curves of the complex frequency problem, as wavenumber versus the real part of the complex non-dimensional frequency kb, and a validation of those against contour plots of the logarithm of $|\det[\boldsymbol{D}(\omega,\nu)]|$. For the contour plots of Figure 4.6(b), the value

of $|\det[\boldsymbol{D}(\omega,\nu)]|$ was evaluated on a grid of non-dimensional frequencies, and fixed wavenumber $\nu = 10$. Again, predicted solutions can be seen to lie in divergent regions of the contour plot, validating them as true roots of $\det[\boldsymbol{D}(\omega,\nu)]$. Note that, just like for the leaky modes of Figure 4.4(b), some modes are missing from Figure 4.6(b), see divergent regions without SCM predictions; those modes are retrievable and satisfactorily converge when N_f is increased.

To illustrate the temporal amplitude variation of circumferential waves of complex frequencies, wave fields are computed and propagated in time in accordance to $e^{-i\omega t}$. Figure 4.7 depicts the exponentially growing field of radial displacements around the annulus and surrounding fluid, $\Re(u_r e^{-i\omega t})$, as it propagates through time, for the leaky wave annotated in Figure 4.6(a) at $\nu = 10$ and $\Re(kb) \approx 38$.

4.5 Conclusion

In this chapter a unified SCM was proposed for the computation of the dispersion curves of leaky circumferential waves, for both complex wavenumbers and frequencies, radiating from immersed hollow cylinders. A complex coordinate map transformed the leaky wave field in the surrounding fluid into a numerically decaying function in the complex plane, with the transformation preserving all the important physical characteristics of the original leaky wave field. This enabled the proposed SCM to effectively capture the complete set of leaky circumferential waves in the frequency and wavenumber ranges of interest.

The validation of the method was carried out initially through a comparison of two limiting cases of the structure – that of a weak fluid surrounding the annulus and that of an immersed annulus of small curvature – against

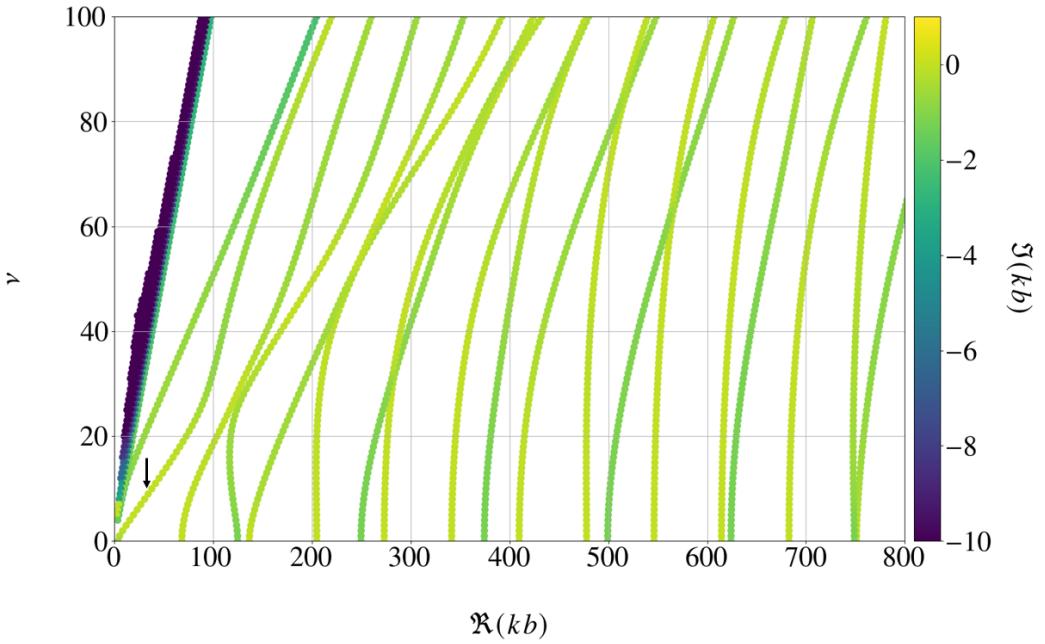

(a)

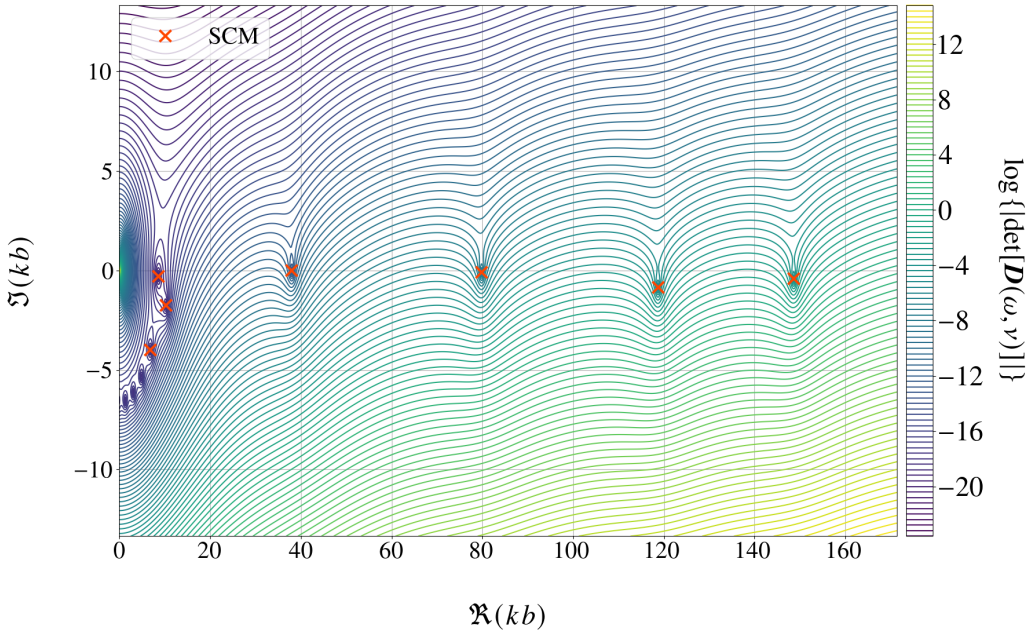

(b)

Figure 4.6: Dispersion curves of wavenumber against the real part of non-dimensional frequency, $\Re(kb)$, in 4.6(a), and a contour plot validation of pairs (ω, ν), for $\nu = 10$, in 4.6(b).

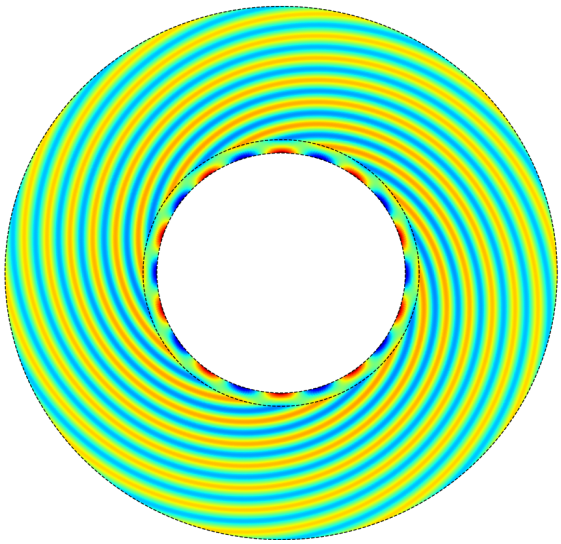

(a) $t = 0\ \mu s$

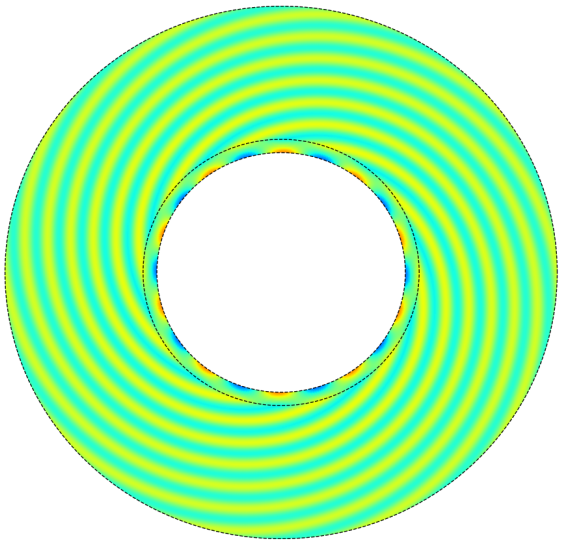

(b) $t = 500\ \mu s$

Figure 4.7: The wave field of the leaky circumferential wave of complex frequency at $\nu = 10$, and $\Re(kb) \approx 38$ from Figure 4.6(a), propagated 500 μs in time.

dispersion curves from DISPERSE. Subsequently, the general case of leaky circumferential waves, for both complex wavenumbers and complex frequencies, was carried with a comparison against analytic formulations.

While this chapter only investigated leaky circumferential waves radiating from submerged hollow cylinders made of isotropic material, the SCM presented here is believed to be a simple yet powerful tool for the effective computation of dispersion curves in cylindrical geometries and lays the foundations for a black-box approach to solving more complicated systems. The proposed methodology should readily extend to fluid-filled cylinders, shear waves that have their displacements in the axial direction, multilayered cylinders made of anisotropic materials and cylinders embedded in solids.

Chapter 5

Underwater Scattering from Submerged Elastic Hollow Cylinders

5.1 Introduction

Thus far, the modal responses of systems were investigated, i.e. no external forcing was ever present. However, in real life applications immersed or embedded objects are often studied based on their response to incoming waves; the dispersion curves of the object are closely related with its responses to wave fields that emerge from distant sources and are incident upon it, with useful insight into the object's characteristics and material properties being retrievable from the scattered field. To that end, in this chapter, the interactions between incoming waves and the immersed elastic cylinder introduced in Chapter 4 are investigated.

Resonance scattering theory [131] suggests that information about the im-

mersed structure's resonances, i.e. its dispersion curves, lie in the scattered field echoes. The study of that response has been the focus of the work of many, with the literature on scattering problems spanning over a decade and a range of applications. Gaunaurd [132] provides an excellent report on the advances in the field over the last century. Some notable contributions concerning spherical and cylindrical scatterers are those of Faran [133] for elastic scatterers in fluid, of Einspruch and Truell [134] for fluid scatterers in solids, and more recently of Sun and Marston [135] on leaky wave contributions to the backscattering from thick cylindrical shells and of Marston [136] on the scattering of a Bessel beam by a sphere.

As attested by an extensive literature on the field, being able to compute the response of a known scatterer, or inversely, distinguish one scatterer from another by interpreting a monitored response, remain longstanding challenges of both scientific and industrial interest. For objects of simple geometries, like spheres or cylinders, the computation of the scattered field involves the numerical solution of matrix equations of Bessel functions that result from assuming analytic forms for the unknown wave fields of the problem and applying boundary conditions [121,132,137,138]. Unfortunately, the numerical instabilities associated with Bessel functions one encounters when computing leaky circumferential wave dispersion curves, which were discussed in Chapter 4, also extend to the analytic matrix formulations of scattering problems.

This chapter is dedicated to overcoming these challenges for elastic cylindrical scatterers in fluid. The similarities in the underlying physics, i.e. the equations of motion and boundary conditions, between the propagation of leaky circumferential waves in an immersed cylindrical structure and the response of the same structure when viewed as a sound scatterer subjected to an incident wave field will be exploited. Owning to those similarities, the SCM presented in Chapter 4 for the dispersion curve computations of the former

problem will be tailored to the scattered field computations of the latter; computations will be validated against analytic formulations. Finally, resonance scattering theory will enable the decomposition of the scattered field into its constituent components and the relationship between the dispersion curves of the structure and the field scattered by it to be demonstrated.

The chapter is organised as follows: Section 5.2 presents the theoretical framework and analytic formulations of the scattering response problem for an elastic hollow cylinder subjected to incident acoustic waves, while Section 5.3 presents how the SCM for leaky circumferential wave computations is modified for scattered field computations. The chapter concludes by presenting and validating results in Section 5.4 and a discussion on key findings and future work in Section 5.5.

5.2 Theory

5.2.1 Problem Statement

Consider a hollow cylinder submerged in inviscid fluid and an incoming plane wave of known angular frequency, ω, that is incident upon the cylinder at an angle θ_{inc} and is perpendicular to the axis of the cylinder (broadside). Assume the geometry and material properties of the system to be the same as those considered in Chapter 4. A schematic of the forced system, depicting the cross-section of the hollow cylinder and the incoming wave field, is given in Figure 5.1.

Assuming again two-dimensional, time-harmonic waves of angular wavenumber ν, denote the displacement field in the annulus by $\boldsymbol{u_c} = (u_r, u_\theta, 0)$ and that in the fluid by $\boldsymbol{u_f} = (u_{r_f}, u_{\theta_f}, 0)$. In both fields, a common exponential term $\exp[i(\nu\theta - \omega t)]$, is assumed and suppressed and the Helmholtz decom-

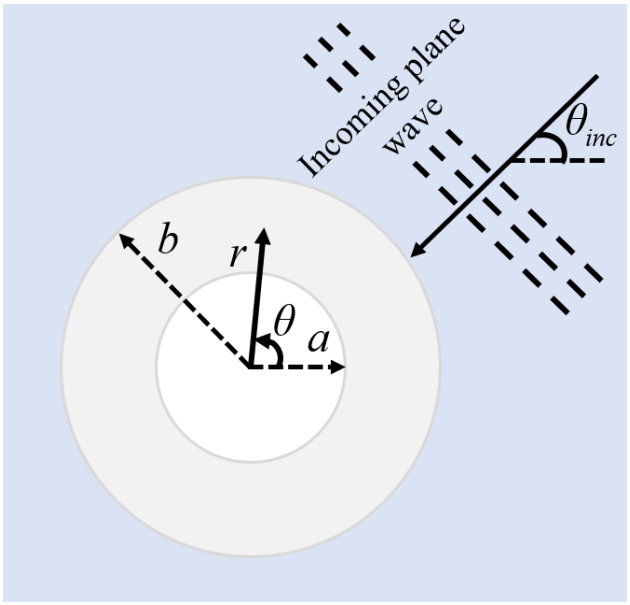

Figure 5.1: Incoming plane waves incident upon an annulus of inner radius a and outer radius b, immersed in fluid.

position of Eqs. (4.4) and (4.6), in terms of the elastic wave potentials ϕ and Ψ in the annulus and the wave potential ϕ_f in the fluid, is applied.

The field in the surrounding fluid, ϕ_f, is now composed of two parts for the forced problem – the incoming wave field and the field scattered by the immersed annulus. Thus, the forcing imposed upon the system by the incoming wave is incorporated into the fluid wave potential through its decomposition as

$$\phi_f = \phi_{\text{sc}} + \phi_{\text{inc}}, \tag{5.1}$$

where, ϕ_{sc} and ϕ_{inc} are the wave potentials of the scattered and incoming wave fields respectively.

The incoming plane wave's pressure field may be expressed [121, 133] as a

sum of normal modes as

$$\begin{aligned} p_{\text{inc}}(r,\theta) &= A_{\text{inc}} \exp\left[-ikr\cos(\theta-\theta_{\text{inc}})\right] \\ &= A_{\text{inc}} \sum_{\nu=-\infty}^{\infty} (-i)^{|\nu|} J_{|\nu|}(kr) \exp\left[i\nu(\theta-\theta_{\text{inc}})\right], \end{aligned} \tag{5.2}$$

with A_{inc} a predefined pressure amplitude and the exponential $e^{-i\omega t}$ assumed throughout. Each term of the incoming pressure field sum given above is the incoming pressure field of the ν^{th} normal mode; the corresponding incoming wave potential is expressed in terms of the incoming wave pressure field as $\phi_{\text{inc}} = -p_{\text{inc}}/(\rho_f \omega^2)$, with ρ_f the density of the fluid.

Since the geometry and material properties of the system remain identical to those studied earlier, the fields in the elastic annulus and the surrounding fluid of the forced system must still satisfy the same wave equations, Eqs. (4.7)-(4.9), and boundary and interface conditions, Eqs. (4.10) and (4.11), for stresses given by Eqs. (4.15)-(4.17).

By substituting Eq. (5.1) into Eq. (4.9), the fluid equation of motion for the forced system is expressed in terms of the incoming and scattered fluid potentials as

$$\left(\frac{\partial^2}{\partial r^2} + \frac{1}{r}\frac{\partial}{\partial r} - \frac{\nu^2}{r^2}\right)\phi_{\text{sc}} + \frac{\omega^2}{c_f^2}\phi_{\text{sc}} = -\left(\frac{\partial^2}{\partial r^2} + \frac{1}{r}\frac{\partial}{\partial r} - \frac{\nu^2}{r^2}\right)\phi_{\text{inc}} - \frac{\omega^2}{c_f^2}\phi_{\text{inc}}, \tag{5.3}$$

and similarly for the stresses and displacements in the fluid

$$\sigma_{r_f} = \lambda_f \left(\frac{\partial^2}{\partial r^2} + \frac{1}{r}\frac{\partial}{\partial r} - \frac{\nu^2}{r^2}\right)(\phi_{\text{sc}} + \phi_{\text{inc}}), \tag{5.4}$$

$$u_{r_f} = \frac{\partial}{\partial r}(\phi_{\text{sc}} + \phi_{\text{inc}}), \quad u_{\theta_f} = \frac{i\nu}{r}(\phi_{\text{sc}} + \phi_{\text{inc}}). \tag{5.5}$$

Under this notation, the interface conditions of Eq. (4.11) may explicitly be

expressed in terms of the wave potentials in the annulus and the scattered and incoming wave potentials in the fluid as

$$\left[2\nu\left(\frac{1}{r^2}-\frac{1}{r}\frac{\partial}{\partial r}\right)\phi+\left(\frac{\partial^2}{\partial r^2}-\frac{1}{r}\frac{\partial}{\partial r}+\frac{\nu^2}{r^2}\right)\psi\right]\Bigg|_{r=b}=0, \tag{5.6}$$

$$\begin{aligned}\left\{\left[\kappa^2\frac{\partial^2}{\partial r^2}+(\kappa^2-2)\left(\frac{1}{r}\frac{\partial}{\partial r}-\frac{\nu^2}{r^2}\right)\right]\phi+2\nu\left(\frac{1}{r^2}-\frac{1}{r}\frac{\partial}{\partial r}\right)\psi\right.\\ \left.-\frac{\lambda_f}{\mu}\left(\frac{\partial^2}{\partial r^2}+\frac{1}{r}\frac{\partial}{\partial r}-\frac{\nu^2}{r^2}\right)\phi_{\rm sc}\right\}\Bigg|_{r=b}=\left[\frac{\lambda_f}{\mu}\left(\frac{\partial^2}{\partial r^2}+\frac{1}{r}\frac{\partial}{\partial r}-\frac{\nu^2}{r^2}\right)\phi_{\rm inc}\right]\Bigg|_{r=b},\end{aligned} \tag{5.7}$$

$$\left[\frac{\partial\phi}{\partial r}-\frac{\nu}{r}\psi-\frac{\partial\phi_{\rm sc}}{\partial r}\right]\Bigg|_{r=b}=\left[\frac{\partial\phi_{\rm inc}}{\partial r}\right]\Bigg|_{r=b}. \tag{5.8}$$

The equations of motion, Eqs. (4.7),(4.8) and (5.3) are Bessel equations and, subject to amplitudes determined by the boundary and interface conditions of Eqs. (4.18), (4.19) and (5.6)-(5.8), admit solutions of the form [121]

$$\phi=\sum_{\nu=-\infty}^{\infty}A_\nu J_{|\nu|}(k_l r)+B_\nu Y_{|\nu|}(k_l r), \tag{5.9}$$

$$\psi=\sum_{\nu=-\infty}^{\infty}C_\nu J_{|\nu|}(k_t r)+D_\nu Y_{|\nu|}(k_t r), \tag{5.10}$$

$$\phi_{\rm sc}=\sum_{\nu=-\infty}^{\infty}E_\nu H_{|\nu|}(kr)\,. \tag{5.11}$$

Due to the linearity of the formulation, the scattering problem may be solved for each normal mode individually. That is, for an incoming plane wave of known frequency ω one may run over each ν and term in the sum of Eq. (5.2) and compute the corresponding terms of sums in Eqs. (5.9)-(5.11). The potential fields of Eqs. (5.9)-(5.11) are then retrieved by summing over the contributions of normal modes for all ν.

Similarly to what was done in Eq. (4.26), by substituting the exact form of

the wave potentials of normal modes in the boundary and interface conditions of Eqs. (4.18), (4.19) and (5.6)-(5.8), an analytic formulation of the forced problem is achieved, expressed as the matrix equation

$$\boldsymbol{D}(\omega,\nu)\boldsymbol{A}_\nu = \boldsymbol{F}_\nu, \tag{5.12}$$

with $\boldsymbol{D}(\omega,\nu)$ the matrix of Eq. (4.26) whose entries are given in Appendix B, $\boldsymbol{A}_\nu = [A_\nu, B_\nu, C_\nu, D_\nu, E_\nu]^T$ a vector of the amplitudes to be computed, and $\boldsymbol{F}_\nu$ a column vector of forcing terms, explicitly given as

$$\boldsymbol{F}_\nu = -A_{\text{inc}}(-i)^{|\nu|}(\rho_f\omega^2)^{-1}\begin{pmatrix} 0 \\ 0 \\ 0 \\ \frac{\lambda_f}{\mu}\left[k^2 J''_{|\nu|}(kb) + \frac{k}{b}J'_{|\nu|}(kb) - \frac{\nu^2}{b^2}J_{|\nu|}(kb)\right] \\ kJ'_{|\nu|}(kb) \end{pmatrix}. \tag{5.13}$$

In the above, $'$ denotes differentiation with respect to the radial direction, r. The non-zero terms of $\boldsymbol{F}_\nu$ are exactly the contributions of the incoming wave potential in the stresses and displacements, σ_{rf} and u_{rf}, of Eqs. (5.4) and (5.5), that appear on the RHS of the last two interface condition equations of Eqs. (5.7) and (5.8). If no forcing is present, i.e. $A_{\text{inc}} = 0$, then $\boldsymbol{F}_\nu = \boldsymbol{0}$ and the scattering equation of Eq. (5.13) reduces to the resonance equation of Eq. (4.26).

Notice that because both ω and integer ν are assumed known for each normal mode of the forced problem, the analytic formulation of Eq. (5.12) presents a set of simultaneous equations from which the amplitudes vector of the ν^{th} normal mode can be retrieved as $\boldsymbol{A}_\nu = \boldsymbol{D}^{-1}(\omega,\nu)\boldsymbol{F}_\nu$. This analytic formulation will be used as a benchmark for the validation of SCM computations to follow.

5.2.2 Resonance Scattering Theory

Resonance scattering theory [131] states that in the acoustic far-field, $r \gg b^2/\lambda$ with λ the wavelength of bulk waves in fluid, the pressure field scattered by an immersed object contains insight into the characteristics of the scatterer itself, and is therefore what is ultimately sought in this study. In this section, ideas from resonance scattering theory, that will allow the relationship between the dispersion curves and the scattered field response of an immersed object to be established, are reproduced from [121, 138] in the notation of this thesis.

When a penetrable object acts as a sound scatterer subjected to an incident wave field, elastic or acoustic energy penetrates into the scatterer when the incident field's frequency passes through a frequency interval centred at the scatterer's resonance frequencies [132]. For the immersed annulus of interest in this study, those resonance frequencies are the complex frequencies of leaky circumferential waves studied in Chapter 4, while the width of each frequency interval is dependent on the strength of the coupling between the scatterer and its surroundings [139] and is proportional to the imaginary part of the complex frequency of the resonance [138, 140]. Away from resonance frequencies, the body behaves as perfectly impenetrable, e.g. an elastic object immersed in fluid behaves as if it were rigid or a fluid-filled cavity in an elastic matrix behaves as if it were empty.

This behaviour underpins an immersed penetrable object's response to an incident wave field, i.e. the field scattered by the object, which may be decomposed into two distinct components: a background that is smoothly varying with frequency and would be present were the immersed object impenetrable, and a resonant component that is superimposed upon the smooth background and contains a number of resonance peaks coinciding with the resonances or eigenfrequencies of the immersed object. Resonance scattering theory allows

the resonance spectrum of the scatterer to be studied separately by removing the smooth impenetrable scatterer background from the scattered field response of the object.

To do so, consider first scattering from impenetrable scatterers in fluid. An impenetrable scatterer is assumed a perfect reflector that does not absorb energy. The simplest impenetrable scatterers possible are the two extreme cases of a sound-soft (zero acoustic and shear impedance) and a sound-hard (infinite acoustic and shear impedance) scatterer. For a sound-soft scatterer, the total pressure field vanishes at the boundary, while for a sound-hard scatterer, the radial derivative of the fluid wave potential, i.e. radial displacement, vanishes at the boundary. Expressed mathematically one has [121]

$$\phi_f\Big|_{r=b} = 0, \qquad \text{for sound-soft scatterers,} \tag{5.14}$$

$$\frac{\partial \phi_f}{\partial r}\bigg|_{r=b} = 0, \qquad \text{for sound-hard scatterers,} \tag{5.15}$$

and it follows that for the incident plane wave under consideration here, the scattered field amplitudes from soft and hard scatterers, say $E_\nu^{(\mathrm{s})}$ and $E_\nu^{(\mathrm{h})}$, are

$$E_\nu^{(\mathrm{s})} = A_{\mathrm{inc}}(-i)^{|\nu|}(\rho_f\omega^2)^{-1}\frac{J_{|\nu|}(kb)}{H_{|\nu|}(kb)}, \tag{5.16}$$

$$E_\nu^{(\mathrm{h})} = A_{\mathrm{inc}}(-i)^{|\nu|}(\rho_f\omega^2)^{-1}\frac{J'_{|\nu|}(kb)}{H'_{|\nu|}(kb)}. \tag{5.17}$$

The field scattered from the elastic annulus may then be separated into the contributions of the resonance spectrum and those of a sound-soft or sound-hard background, through the scattered field amplitudes of normal modes. The ν^{th} normal mode's resonant spectrum amplitudes are retrieved here by removing the sound-soft or sound-hard background amplitudes from the am-

plitudes of the field scattered by the elastic scatterer, E_ν, through [141]

$$E_\nu^{(\mathrm{res})} = 2\frac{E_\nu - E_\nu^{(\mathrm{s})}}{1 + 2E_\nu^{(\mathrm{s})}}, \quad \text{or} \quad E_\nu^{(\mathrm{res})} = 2\frac{E_\nu - E_\nu^{(\mathrm{h})}}{1 + 2E_\nu^{(\mathrm{h})}}. \tag{5.18}$$

As the behaviour of scattered spectra in the acoustic far-field is of interest here, the Hankel functions of Eq. (5.11) are replaced with their asymptotic approximations for large arguments from Eq. (4.34). This allows the pressure field scattered by the elastic annulus, $p_{\mathrm{sc}} = -\rho_f \omega^2 \phi_{\mathrm{sc}}$, to be approximated as

$$p_{\mathrm{sc}} \approx \frac{D(\omega,\theta)\exp(ikr)}{\sqrt{r}}, \text{ for } r \to \infty, \tag{5.19}$$

with $D(\omega,\theta)$ the directivity of the scattered pressure field given as a function of angular frequency and azimuthal direction. In the above, the directivity $D(\omega,\nu)$, is given explicitly as a sum of normal mode directivities, $D_\nu(\omega,\theta)$, as

$$D(\omega,\theta) = \sum_{\nu=-\infty}^{\infty} D_\nu(\omega,\theta), \tag{5.20}$$

where

$$D_\nu(\omega,\theta) = -\rho_f \omega^2 E_\nu \sqrt{\frac{2}{\pi k}} \exp\left[-i\left(\frac{1}{2}|\nu|\pi + \frac{1}{4}\pi\right)\right] \exp\left[i\nu(\theta - \theta_{\mathrm{inc}})\right]. \tag{5.21}$$

In an analogous way, a directivity of the resonance spectrum may be defined and expressed as a sum of normal mode resonance directivities as

$$D^{(\mathrm{res})}(\omega,\theta) = \sum_{\nu=-\infty}^{\infty} D_\nu^{(\mathrm{res})}(\omega,\theta), \tag{5.22}$$

with the $D_\nu^{(\mathrm{res})}(\omega,\theta)$ obtained by replacing the scattered wave amplitudes, E_ν in Eq. (5.21) with the resonant amplitudes, $E_\nu^{(\mathrm{res})}$ of Eq. (5.18).

These directivities hold all the important characteristics of the scattered field

and the elastic scatterer, and to compute them for a pair of frequency and angle the infinite sums of Eqs. (5.20) and (5.22) are approximated with finite ones. Specifically, sums are truncated so that the wavenumber ν ranges between $-M$ and M, where M is chosen sufficiently large to ensure the convergence of the sum. For every term of the truncated sum and integer wavenumber ν, the amplitudes of the scattered and resonance fields of the ν^{th} normal mode, E_ν and $E_\nu^{(\text{res})}$, are calculated. Directivities are then computed by summing over all normal mode directivities of the truncated sum. The procedure is repeated for multiple frequencies and angles of interest, with results typically [121] presented as target strength plots, in decibels, on a logarithmic scale.

5.3 Discretisation

A spectral collocation discretisation that enables the computation of the unknown scattered field amplitudes and desired directivities of the response problem is presented next. It was already demonstrated how the response problem investigated here is closely related to the problem of leaky circumferential waves of Chapter 4; one may obtain the unforced leaky wave problem by simply setting $A_{\text{inc}} = 0$ in the forced problem. In the discussion to follow, this relationship between the two problems is exploited and the SCM developed for the computation of leaky circumferential waves of complex wavenumbers is tailored to the computation of the scattered field response from submerged hollow cylinders. Finally, it will further be demonstrated how the discretisation may be reduced to a more efficient boundary value problem, when both wavenumber and frequency are assumed known.

Start by fixing both real ω and integer ν, and assume that the incoming pressure field is that of the ν^{th} normal mode, given by the ν^{th} term in the sum

of Eq. (5.2); denote this incoming pressure field, and corresponding incoming wave potential, by p^{ν}_{inc} and ϕ^{ν}_{inc} respectively. Under this notation,

$$\phi^{\nu}_{\text{inc}} = -A_{\text{inc}}(-i)^{|\nu|}(\rho_f\omega^2)^{-1}J_{|\nu|}(kr)\exp[i\nu(\theta-\theta_{\text{inc}})]. \tag{5.23}$$

For the incoming wave of Eq. (5.23), one is interested in computing the wave potentials

$$\phi^{\nu} = A_{\nu}J_{|\nu|}(k_l r) + B_{\nu}Y_{|\nu|}(k_l r), \tag{5.24}$$

$$\psi^{\nu} = C_{\nu}J_{|\nu|}(k_t r) + D_{\nu}Y_{|\nu|}(k_t r), \tag{5.25}$$

$$\phi^{\nu}_{\text{sc}} = E_{\nu}H_{|\nu|}(kr), \tag{5.26}$$

of the ν^{th} normal mode, given by the ν^{th} term in each of the sums of Eqs. (5.9)-(5.11).

To compute those wave potentials, the SCM of Section 4.3 for both the immersed annulus and the fluid space is adopted here. Under the discretisation presented in that section, Eq. (4.29) gives the first and second order differentiation matrices, based on Chebyshev collocation points, over the annular cross-section of the cylinder, while Eqs. (4.31) and (4.32) give the differentiation matrices in the fluid. Of course, the choice of complex ζ_f is again important here as it defines a complex path, say $\mathbb{C}^{\nu}_f$, in which the fluid wave potentials of the problem, ϕ^{ν}_{sc} and ϕ^{ν}_{inc}, are made to numerically decay while also preserving their amplitudes and wavenumber.

As done previously, consider the problem in terms of the decaying complex wave potentials $\tilde{\phi}^{\nu}_{\text{sc}}$ and $\tilde{\phi}^{\nu}_{\text{inc}}$, and utilise differentiation matrices to discretise the equations of motion of the forced problem, Eqs. (4.7), (4.8) and (5.3).

The resulting matrix equation reads

$$\begin{pmatrix} L_\phi & 0 & 0 \\ 0 & L_\Psi & 0 \\ 0 & 0 & L_{\phi_f} \end{pmatrix} \begin{pmatrix} \boldsymbol{\phi}^\nu \\ \boldsymbol{\Psi}^\nu \\ \tilde{\boldsymbol{\phi}}^\nu_{\text{sc}} \end{pmatrix} = - \begin{pmatrix} 0 & 0 & 0 \\ 0 & 0 & 0 \\ 0 & 0 & L_{\phi_f} \end{pmatrix} \begin{pmatrix} \mathbf{0} \\ \mathbf{0} \\ \tilde{\boldsymbol{\phi}}^\nu_{\text{inc}} \end{pmatrix}, \tag{5.27}$$

where L_ϕ, L_Ψ and L_{ϕ_f} are exactly the $N \times N$ operators of Eqs. (4.38)-(4.40) and

$$\boldsymbol{u}_{\text{sc}} = \begin{pmatrix} \boldsymbol{\phi}^\nu \\ \boldsymbol{\Psi}^\nu \\ \tilde{\boldsymbol{\phi}}^\nu_{\text{sc}} \end{pmatrix} \quad \text{and} \quad \boldsymbol{u}_{\text{inc}} = \begin{pmatrix} \mathbf{0} \\ \mathbf{0} \\ \tilde{\boldsymbol{\phi}}^\nu_{\text{inc}} \end{pmatrix}, \tag{5.28}$$

are column vectors of length $3N$, containing the wave potentials in the annulus and the complex scattered and incoming wave potentials in $\mathbb{C}^\nu_f$, each evaluated on the collocation points discretising their domains of definition.

The boundary and interface conditions of Eqs. (4.18), (4.19) and (5.6)- (5.8), are similarly discretised and represented by two matrix equations as

$$BC\boldsymbol{u}_{\text{sc}} = \mathbf{0}, \tag{5.29}$$

$$IC\boldsymbol{u}_{\text{sc}} = -IC\boldsymbol{u}_{\text{inc}}, \tag{5.30}$$

with BC, IC the boundary and interface conditions matrices of Eqs. (4.42) and (4.43).

To impose boundary and interface conditions to the discrete problem, rows $1, N+1$ and $N, 2N, 2N+1$ of each of the two operators acting on the column vectors $\boldsymbol{u}_{\text{sc}}$ and $\boldsymbol{u}_{\text{inc}}$ in Eq. (5.27) are, respectively, replaced by rows of the boundary and interface condition operators of Eqs. (5.29) and (5.30) which are acting on the same column vectors. To ensure the vanishing of the wave field, Dirichlet zero boundary conditions are again imposed at the collocation

point at infinity. After rearranging, the resulting equation reads

$$\left(L - \omega^2 \mathcal{M}\right) \boldsymbol{u}_{\text{sc}} = \boldsymbol{P}, \tag{5.31}$$

where L and $\mathcal{M}$ are the matrix operators introduced in Eq. (4.47) and $\boldsymbol{P}$ is a column vector of $3N$ entries. Column vector $\boldsymbol{P}$ is zero everywhere except at its last N entries which contain the RHS of Eq. (5.3), evaluated on the set of the N collocation points in the complex interval $\mathbb{C}_f^{\nu}$, and at rows $1, N+1$ and $N, 2N, 2N+1$ which were replaced with the contributions of the incoming wave potential in the boundary and interface conditions of Eqs. (4.18), (4.19) and (5.6)-(5.8). Column vector $\boldsymbol{P}$ is effectively the forcing vector of the discrete problem.

Since both wavenumber and frequency are fixed here, Eq. (5.31) is no longer an eigenvalue problem; it is rather a set of simultaneous equations which allows the retrieval of the field in the annulus and the fluid, and consequently the amplitudes $\boldsymbol{A}_{\nu}$, as $\boldsymbol{u}_{\text{sc}} = \left(L - \omega^2 \mathcal{M}\right)^{-1} \boldsymbol{P}$. By sweeping through a range of frequencies, each time calculating the amplitudes $\boldsymbol{A}_{\nu}$ for all integer wavenumbers between $\pm M$, the directivity, $D(\omega, \theta)$, can be computed for any given angle of interest as a sum of normal mode directivities.

Even though the presented discretisation fully encapsulates the problem, its efficiency may be improved by making some adjustments. Since an exact form for the incoming wave potential is assumed, analytical expressions for

its derivatives with respect to the radial direction may be obtained as

$$\frac{\partial \phi^{\nu}_{\text{inc}}}{\partial r} = -\frac{kA_{\text{inc}}(-i)^{|\nu|}(\rho_f \omega^2)^{-1}}{2}\left[J_{|\nu|-1}(kr) - J_{|\nu|+1}(kr)\right] \times \exp\left[i\nu(\theta - \theta_{\text{inc}})\right], \tag{5.32}$$

$$\frac{\partial^2 \phi^{\nu}_{\text{inc}}}{\partial r^2} = -\frac{k^2 A_{\text{inc}}(-i)^{|\nu|}(\rho_f \omega^2)^{-1}}{4}\left[J_{|\nu|-2}(kr) - 2J_{|\nu|}(kr) + 2J_{|\nu|+2}(kr)\right] \times \exp\left[i\nu(\theta - \theta_{\text{inc}})\right]. \tag{5.33}$$

Evaluating Eqs. (5.32) and (5.33) on the set of collocation points in the fluid avoids the need of approximating the potential's derivatives with differentiation matrices – this is particularly helpful when computing the non-zero entries of $\boldsymbol{P}$. It is important to recognise that this would not have been possible if Eq. (5.31) was an eigenvalue problem. If complex ν or ω, which respectively appear in the order and the argument of the Bessel functions of Eq. (5.2), were to be solved for, a non-linear eigenvalue problem would emerge, compromising the discretisation.

In a similar way, the exact form of the scattered field from Eq. (5.26) may also be assumed and an exact form for its derivatives be obtained as

$$\frac{\partial \phi^{\nu}_{\text{sc}}}{\partial r} = \frac{kE_{\nu}}{2}\left[H_{|\nu|-1}(kr) - H_{|\nu|+1}(kr)\right]\exp\left[i\nu(\theta - \theta_{\text{inc}})\right], \tag{5.34}$$

$$\frac{\partial^2 \phi^{\nu}_{\text{sc}}}{\partial r^2} = \frac{k^2 E_{\nu}}{4}\left[H_{|\nu|-2}(kr) - 2H_{|\nu|}(kr) + 2H_{|\nu|+2}(kr)\right] \times \exp\left[i\nu(\theta - \theta_{\text{inc}})\right], \tag{5.35}$$

eliminating the need to approximate scattered field derivatives with differentiation matrices. Under these assumptions, there is no longer a need to approximate any derivatives in the fluid domain as all derivatives can explicitly be evaluated through Eqs. (5.32)-(5.35).

What is more, by assuming their exact forms, the scattered and incoming

fields are fully determined by their amplitudes, A_{inc} and E_ν. Those amplitudes are computed through the interface conditions at the solid-fluid interface, and placing a single collocation point at the solid-fluid interface, upon which interface conditions are imposed, enables the computation of the unknown amplitudes and fully captures fluid motion. Thus, assuming exact forms for the fluid wave potentials and placing a single collocation point at the interface at $r = b$, circumvents the discretisation of the fluid domain altogether, and casts the problem of Eq. (5.31) onto a boundary value problem of the form

$$\left(\tilde{L} - \omega^2 \tilde{\mathcal{M}}\right) \tilde{\boldsymbol{U}}_{\text{sc}} = \tilde{\boldsymbol{P}}, \tag{5.36}$$

with

$$\tilde{\boldsymbol{u}}_{\text{sc}} = \begin{pmatrix} \boldsymbol{\phi}^\nu \\ \boldsymbol{\psi}^\nu \\ E_\nu \end{pmatrix}, \tag{5.37}$$

$$\tilde{\boldsymbol{P}} = -A_{inc}(-i)^{|\nu|}\left(\rho_f \omega^2\right)^{-1} \begin{pmatrix} 0 \\ \vdots \\ 0 \\ \frac{\lambda_f}{\mu}\left[k^2 J''_{|\nu|}(kb) + \frac{k}{b} J'_{|\nu|}(kb) - \frac{\nu^2}{b^2} J_{|\nu|}(kb)\right] \\ k J'_{|\nu|}(kb) \end{pmatrix} \tag{5.38}$$

two column vectors of $2N + 1$ entries and $\tilde{L}, \tilde{\mathcal{M}}$ matrix operators of size $(2N + 1) \times (2N + 1)$. Because rows $1, N + 1$ and $N, 2N, 2N + 1$ of the matrix operators of Eq. (5.36) correspond to boundary and interface conditions respectively, it should come as no surprise that the last two entries of $\tilde{\boldsymbol{P}}$ from the discrete formulation, and the last two entries of $\boldsymbol{F}_\nu$ from the analytic formulation, are the same – exact forms of the fluid fields were assumed in both. This adjustment of the SCM method reduces matrix sizes and improves computational times, while it also avoids the use of complex maps and the

choice of complex parameter ζ_f.

An important comment needs to be made here: since no non-linear eigenvalue problems arise from assuming the exact form of the unknown potentials of the problem, it is tempting to keep repeating the same process and assume exact forms for the elastic wave potentials in the annulus. This would reduce the discrete formulation even further to exactly the analytic one. Crucially, that is not done here, because discretising the immersed annulus with SCM makes the method versatile, and enables a wide range of different problems, like scattering from multilayered, viscoelastic and anisotropic annuli, to be studied. That may be achieved by discretising motion in annuli of more complex compositions with established generalisations of SCM from the literature – see for instance the SCM discretisation of multilayered or anisotropic annuli of Adamou and Craster [24] or of multilayered, viscoelastic and generally anisotropic flat waveguides of Quintanilla *et al.* [27, 29] – and coupling that discretisation with the proposed methodology for scattering problems. Equivalent generalisations of the analytic approach are increasingly difficult and costly to achieve – especially for anisotropy [142, 143] – and can lead to numerically unstable matrices of Bessel and Hankel functions of different arguments.

5.4 Results & Discussion

In this section, the SCM discretisation of the forced problem is employed for the computation of the scattered field response from a steel hollow cylinder immersed in water, of material properties and dimensions taken from Section 4.4.1.3. Target strength plots are presented and validated against calculations using the analytic formulation of Eq. (5.12), while resonance spectra of normal modes are evaluated through Eq. (5.18) and their relation to leaky

circumferential waves of complex frequencies is demonstrated.

In Figure 5.2, target strength plots of $D(\omega, \theta)$, as computed by the SCM formulation with $N = 30$ alongside those computed by the analytic formulation of Eq. (5.12), are depicted. The presented response is a result of an incoming plane wave of unit amplitude, $A_{\text{inc}} = 1$, taken to be incident at an angle $\theta_{\text{inc}} = \pi$ at all instances. Figures 5.2(a) and 5.2(b) depict SCM and analytic target strength plots respectively, for a range of frequencies and angles, in decibels, as heat maps of [121]

$$TS = 20 \log_{10} |D(\omega, \theta)|. \tag{5.39}$$

The computation of target strength plots was carried out at 1000 frequencies in the non-dimensional frequency range, $kb \in [0, 100]$ and 1000 angles in the range $[0, 2\pi]$, with both SCM and analytic computations performed for every integer wavenumber between $\pm M$, for $M = 100$.

As a validation, line target strength plots computed by the SCM are compared with those obtained from the analytic formulation, for particular angles of interest and non-dimensional frequencies. That is equivalent to comparing horizontal or vertical slices of the target strength plots of Figures 5.2(a) and 5.2(b). Figure 5.3 compares the line target strength plots between the two methods for fixed angles of interest – the vertical lines in the two plots of Figure 5.2. Line target strength plots for $\theta = \pi/4$ are shown in Figure 5.3(a) and for $\theta = 7\pi/13$ in Figure 5.3(b), as a function of the non-dimensional frequency, kb. Figure 5.4 compares the line target strength plots between the two methods for fixed non-dimensional frequencies – the horizontal lines in the two plots of Figure 5.2. Those are shown in Figure 5.4(a) for $kb = 10$ and in Figure 5.4(b) for $kb = 75$, as a function of angle in polar plot format. Excellent agreement between SCM and analytical results is seen in all instances.

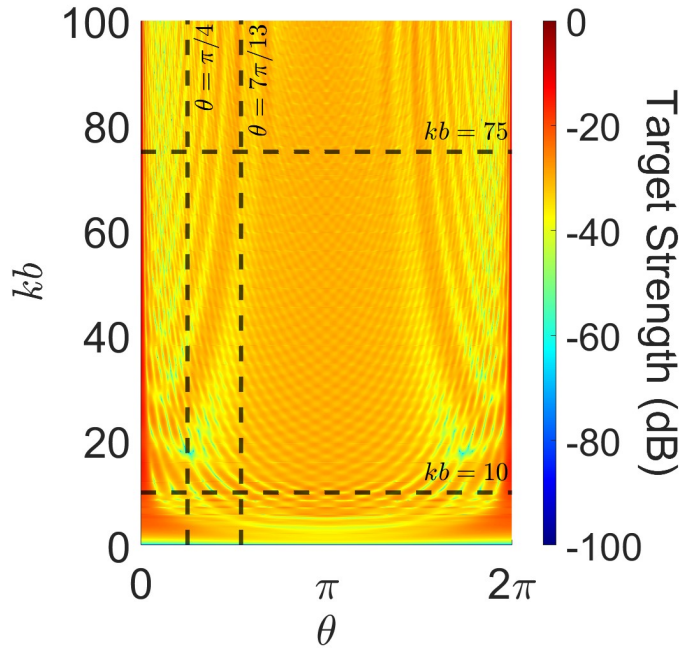

(a)

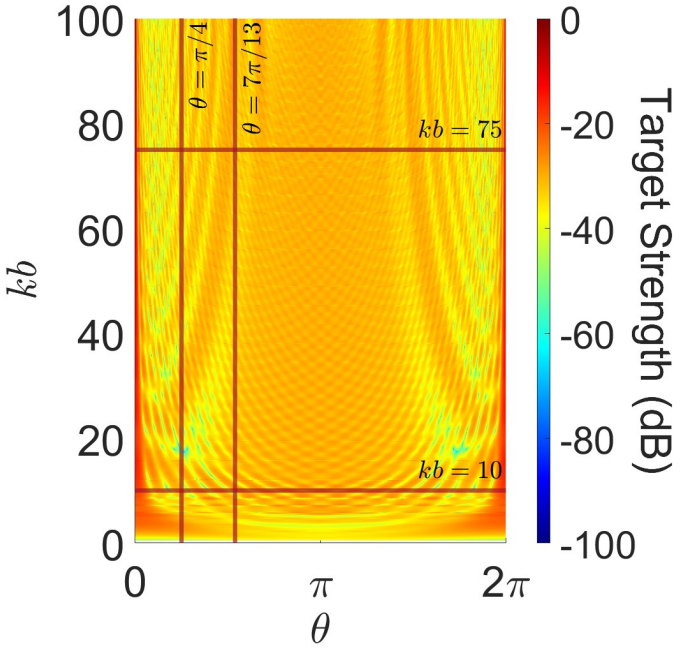

(b)

Figure 5.2: Target strength plots of a steel hollow cylinder in water subjected to an incident plane wave at an angle $\theta_{\text{inc}} = \pi$, calculated with SCM in 5.2(a) and analytical formulation in 5.2(b), for $\theta \in [0, 2\pi]$ and $kb \in [0, 100]$.

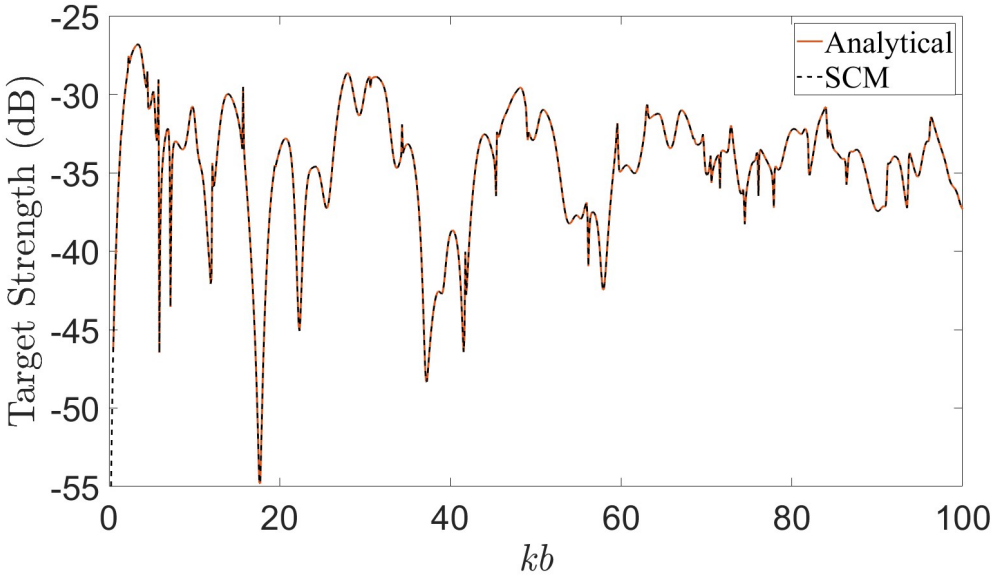

(a)

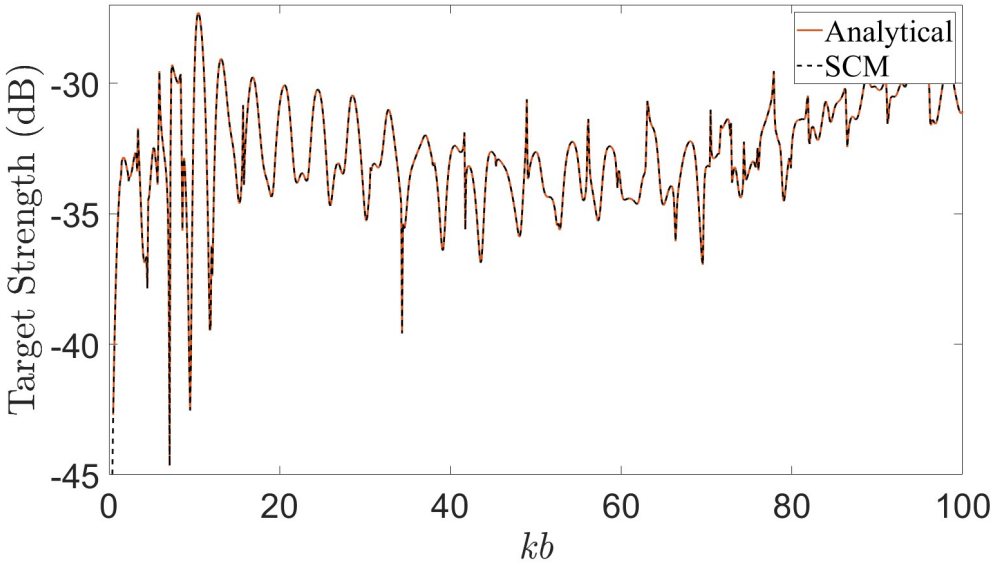

(b)

Figure 5.3: Comparisons between line target strength plots as computed with SCM against analytical formulations, for angles of interest $\theta = \pi/4$ in Figure 5.3(a) and $\theta = 7\pi/13$ in Figure 5.3(b).

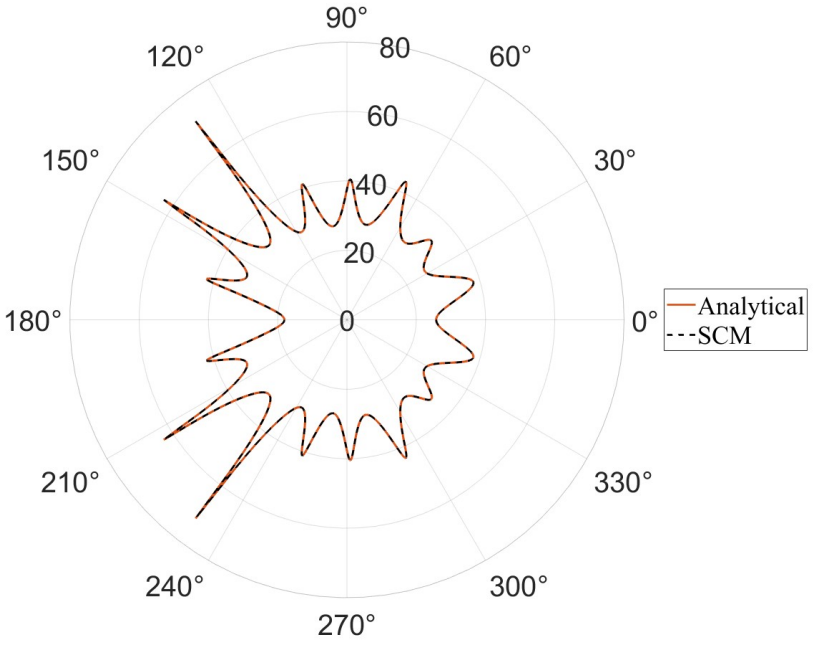

(a)

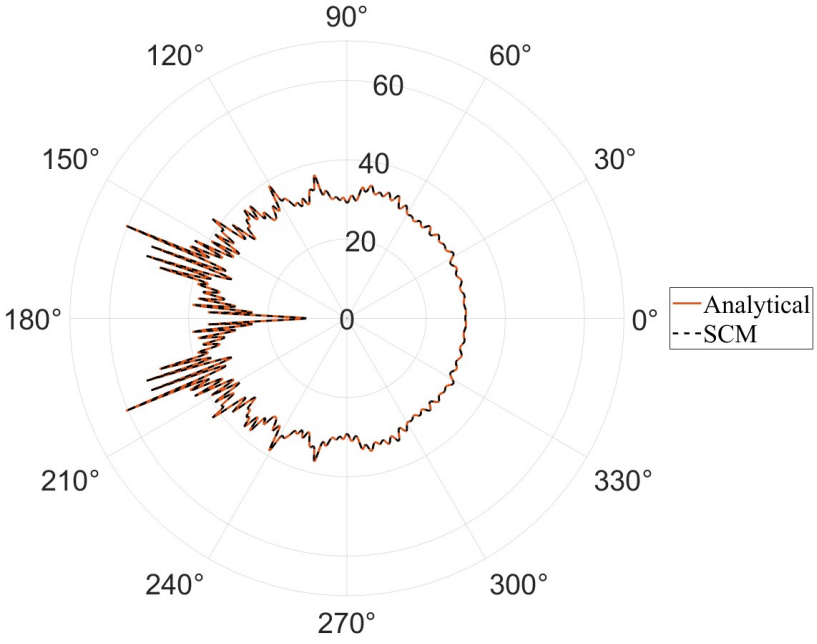

(b)

Figure 5.4: Comparisons between line target strength plots as computed with SCM against analytical formulations for non-dimensional frequencies, $kb = 10$ in Figure 5.4(a) and $kb = 75$ in Figure 5.4(b).

To demonstrate the relationship between the resonance spectrum of the scattered response problem and the leaky circumferential waves of complex frequencies of Section 4.4.2, the resonance spectrum amplitudes of Eq. (5.18) and corresponding normal mode resonance directivity functions of Eq. (5.22) are computed next for a range of frequencies. From [139], any submerged elastic cylinder of density greater than that of the surrounding fluid, and shear and compressional bulk wave speeds greater than the speed of sound in the fluid, acts as a rigid body away from its resonance frequencies. Thus, when computing the resonance spectrum amplitudes of Eq. (5.18), sound-hard amplitudes ought to be removed from the computed scattered field ones.

Figure 5.5 depicts line target strength plots of normal mode resonance directivities $D_{\nu}^{(\mathrm{res})}(\omega, \theta)$ for the back-scattered response ($\theta = \pi$) of the normal mode with $\nu = 10$ in Figure 5.5(a), and $\nu = 50$ in Figure 5.5(b). Their computation was carried out in a wider non-dimensional frequency range, $kb \in [0, 500]$, with the same resolution as before. Overlaying each target strength plot are the real parts of the complex non-dimensional frequencies of modes of the same wavenumber, as predicted by the proposed SCM in Section 4.4.2 and taken from the dispersion curves of leaky circumferential waves in Figure 4.6.

As attested by Figure 5.5, resonance peaks predicted by resonance scattering theory coincide with the real parts of the non-dimensional eigenfrequencies of leaky circumferential waves in the submerged steel cylinder. In-between resonances, sharp anti-resonances are also visible, indicating that at those frequencies, resonance directivities approach zero. It follows that the resonance amplitudes of Eq. (5.18) must vanish at those locations and that implies that the scattered field amplitudes approximate those of the impenetrable rigid body background; the elastic cylinder behaves exactly like a rigid body in-between resonances, consistent with resonance scattering theory.

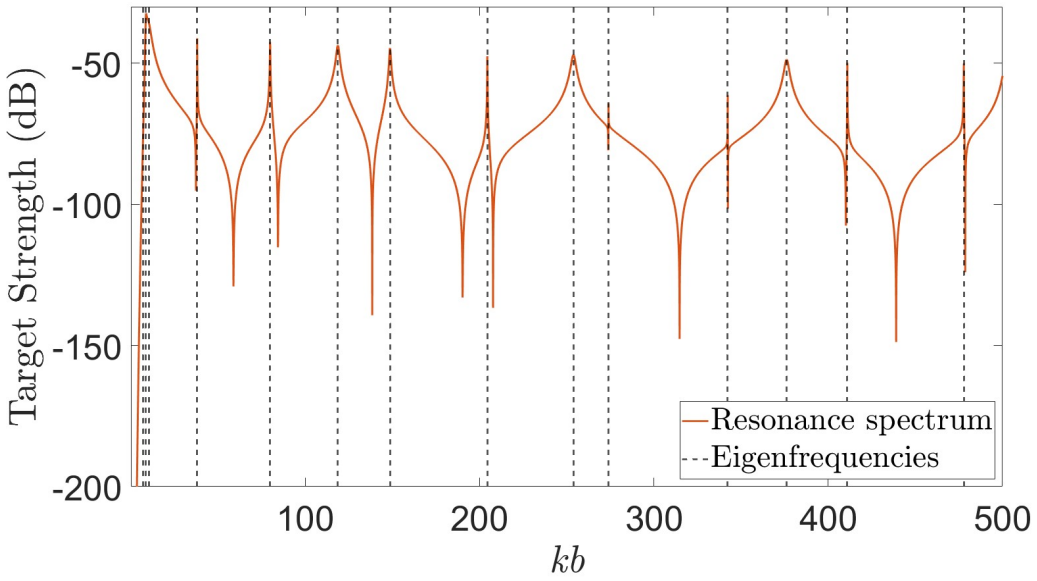

(a)

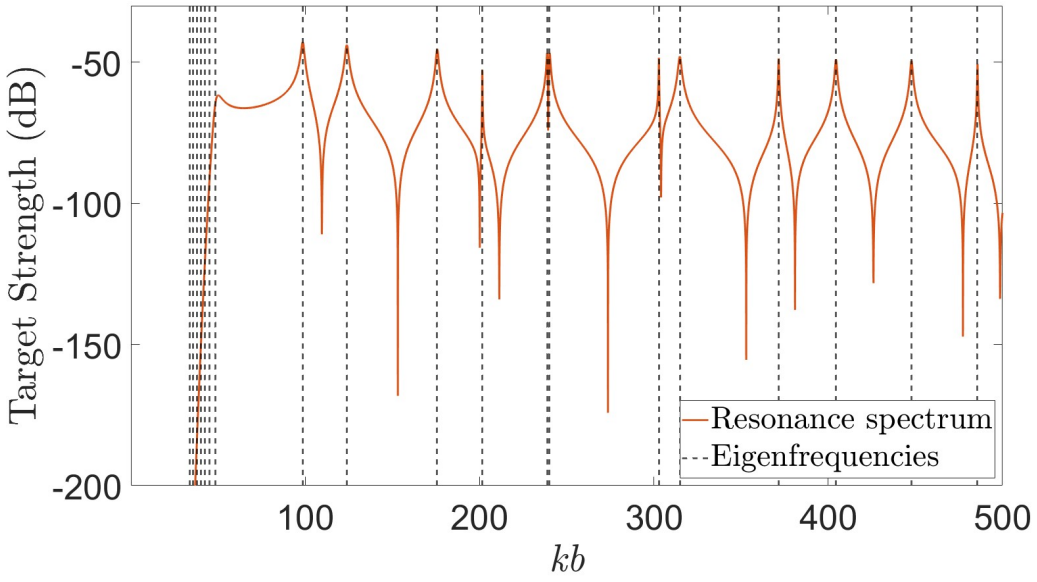

(b)

Figure 5.5: The resonance spectrum of the field scattered by an immersed steel hollow cylinder, for the normal modes of $\nu = 10$ in Figure 5.5(a) and $\nu = 50$ in Figure 5.5(b), with resonant peaks coinciding with eigenfrequencies from the complex frequency dispersion curves of Figure 4.6 for the same values of wavenumber.

5.5 Conclusion

In this chapter a SCM was proposed for the computation of the response of immersed hollow cylinders when subjected to an incident plane wave of known wavenumber and frequency. On account of the close relation to the problem of leaky circumferential waves propagating around the immersed cylinder, the SCM developed in previous work was exploited here and adapted for the computation of the scattered field amplitudes of the response problem. Therein, the assumption of known wavenumber and frequency allowed the SCM discretisation to be reduced to a boundary value problem.

Results from the SCM were obtained for a range of frequencies and angles of interest and were presented as target strength plots on a logarithmic scale. Upon comparing line target strength plots of single frequency or angle of interest, SCM results were found to be consistent with those from analytical formulations. Through resonance scattering theory, which enabled the separation of the scattered field in its resonant and sound-hard constituents, it was demonstrated how the resonance peaks of the resonant spectrum coincided with the complex frequencies of leaky circumferential waves computed in the previous chapter, and how away from those frequencies, the immersed cylinder behaved like a rigid body.

The proposed SCM is a simple yet powerful tool for the effective computation of scattering response problems. Under established generalisations of SCMs for the discretisation of complex annular waveguides, it is believed that the scattering formulation presented here will prove to be an accurate and versatile tool, able to handle scattering from cylinders of increased material complexities (viscoelastic, anisotropic, multilayered); problems that are increasingly difficult to solve otherwise.

Chapter 6

Conclusion

In this thesis the numerical evaluation of dispersion curves of leaky waves propagating in submerged or buried waveguides was investigated using the method of spectral collocation. It is believed that the work presented here lays the foundations for a fully automated numerical tool for the computation of leaky wave dispersion curves in planar and cylindrical geometries, for leaky waves in immersed or embedded waveguides where the material of both the waveguide and exterior may be arbitrary.

In this chapter, a review of the thesis is presented as well as a summary of main findings and a discussion on suggested future work.

6.1 Review of Thesis

The thesis began by discussing the motivation of the work; a thorough understanding of the underlying physics of wave propagation in leaky systems is crucial for a broad range of applications within physics, medicine and engineering. When it comes to identifying leaky waves and accurately computing their dispersion curves and mode shapes, the complex wavenumbers and ex-

ponentially growing wave fields which characterise them compromise the performance of computational methods traditionally used. There is, therefore, a need for a robust, versatile and accurate method for the identification of leaky waves, that does not suffer from the computational challenges associated with the aforementioned complex wavenumbers and exponential growth.

Leaky waves were first introduced in Chapter 1, where their characteristics and the numerical challenges associated with their computation were discussed in detail. Accompanying the discussion on leaky waves, the equations underlying wave propagation in isotropic elastic media were presented, alongside an introduction to the fundamental principles of spectral collocation; the solution method of choice throughout this thesis. The chapter concluded with a brief exposition on FE modelling which was later used in the thesis as a validation for the dispersion curves and modal profiles of waves radiating from buried waveguides.

The specific example of leaky waves in a straight elastic waveguide coupled with different inviscid fluid half-spaces on each side was subsequently investigated in Chapter 2. Note that the problem of leaky waves in a waveguide loaded only on one side by an inviscid fluid or on both sides by the same fluid was solved in the contribution of Kiefer *et. al.* [43], where a non-linear eigenvalue problem, of a single non-linear term, was linearised with a neat change of variables. Analogous formulations for waveguides coupled to two different fluid or solid spaces would unfortunately result in non-linear problems, of more than one non-linear terms, which do not reduce as nicely. Thus, the problem under consideration in Chapter 2 is regarded as an exemplar of leaky waves that exhibits the key difficulties associated with solving such systems to date; root-finding techniques struggle with the complex wavenumbers of leaky waves in analytic matrix formulations, discretising the problem results in non-linear eigenvalue problems that are difficult to solve, and dealing with

the exponential growth of leaky waves through absorbing layers results in the accuracy of the solution being dependent on a choice of absorbing parameters.

In the same chapter, a spectral collocation discretisation for the computation of leaky wave dispersion curves that manages to circumvent the numerical challenges associated with their exponential growth and complex wavenumbers was proposed. Chebyshev nodes discretised the waveguide while collocation points that would otherwise discretise the exterior fluid domains were mapped onto appropriately chosen complex paths via carefully selected complex maps. The chosen maps guaranteed a single collocation point at the physical space of each of the two solid-fluid interfaces of the problem, thereby achieving the discretisation of complex paths in the complex plane which originated from the two solid-fluid interfaces in real space. Importantly, when the exponentially growing fluid wave potentials of leaky waves were considered as functions defined over those complex paths, it was deduced that subject to an appropriate choice of complex maps, they could be made to numerically decay with distance from the waveguide for the same wavenumber and amplitudes. Thus, under the proposed methodology, solving the problem of exponentially growing leaky waves became a matter of solving for numerically decaying functions while all essential physics were preserved (wavenumber and amplitudes of wave fields).

The proposed discretisation resulted in a polynomial eigenvalue problem for the numerically decaying wave potentials that was easy to solve with conventional solvers. Results were obtained robustly, accurately, without the need of user intervention and were validated against commercially available software (DISPERSE). Importantly, as was demonstrated in [80], the underlying spectral collocation discretisation of the domain of the waveguide can handle more complex waveguides (anisotropic, viscoelastic, multilayered), and

thus, together with the proposed treatment of fluid domains for leaky waves, spectral collocation provides a methodology for all leaky wave systems and radiation into fluids.

Following the development of a SCM for leaky waves radiating from straight elastic waveguides into spaces of fluid, a problem of increased complexity was subsequently considered in Chapter 3; leaky wave radiation from elastic waveguides buried between two elastic spaces, each composed of isotropic solid materials distinct from both the waveguide and each other. In such systems, elastodynamic energy is radiated into the exterior spaces of isotropic solids as a superposition of longitudinal and shear waves, with either one or both partial waves exhibiting an exponential growth of amplitude with distance from the waveguide for leaky waves; a step-change in complexity when compared to the purely compressive polarisations of waves radiating into inviscid fluids considered in Chapter 2. To overcome the added complexity, a solution framework was proposed whereby the phase velocity domain was separated into several regions depending on the type of radiation expected in each region (non-leaky, shear-leaky, fully-leaky). In each region some or all partial waves were exponentially growing, and by judiciously applying the SCM of Chapter 2 to each growing partial wave, exponential growth was removed from the numerical scheme at all instances and leaky wave solutions were retrieved as eigenvalues of polynomial eigenvalue problems.

Results were verified against Disperse and FE simulations (Pogo) of two types of excitations: multi-modal and single-mode. In simulations of multi-modal excitations, the source nodes of the FE model were displaced based on broadband excitation tonebursts, resulting in multiple modes being excited at the same time. Performing a 2D-FFT of monitored signals then extracted the dispersion curves of excited modes which were subsequently overlaid with predictions from the proposed SCM. This approach qualitatively validated

multiple modes of the predicted SCM at once. In simulations of single-mode excitations, source nodes were excited with the "centre mode shape" [65] technique. There, individual modes were preferentially excited by modifying excitation signals in accordance to the mode shapes of the desired mode at the central frequency of the simulation. This allowed for individual modes to be investigated, and their mode shapes and dispersion curves be validated even for cases where a DISPERSE solution was not available. The proposed SCM for leaky waves in elasticity was found to be accurate, versatile (it can be simplified to handle other cases of loading like a waveguide with a solid on one side and a fluid on the other), and it identified all leaky modes without requiring knowledge of their existence or any tuning *a priori*.

Moving away from planar geometries, in Chapter 4 the proposed SCM was extended to elastic cylinders and specifically to leaky circumferential waves propagating around a hollow cylinder submerged in fluid. An analytic description of the problem was presented prior to discretisation with spectral collocation; the analytic description served as a tool for the validation of the SCM in cylindrical geometries. In the same fashion as in previous chapters, complex paths were discretised instead of the physical domain of the fluid surrounding the cylinder, in which the fluid wave potential was made to exponentially decay. Leaky wave solutions were again retrieved as eigensolutions of linear eigenvalue problems.

The proposed discretisation enabled the computation of dispersion curves for two types of leaky waves, each of distinct physical interpretation. Those were the leaky waves of complex wavenumbers and real frequencies, which correspond to waves that attenuate as they propagate around the cylinder, and the leaky waves of complex frequencies and real wavenumbers, which correspond to waves that decay with time. The SCM in cylindrical geometries was initially validated for complex wavenumbers through a comparison of

results for two limiting cases of the materials and geometry of the system – a cylinder in weak fluid and an immersed cylinder of small curvature – against dispersion curves from DISPERSE. The general case for both complex wavenumbers and complex frequencies was conclusively validated through contour plots, generated from computing the determinant of matrices coming from the analytic formulation of the problem over a range of frequencies and wavenumbers. Predicted dispersion curves were seen to lie in divergent regions of the contour plots, indicating their validity as solutions of the leaky circumferential waves problem.

Closely related to the problem of leaky circumferential waves propagating around a submerged hollow cylinder is the response of the same cylinder when viewed as a scatterer of sound subjected to an incoming wave field that is incident upon it. The response problem was the focus of the final chapter of this thesis, Chapter 5. There, the forcing imposed upon the immersed cylinder by the incident field was accounted for by decomposing the total field in the fluid in two parts: the incoming wave field and the field scattered by the cylinder. To compute the scattered field response of the scatterer, the similarities between the computation of the dispersion curves of leaky circumferential waves propagating around an immersed cylinder and the computation of the scattered field response of the same cylinder when subjected to an incoming plane wave were exploited here. Specifically, the SCM proposed in Chapter 4 for the computation of the former was modified and reduced here to a boundary value problem for the computation of the latter. The immersed cylinder's response was presented as target strength plots and was validated against calculations of the same response through an analytic formulation of the problem. Crucially, as is the case for planar geometries, the spectral collocation discretisation of the annular cross-section of the cylinder allows for the scattered field response from more complex

structures, e.g. multilayered anisotropic cylinders, to be easily calculated by combining the spectral collocation discretisation of the complex structure, e.g. [24] for multilayered and anisotropic annuli, with the treatment for scattering problems proposed in this thesis.

The chapter concluded by demonstrating the strong relation between the dispersion curves of leaky circumferential waves in the immersed cylinder of Chapter 4 and the scattered field response of the same object computed in Chapter 5. For a known, real, wavenumber, it was shown that the real parts of complex frequencies from the complex frequency dispersion curves of Chapter 4 coincided with resonance peaks of the resonance spectrum of the scattered field response of Chapter 5. In line with resonance scattering theory, this implied that sound penetrated the immersed cylinder only when the frequency of the incoming wave was close to one of its resonance frequencies, while between those resonance frequencies the cylinder scattered sound as if it was impenetrable.

6.2 Reflection on Objectives

This thesis was motivated by a real scientific and industrial need of an automated method for computing the dispersion curves of leaky waves radiating from any immersed or buried waveguide, in both planar and cylindrical geometries. That is, leaky waves in systems where the material of the waveguide and its surroundings may be taken to be arbitrary.

To address this challenge, this thesis presents the development of a novel SCM for the identification of leaky waves in immersed and buried structures. The SCM, originally introduced in Chapter 2, has demonstrated its ability to effectively identify leaky waves radiating from straight waveguides that are coupled to dissimilar inviscid fluids on either side; a problem with which

existing methods are known to struggle. This SCM is really the backbone of this thesis and it underpins all subsequent investigations whose aim was to demonstrate the versatility of the proposed methodology and establish its potential as a tool for automated leaky wave computations in general systems.

Subsequent chapters extended the application of the SCM to increasingly difficult problems, including leaky waves in waveguides buried between dissimilar elastic spaces, leaky circumferential waves radiating from submerged hollow cylinders and underwater scattering problems. Although the range of leaky wave problems considered here is not exhaustive, the selected problems span across a range of complexities: from radiation into fluids, where a single wave potential exponentially grows, to radiation into solids and possibly two exponentially growing potentials, and finally to leaky circumferential waves in submerged cylinders that would require non-linear complex-ordered Hankel and Bessel functions if approached analytically. At all instances the SCM yielded excellent results when compared to commercial software, FE modelling and analytic computations, proving its versatility and validating its reliability and accuracy.

While much still remains to be done in rolling out the new capability to all classes of cases (see Section 6.3), it is believed that this thesis has successfully achieved its objective of developing an effective candidate for an automated method to compute the dispersion curves of leaky waves in general systems, addressing a longstanding gap in the field.

6.3 Future Work

In this final section of the thesis, potential avenues for further research are discussed, aiming at improving the proposed methodology and progressing it

towards a "black-box" approach for the computation of leaky wave dispersion curves for systems of the generic type.

Throughout the thesis, as a result of the proposed discretisation and choices of complex parameters or numbers of collocation points, non-physical, spurious or non-converged solutions emerged and were discarded through several different filtering procedures. In Chapter 2 solutions were filtered out based on their speeds. In Chapter 3 solutions were filtered out when they did not attain a particular form (and thus did not satisfy boundary conditions). Similarly, in Chapter 4 solutions were filtered out if they did not converge within a chosen tolerance. These filtering procedures were relatively simple and effective, however, when it comes to producing a fully automated tool for the computation of dispersion curves of leaky waves in arbitrary systems, it is important to formalise what a satisfactory solution is and streamline the filtering process. Therefore investigating filtering methods is an important area of future research.

Another aspect of the method that merits further investigation is that of the choice of complex parameters. When it came to the choice of complex paths that would enable the retrieval of leaky waves in this thesis, the same complex parameter was chosen for all frequencies. That is, a constant (frequency-independent) choice of complex parameter was always made. This frequency-independent choice can be seen to produce excellent results for all leaky wave problems investigated in this thesis and within the frequency range of interest. Numerical experimentation revealed that the proposed SCM remained robust to the variations in complex parameter within the frequency range of interest. However, at higher frequencies, performance was compromised unless the complex parameter was adjusted or the number of collocation points in the exterior domain was increased. It is therefore believed that the success of the method with a frequency-independent choice of complex parameter is in

part attributed to the liberal choices of the number of collocation points that were made in the various open spaces under consideration and the inherent convergence properties of spectral collocation, even if a poor choice of complex parameter was made. Thus, to improve the efficiency of the proposed method, a thorough investigation on the impact of complex parameter selection ought to be made, possibly considering frequency dependent choices.

Additionally, while this thesis only studied leaky waves radiating from isotropic waveguides into inviscid fluids or isotropic solid media, the treatment of leaky waves presented in this thesis in combination with the spectral collocation discretisation of complex waveguides in planar [29] and cylindrical [24] geometries enables the study of leaky waves leaking from waveguides of arbitrary material in contact with spaces of inviscid fluid or isotropic solids. To be able to deal with arbitrary systems, more complex exteriors must be addressed. Next steps could therefore include investigating the effectiveness of the proposed SCM to elastic cylinders buried in isotropic solids and to systems of waveguides in contact with viscous fluids and viscoelastic or anisotropic media. Importantly, it is expected that no new maths or physics are needed for these, i.e. this will be a process of implementing, not new discovery.

Inspired by the inspection of submerged or buried pipes in NDE, and in line with extending the capabilities of the proposed SCM, it would be interesting to apply the proposed methodology to the problem of leaky waves propagating in helical paths along submerged or buried cylindrical waveguides. That would involve a formulation of the 3D problem in terms of radially dependent displacements and the application of the proposed SCM for a given a choice of axial wavenumber. By investigating problems in order of increasing complexity, first simple cylinders (made of fluid or isotropic solids) in inviscid and viscous fluids and then cylinders in a matrix of isotropic then viscoelastic and then anisotropic solids, it is believed that a versatile SCM for leaky

helical waves in general systems is possible. Again, this will be a matter of implementation rather than of new discovery.

In Chapter 5 a SCM for the computation of the field scattered from an elastic cylindrical scatterer in fluid subjected to an incident wave field was presented. This computation altogether circumvented the need for Bessel functions in the descriptions of displacement fields in the scatterer, which were instead approximated with spectral collocation. Crucially, due to the versatility of the spectral collocation discretisation of the domain of the scatterer, the presented methodology is applicable to more complex scatterers in fluid, like multilayered anisotropic annuli, whose modelling is increasingly difficult to achieve due to the inherent complexities of Bessel functions. Consequently, the proposed SCM provides a framework for addressing a broad spectrum of scattering problems and progressing this work would be of both industrial and scientific interest. Future work could include applying the proposed SCM to instances of scattering from fluid-filled cylinders in water, cylindrical inclusions in a solid matrix of arbitrary material, and scattering from straight waveguides and spheres.

Finally, carrying out the work outlined above would result in a fully automated method for the computation of leaky wave dispersion curves and scattering response problems in general systems. For the methodology to have any real impact, however, it must become accessible to everyone. That is, it must ultimately be converted into a computer tool (like DISPERSE) that is easy to use and does not require user expertise. A critical future work is therefore the investment of sufficient time and effort in incorporating codes from this thesis, and any developments thereafter, into a numerical tool that is intuitive and does not require any user intervention; a significant yet essential challenge in itself.

Appendix A

Relationship to PMLs

PMLs were originally introduced by Berenger [47] for the simulation of free-space for electromagnetic scattering problems using the finite-difference time-domain method. Therein, a layer of perfectly matched impedance was placed around the edges of the finite computational domain. The layer is defined through a change in the magnetic and electric conductivities; these were chosen to have a power law dependence on the ratio of distance from the interface between PML and unaltered material to the thickness of the PML:

$$\sigma(r) = \sigma_m \left(\frac{r}{\delta}\right)^n, \tag{A.1}$$

with σ_m the limiting magnetic or electric conductivity inside the PML, r the distance from the interface inside the matched layer, δ the PML's thickness and n a non-negative integer. The choice of conductivities in Eq. (A.1) ensure that waves enter the PML without reflections and are absorbed; in practical terms the choices of the parameters σ_m, δ and n are all important in achieving the optimal outcome.

Later, Chew and Weedon [144] proposed an alternative viewpoint of PML

using the modified Maxwell's equations in terms of a complex coordinate stretching. The same idea was extended to elastodynamics [145–147] to produce a medium that absorbs outgoing waves. The coordinate stretching is generally (see for instance [48,144,147–149]) given by

$$r \to \tilde{r} = \int_0^r \gamma(s)\, \mathrm{d}s, \tag{A.2}$$

with γ a complex-valued function such that

$$\begin{cases} \Im\{\gamma(r)\} > 0 & \text{inside the PML,} \\ \gamma(r) = 1 & \text{elsewhere.} \end{cases} \tag{A.3}$$

A typical choice for γ in Eq. (A.2) that satisfies the conditions of Eq. (A.3) is

$$\gamma(r) = 1 + \frac{i}{\omega}\sigma(r), \tag{A.4}$$

with $\sigma(r)$ taken from Berenger's conductivity Eq. (A.1) inside the PML and zero everywhere else. In essence the undisturbed material is surrounded by an impedance matched layer with material properties gradually changing throughout the layer to minimise any reflections back into the computational domain of interest; constant, rather than gradually changing, choices, i.e. $n = 0$, tend to perform poorly.

In theory PMLs are layers of perfectly matched impedance, however, in practice, reflections can occur from the interface between the PML and unaltered material due to the discretisation of the wave equation for use in a computer simulation [46,150]. Skelton *et al.* [151] provide the mathematical grounds for those reflections, where they can be interpreted as emitted disturbances

propagating away from a collection of sources placed at the elastic-PML interface; it was concluded that to minimise reflections, the power dependence of Eq. (A.1) must at least be a quadratic ($n \geq 2$).

Turning away from diffraction and scattering to now consider eigenmodes of structures, Treyssède *et al.* [48] used PMLs surrounding a region of unaltered material for the computation of modes of an open stratified waveguide; results from a constant PML ($n = 0$) – previously adopted in the literature for open waveguides [152–154] – and from a parabolic PML ($n = 3$) were compared and computational accuracy improved when the continuously increasing absorbing function of the parabolic PML was used.

The methodology used in the body of this thesis can be viewed as a constant PML (or of constant conductivity under Berenger's definition), like that in [48], but now attached directly onto the waveguide. Considering $n = 0$ in Eq. (A.1), the complex coordinate stretching of Eq. (A.2), for a PML attached at the waveguide interface at $y = d$, becomes

$$r \to \tilde{r} = d + \left(1 + \frac{i}{\omega}\sigma_m\right) r, \tag{A.5}$$

inside the PML. With a choice of

$$\sigma_m = -i\omega \left(\zeta_{\Psi_2} - 1\right), \tag{A.6}$$

and $r = \pm(y \mp d)$, Eq. (A.5) maps collocation points from the real line $[d, \infty]$ to the complex paths defined by Eqs. (3.26) and (3.28). Crucially, now both the elastic waveguide and the PML have collocation points on the same physical spaces of the waveguide-exterior interfaces and, by enforcing continuity of normal tractions and displacements and vanishing of shear stresses, there is no impedance mismatch at the elastic-PML interface; the disadvantages of a constant PML are negated as reflections from the elastic-PML interface do

not pollute the computation and the constant map effectively computes leaky waves.

Appendix B

Explicit Form of $\boldsymbol{D}(\omega, \nu)$

The entries d_{lq}, for $l, q = 1 \dots 5$, of matrix $\boldsymbol{D}(\omega, \nu)$ in Eq. (4.26) read

$$
\begin{aligned}
d_{11} &= \kappa^2 k_l^2 J_\nu''(k_l a) + \frac{(\kappa^2-2)k_l}{a} J_\nu'(k_l a) - \frac{(\kappa^2-2)\nu^2}{a^2} J_\nu(k_l a),\\
d_{12} &= \kappa^2 k_l^2 Y_\nu''(k_l a) + \frac{(\kappa^2-2)k_l}{a} Y_\nu'(k_l a) - \frac{(\kappa^2-2)\nu^2}{a^2} Y_\nu(k_l a),\\
d_{13} &= \frac{2\nu}{a^2} J_\nu(k_t a) - \frac{2\nu k_t}{a} J_\nu'(k_t a),\\
d_{14} &= \frac{2\nu}{a^2} Y_\nu(k_t a) - \frac{2\nu k_t}{a} Y_\nu'(k_t a),\\
d_{15} &= 0,\\
d_{21} &= \frac{2\nu}{a^2} J_\nu(k_l a) - \frac{2\nu k_l}{a} J_\nu'(k_l a),\\
d_{22} &= \frac{2\nu}{a^2} Y_\nu(k_l a) - \frac{2\nu k_l}{a} Y_\nu'(k_l a),\\
d_{23} &= k_t^2 J_\nu''(k_t a) - \frac{k_t}{a} J_\nu'(k_t a) + \frac{\nu^2}{a^2} J_\nu(k_t a),\\
d_{24} &= k_t^2 Y_\nu''(k_t a) - \frac{k_t}{a} Y_\nu'(k_t a) + \frac{\nu^2}{a^2} Y_\nu(k_t a),\\
d_{25} &= 0,
\end{aligned}
$$

$$
\begin{aligned}
d_{31} &= \frac{2\nu}{b^2} J_\nu(k_l b) - \frac{2\nu k_l}{b} J'_\nu(k_l b), \\
d_{32} &= \frac{2\nu}{b^2} Y_\nu(k_l b) - \frac{2\nu k_l}{b} Y'_\nu(k_l b), \\
d_{33} &= k_t^2 J''_\nu(k_t b) - \frac{k_t}{b} J'_\nu(k_t b) + \frac{\nu^2}{b^2} J_\nu(k_t b), \\
d_{34} &= k_t^2 Y''_\nu(k_t b) - \frac{k_t}{b} Y'_\nu(k_t b) + \frac{\nu^2}{b^2} Y_\nu(k_t b), \\
d_{35} &= 0, \\
d_{41} &= \kappa^2 k_l^2 J''_\nu(k_l b) + \frac{(\kappa^2 - 2) k_l}{b} J'_\nu(k_l b) - \frac{(\kappa^2 - 2)\nu^2}{b^2} J_\nu(k_l b), \\
d_{42} &= \kappa^2 k_l^2 Y''_\nu(k_l b) + \frac{(\kappa^2 - 2) k_l}{b} Y'_\nu(k_l b) - \frac{(\kappa^2 - 2)\nu^2}{b^2} Y_\nu(k_l b), \\
d_{43} &= \frac{2\nu}{b^2} J_\nu(k_t b) - \frac{2\nu k_t}{b} J'_\nu(k_t b), \\
d_{44} &= \frac{2\nu}{b^2} Y_\nu(k_t b) - \frac{2\nu k_t}{b} Y'_\nu(k_t b), \\
d_{45} &= -\frac{\lambda_f k^2}{\mu} H''_\nu(kb) - \frac{\lambda_f k}{\mu b} H'_\nu(kb) + \frac{\lambda_f \nu^2}{\mu b^2} H_\nu(kb), \\
d_{51} &= k_l J'_\nu(k_l b), \\
d_{52} &= k_l Y'_\nu(k_l b), \\
d_{53} &= -\frac{\nu}{b} J_\nu(k_t b), \\
d_{54} &= -\frac{\nu}{b} Y_\nu(k_t b), \\
d_{55} &= -k H'_\nu(kb).
\end{aligned}
$$

with $'$ denoting derivative with respect to the radial direction, r.

References

[1] M. J. Lowe, "Guided Waves in Structures," in *Encyclopedia of vibration* (S. G. Braun, D. J. Ewins, and S. S. Rao, eds.), London: Academic Press, 2002.

[2] J. W. S. B. Rayleigh, *Theory of Sound*, vol. 2. MacMillan and Co, 1878.

[3] J. S. Popovics, N. Ryden, A. Gibson, S. Alzate, I. L. Al-Qadi, W. Xie, D. O. Thompson, and D. E. Chimenti, "New developments in NDE methods for pavements," in *Review of Progress in QNDE* (D. O. Thompson and D. E. Chimenti, eds.), vol. 975, pp. 1320–1327, AIP Publishing, 2 2008.

[4] T. N. Tran, L. H. Le, and D. Ta, "Ultrasonic guided waves in bone: A decade of advancement in review," *IEEE Trans. Ultrason. Ferroelectr. Freq. Control*, vol. 69, pp. 2875–2895, 10 2022.

[5] P. Moilanen, P. H. Nicholson, V. Kilappa, S. Cheng, and J. Timonen, "Assessment of the cortical bone thickness using ultrasonic guided waves: Modelling and in vitro study," *Ultrasound Med. Biol.*, vol. 33, pp. 254–262, 2 2007.

[6] J. L. Rose, J. J. Ditri, A. Pilarski, K. Rajana, and F. Carr, "A guided wave inspection technique for nuclear steam generator tubing," *NDT Int.*, vol. 27, pp. 307–310, 12 1994.

[7] H. Farheen, T. Leuteritz, S. Linden, V. Myroshnychenko, and J. Förstner, "Optimization of optical waveguide antennas for directive emission of light," *J. Opt. Soc. Am. B: Opt. Phys.*, vol. 39, p. 83, 1 2022.

[8] B. Drafts, "Acoustic wave technology sensors," *IEEE Trans. Microw. Theory Tech*, vol. 49, 4 2001.

[9] M. J. S. Lowe, D. N. Alleyne, and P. Cawley, "The mode conversion of a guided wave by a part-circumferential notch in a pipe," *J. Appl. Mech.*, vol. 65, 1998.

[10] P. Cawley, P. Wilcox, D. N. Alleyne, B. Pavlakovic, M. Evans, K. Vine, and M. J. S. Lowe, "Long range inspection of rail using guided waves," in *16th World Conference on NDT*, e-Journal of Nondestructive Testing, 2004.

[11] D. N. Alleyne and P. Cawley, "Optimization of Lamb wave inspection techniques," *NDT Int.*, vol. 25, no. 1, pp. 11–22, 1992.

[12] D. N. Alleyne, B. Pavlakovic, M. J. Lowe, and P. Cawley, "Rapid long-range inspection of chemical plant pipework using guided waves," *Insight*, vol. 43, pp. 93–96, 2 2001.

[13] P. Fromme, P. Wilcox, M. Lowe, and P. Cawley, "On the development and testing of a guided ultrasonic wave array for structural integrity monitoring," *IEEE Trans. Ultrason. Ferroelectr. Freq. Control*, vol. 53, pp. 777–785, 4 2006.

[14] R. Long, M. J. S. Lowe, and P. Cawley, "Attenuation characteristics of the fundamental modes that propagate in buried iron water pipes," *Ultrasonics*, vol. 41, pp. 509–519, 9 2003.

[15] P. D. Wilcox, M. J. S. Lowe, and P. Cawley, "Mode and transducer selection for long range Lamb wave inspection," *J. Intell. Mater. Syst.*

Struct., vol. 12, no. 8, pp. 553–565, 2001.

[16] B. Pavlakovic, M. Lowe, D. Alleyne, and P. Cawley, "Disperse: A general purpose program for creating dispersion curves," in *Review of Progress in QNDE* (D. O. Thompson and D. E. Chimenti, eds.), vol. 16, pp. 185–192, Boston, MA: Springer US, 1997.

[17] M. J. S. Lowe, "Matrix techniques for modeling ultrasonic waves in multilayered media," *IEEE Trans. Ultrason. Ferroelectr. Freq. Control*, vol. 42, no. 4, pp. 525–542, 1995.

[18] W. T. Thomson, "Transmission of elastic waves through a stratified solid medium," *J. Appl. Phys.*, vol. 21, no. 2, pp. 89–93, 1950.

[19] N. A. Haskell, "The dispersion of surface waves on multilayered media," *Bull. Seismol. Soc. Am.*, vol. 54, no. 1, pp. 431–438, 1964.

[20] L. Knopoff, "A matrix method for elastic wave problems," *Bull. Seismol. Soc. Am.*, vol. 54, no. 1, pp. 431–438, 1964.

[21] L. Gavrić, "Computation of propagative waves in free rail using a finite element technique," *J. Sound Vib.*, vol. 185, no. 3, pp. 531–543, 1995.

[22] I. Bartoli, A. Marzani, F. Lanza di Scalea, and E. Viola, "Modeling wave propagation in damped waveguides of arbitrary cross-section," *J. Sound Vib.*, vol. 295, pp. 685–707, 8 2006.

[23] A. Marzani, E. Viola, I. Bartoli, F. Lanza di Scalea, and P. Rizzo, "A semi-analytical finite element formulation for modeling stress wave propagation in axisymmetric damped waveguides," *J. Sound Vib.*, vol. 318, pp. 488–505, 12 2008.

[24] A. T. I. Adamou and R. V. Craster, "Spectral methods for modelling guided waves in elastic media," *J. Acoust. Soc. Am.*, vol. 116, pp. 1524–

1535, 9 2004.

[25] F. Karpfinger, B. Gurevich, and A. Bakulin, "Modeling of wave dispersion along cylindrical structures using the spectral method," *J. Acoust. Soc. Am.*, vol. 124, pp. 859–865, 8 2008.

[26] T. Zharnikov, D. Syresin, and C.-J. Hsu, "Application of the spectral method for computation of the spectrum of anisotropic waveguides," *Proc. Mtgs. Acoust*, vol. 19, p. 045065, 2013.

[27] F. H. Quintanilla, Z. Fan, M. J. S. Lowe, and R. V. Craster, "Guided waves' dispersion curves in anisotropic viscoelastic single and multilayered media," *Proc. R. Soc. A: Math. Phys. Eng. Sci.*, vol. 471, 11 2015.

[28] F. H. Quintanilla, M. J. S. Lowe, and R. V. Craster, "Modeling guided elastic waves in generally anisotropic media using a spectral collocation method," *J. Acoust. Soc. Am.*, vol. 137, pp. 1180–1194, 3 2015.

[29] F. Quintanilla, M. J. S. Lowe, and R. V. Craster, "Full 3D dispersion curve solutions for guided waves in generally anisotropic media," *J. Sound Vib.*, vol. 363, pp. 545–559, 2 2016.

[30] Y. Shen, S. Hirose, and Y. Yamaguchi, "Dispersion of ultrasonic surface waves in a steel-epoxy-concrete bonding layered medium based on analytical, experimental, and numerical study," *Case Stud. Nondestruct. Test. Evaluation*, vol. 2, no. 1, pp. 49–63, 2014.

[31] A. Lellouch, E. Biondi, B. Biondi, B. Luo, G. Jin, and M. Meadows, "Properties of a deep seismic waveguide measured with an optical fiber," *Phys. Rev. Res.*, vol. 3, 2 2021.

[32] D. E. Chimenti and A. H. Nayfeh, "Leaky Lamb waves in fibrous composite laminates," *J. Appl. Phys.*, vol. 58, pp. 4531–4538, 12 1985.

[33] P. Nagy, "Leaky guided wave propagation along imperfectly bonded fibers in composite materials," *J. Nondestruct. Eval.*, vol. 13, no. 3, 1994.

[34] R. Long, T. Vogt, M. Lowe, and P. Cawley, "Measurement of acoustic properties of near-surface soils using an ultrasonic waveguide," *Geophys.*, vol. 69, no. 2, pp. 460–465, 2004.

[35] E. Leinov, M. J. S. Lowe, and P. Cawley, "Ultrasonic isolation of buried pipes," *J. Sound Vib.*, vol. 363, pp. 225–239, 2 2016.

[36] E. Leinov, M. Lowe, and P. Cawley, "Investigation of guided wave propagation and attenuation in pipe buried in sand," *J. Sound Vib.*, vol. 347, pp. 96–114, 7 2015.

[37] M. Castaings and M. Lowe, "Finite element model for waves guided along solid systems of arbitrary section coupled to infinite solid media," *J. Acoust. Soc. Am.*, vol. 123, pp. 696–708, 2 2008.

[38] V. Potsika, K. Grivas, V. Protopappas, M. Vavva, K. Raum, D. Rohrbach, D. Polyzos, and D. Fotiadis, "Application of an effective medium theory for modeling ultrasound wave propagation in healing long bones," *Ultrasonics*, vol. 54, no. 5, pp. 1219–1230, 2014.

[39] A. Guha, M. Aynardi, P. Shokouhi, and C. Lissenden, "Identification of long-range ultrasonic guided wave characteristics in cortical bone by modelling," *Ultrasonics*, vol. 114, 7 2021.

[40] K. Lee and S. Yoon, "Feasibility of bone assessment with leaky Lamb waves in bone phantoms and a bovine tibia," *J. Acoust. Soc. Am.*, vol. 115, pp. 3210–3217, 6 2004.

[41] E. Georgiades, M. J. S. Lowe, and R. V. Craster, "Leaky wave characterisation using spectral methods," *J. Acoust. Soc. Am.*, vol. 152,

pp. 1487–1497, 9 2022.

[42] M. Mazzotti, I. Bartoli, A. Marzani, and E. Viola, "A coupled SAFE-2.5D BEM approach for the dispersion analysis of damped leaky guided waves in embedded waveguides of arbitrary cross-section," *Ultrasonics*, vol. 53, pp. 1227–1241, 9 2013.

[43] D. A. Kiefer, M. Ponschab, S. J. Rupitsch, and M. Mayle, "Calculating the full leaky Lamb wave spectrum with exact fluid interaction," *J. Acoust. Soc. Am.*, vol. 145, pp. 3341–3350, 6 2019.

[44] H. Gravenkamp, B. Plestenjak, D. A. Kiefer, and E. Jarlebring, "Computation of leaky waves in layered structures coupled to unbounded media by exploiting multiparameter eigenvalue problems," *J. Sound Vib.*, vol. 596, 2 2025.

[45] J. R. Pettit, A. Walker, P. Cawley, and M. J. Lowe, "A stiffness reduction method for efficient absorption of waves at boundaries for use in commercial finite element codes," *Ultrasonics*, vol. 54, no. 7, pp. 1868–1879, 2014.

[46] P. Rajagopal, M. Drozdz, E. A. Skelton, M. J. Lowe, and R. V. Craster, "On the use of absorbing layers to simulate the propagation of elastic waves in unbounded isotropic media using commercially available finite element packages," *NDT Int.*, vol. 51, pp. 30–40, 10 2012.

[47] J.-P. Berenger, "A perfectly matched layer for the absorption of electromagnetic waves," *J. Comput. Phys*, vol. 114, pp. 185–200, 1994.

[48] F. Treyssède, K. L. Nguyen, A. S. Bonnet-BenDhia, and C. Hazard, "Finite element computation of trapped and leaky elastic waves in open stratified waveguides," *Wave Motion*, vol. 51, no. 7, pp. 1093–1107, 2014.

[49] Z. Fan, M. J. S. Lowe, M. Castaings, and C. Bacon, "Torsional waves propagation along a waveguide of arbitrary cross section immersed in a perfect fluid," *J. Acoust. Soc. Am.*, vol. 124, pp. 2002–2010, 10 2008.

[50] J. W. Dunkin, "Computation of modal solutions in layered, elastic media at high frequencies," *Bull. Seismol. Soc. Am.*, vol. 55, no. 2, pp. 335–358, 1965.

[51] B. A. Auld, *Acoustic Fields and Waves in Solids*, vol. 1. Wiley, 1973.

[52] J. L. Rose, *Ultrasonic Guided Waves in Solid Media*. Cambridge University Press, 1 2014.

[53] Shuh-Haw Sheen, Hual-Te Chien, and A. Raptis, "Measurement of shear impedances of viscoelastic fluids," in *1996 IEEE Ultrasonics Symposium. Proceedings*, vol. 1, pp. 453–457, IEEE.

[54] H. Lamb, "On waves in an elastic plate," *Proc. R. Soc. A: Math. Phys. Eng. Sci.*, vol. 81, pp. 114–128, 1916.

[55] L. N. Trefethen, *Spectral Methods in MATLAB*. Philadelphia: SIAM, 2008.

[56] B. Fornberg, *A Practical Guide to Pseudospectral Methods*. Cambridge: Cambridge University Press, 1996.

[57] J. P. Boyd, *Chebyshev and Fourier Spectral Methods*. Mineola, New York: Dover Publications, 2 ed., 2000.

[58] J. A. Weideman and S. C. Reddy, "A MATLAB differentiation matrix suite," *ACM Trans. Math. Softw.*, vol. 26, pp. 465–519, 12 2000.

[59] P. Huthwaite, "Accelerated finite element elastodynamic simulations using the GPU," *J. Comput. Phys.*, vol. 257, pp. 687–707, 1 2014.

[60] R. D. Cook, D. S. Malkus, and M. E. Plesha, *Concepts and Applications of Finite Element Analysis*. John Wiley & Sons, 3 ed., 10 1988.

[61] Bathe K. J., *Finite Element Procedures*. Watertown, MA: K.J. Bathe, 2 ed., 2014.

[62] G. Sarris, S. G. Haslinger, P. Huthwaite, P. B. Nagy, and M. J. S. Lowe, "Attenuation of Rayleigh waves due to surface roughness," *J. Acoust. Soc. Am.*, vol. 149, pp. 4298–4308, 6 2021.

[63] S. G. Haslinger, M. J. Lowe, P. Huthwaite, R. V. Craster, and F. Shi, "Appraising Kirchhoff approximation theory for the scattering of elastic shear waves by randomly rough defects," *J. Sound Vib.*, vol. 460, 11 2019.

[64] M. Huang, G. Sha, P. Huthwaite, S. I. Rokhlin, and M. J. S. Lowe, "Maximizing the accuracy of finite element simulation of elastic wave propagation in polycrystals," *J. Acoust. Soc. Am.*, vol. 148, pp. 1890–1910, 10 2020.

[65] B. N. Pavlakovic, *Leaky guided ultrasonic waves in NDT*. PhD thesis, Imperial College London, London, 1998.

[66] D. N. Alleyne, *The nondestructive testing of plates using ultrasonic Lamb waves*. PhD thesis, Imperial College London, 2 1991.

[67] W. Weisstein, Eric, *CRC Concise Encyclopedia of Mathematics*. Boca Raton: CRC Press, 1 ed., 1999.

[68] W. H. Press, W. T. Vetterling, S. A. Teukolsky, and B. P. Flannery, *Numerical Recipes in Fortran: The Art of Scientific Computing*. Cambridge: Cambridge University Press, 2 ed., 9 1992.

[69] J. G. Scholte, "The range of existence of Rayleigh and Stoneley waves," *Geophys. J. Int.*, vol. 5, pp. 120–126, 1947.

[70] P. B. Nagy, W. R. Rose, and L. Adler, "A single transducer broadband technique for leaky Lamb wave detection," in *Review of Progress in QNDE* (D. O. Thompson and D. E. Chimenti, eds.), vol. 6A, (Boston, MA), pp. 483–490, Springer US, 1987.

[71] A. H. Nayfeh and D. E. Chimenti, "Propagation of guided waves in fluid-coupled plates of fiber-reinforced composite," *J. Acoust. Soc. Am.*, vol. 83, pp. 1736–1743, 5 1988.

[72] A. Snyder and J. Love, *Optical Waveguide Theory*. London: Chapman and Hall, 1983.

[73] J. Hu and C. R. Menyuk, "Understanding leaky modes: Slab waveguide revisited," *Adv. Opt. Photonics*, vol. 1, pp. 58–106, 2009.

[74] A. G. Every and G. A. D. Briggs, "Surface response of a fluid-loaded solid to impulsive line and point forces: Application to scanning acoustic microscopy," *Phys. Rev. B*, vol. 58, no. 3, pp. 1601–1612, 1998.

[75] O. Lefeuvre, P. Zinin, and G. A. D. Briggs, "Leaky surface waves propagating on a fast on slow system and the implications for material characterization," *Ultrasonics*, vol. 36, pp. 229–232, 1998.

[76] F. B. Cegla, P. Cawley, and M. J. Lowe, "Fluid bulk velocity and attenuation measurements in non-newtonian liquids using a dipstick sensor," *Meas. Sci. Technol.*, vol. 17, pp. 264–274, 2 2006.

[77] A. D. Stuart, "Acoustic radiation from submerged plates. I. Influence of leaky wave poles," *J. Acoust. Soc. Am.*, vol. 59, no. 5, pp. 1160–1169, 1976.

[78] A. H. Nayfeh and P. B. Nagy, "Excess attenuation of leaky Lamb waves due to viscous fluid loading," *J. Acoust. Soc. Am.*, vol. 101, pp. 2649–2658, 5 1997.

[79] T. Hayashi and D. Inoue, "Calculation of leaky Lamb waves with a semi-analytical finite element method," *Ultrasonics*, vol. 54, no. 6, pp. 1460–1469, 2014.

[80] F. H. Quintanilla, *Pseudospectral collocation method for viscoelastic guided wave problems in generally anisotropic media*. PhD thesis, Imperial College London, London, 2 2016.

[81] F. H. Quintanilla, M. J. S. Lowe, and R. V. Craster, "The symmetry and coupling properties of solutions in general anisotropic multilayer waveguides," *J. Acoust. Soc. Am.*, vol. 141, pp. 406–418, 1 2017.

[82] J. D. Achenbach, *Wave Propagation in Elastic Solids*. North Holland Publishing Company, 1973.

[83] L. Kinsley, A. Frey, A. Coppens, and J. Sanders, *Fundamentals of Acoustics*. John Wiley & Sons, 4 ed., 1 2000.

[84] N. F. Declercq, R. Briers, J. Degrieck, and O. Leroy, "The history and properties of ultrasonic inhomogeneous waves," *IEEE Trans. Ultrason. Ferroelectr. Freq. Control*, vol. 52, no. 5, pp. 776–791, 2005.

[85] D. Kiefer, *Elastodynamic quasi-guided waves for transit-time ultrasonic flow metering*. PhD thesis, University of Erlangen-Nuremberg, Erlangen, 2022.

[86] A. Hood, *Localizing the eigenvalues of matrix-valued functions: Analysis and applications*. PhD thesis, Cornell University, Ithaca, 2017.

[87] A. Abdrabou, A. M. Heikal, and S. S. A. Obayya, "Efficient rational Chebyshev pseudo-spectral method with domain decomposition for optical waveguides modal analysis," *Opt. Express*, vol. 24, p. 10495, 5 2016.

[88] D. S. Mackey, N. Mackey, C. Mehl, and V. Mehrmann, "Structured polynomial eigenvalue problems: Good vibrations from good linearizations," *SIAM J. Matrix Anal. Appl.*, vol. 28, no. 4, pp. 1029–1051, 2006.

[89] O. Diligent, M. J. S. Lowe, E. Le Clézio, M. Castaings, and B. Hosten, "Prediction and measurement of nonpropagating Lamb modes at the free end of a plate when the fundamental antisymmetric mode A0 is incident," *J. Acoust. Soc. Am.*, vol. 113, no. 6, p. 3032, 2003.

[90] T. K. Vogt, M. J. S. Lowe, and P. Cawley, "Measurement of the material properties of viscous liquids using ultrasonic guided waves," *IEEE Trans. Ultrason. Ferroelectr. Freq. Control*, vol. 51, no. 6, 2004.

[91] F. B. Cegla, P. Cawley, and M. J. S. Lowe, "Material property measurement using the quasi-Scholte mode—A waveguide sensor," *J. Acoust. Soc. Am.*, vol. 117, pp. 1098–1107, 3 2005.

[92] J. Ma, M. J. Lowe, and F. Simonetti, "Feasibility study of sludge and blockage detection inside pipes using guided torsional waves," *Meas. Sci. Technol.*, vol. 18, pp. 2629–2641, 8 2007.

[93] S. Tang, J. Yin, C. Wang, and G. Zhu, "Study on leaky Lamb waves in functionally graded composites loaded by asymmetric fluids," *Waves Random Complex Media*, pp. 1–20, 7 2022.

[94] E. Georgiades, M. J. S. Lowe, and R. V. Craster, "Computing leaky Lamb waves for waveguides between elastic half-spaces using spectral collocation," *J. Acoust. Soc. Am.*, vol. 155, pp. 629–639, 1 2024.

[95] M. Gallezot, F. Treyssède, and L. Laguerre, "Contribution of leaky modes in the modal analysis of unbounded problems with perfectly matched layers," *J. Acoust. Soc. Am.*, vol. 141, pp. EL16–EL21, 1 2017.

[96] V. Mozhaev and M. Weihnacht, "Subsonic leaky Rayleigh waves at liquid-solid interfaces," *Ultrasonics*, vol. 40, pp. 927–933, 2002.

[97] E. Viggen and H. Arnestad, "Modelling acoustic radiation from vibrating surfaces around coincidence: Radiation into fluids," *J. Sound Vib.*, vol. 560, p. 117787, 9 2023.

[98] G. Sarris, S. G. Haslinger, P. Huthwaite, and M. J. Lowe, "Ultrasonic methods for the detection of near surface fatigue damage," *NDT Int.*, vol. 135, 4 2023.

[99] M. B. Drozdz, *Efficient finite element modelling of ultrasound waves in elastic media*. PhD thesis, Imperial College London, London, 1 2008.

[100] B. Pavlakovic, D. Alleyne, M. Lowe, and P. Cawley, "Simulation of Lamb wave propagation using pure mode excitation," in *Review of Progress in QNDE* (D. O. Thompson and D. E. Chimenti, eds.), vol. 17, pp. 1003–1010, Boston, MA: Springer US, 1998.

[101] M. Gallezot, F. Treyssède, and L. Laguerre, "A modal approach based on perfectly matched layers for the forced response of elastic open waveguides," *J. Comput. Phys.*, vol. 356, pp. 391–409, 3 2018.

[102] R. Sammut and A. W. Snyder, "Leaky modes on a dielectric waveguide: Orthogonality and excitation," *Appl. Opt.*, vol. 15, no. 4, pp. 1040–1044, 1976.

[103] D. Alleyne and P. Cawley, "A two-dimensional Fourier transform method for the measurement of propagating multimode signals," *J. Acoust. Soc. Am.*, vol. 89, no. 3, pp. 1159–1168, 1991.

[104] Lowe M and Cawley P, "The applicability of plate wave techniques for the inspection of adhesive and diffusion bonded joints," *J. Nondestruct. Eval.*, vol. 13, no. 4, p. 185, 1994.

[105] P. B. Nagy, M. Blodgett, and M. Golis, "Weep hole inspection by circumferential creeping waves," *NDT Int.*, vol. 27, no. 3, pp. 131–142, 1994.

[106] C. Valle, M. Niethammer, J. Qu, and L. J. Jacobs, "Crack characterization using guided circumferential waves," *J. Acoust. Soc. Am.*, vol. 110, pp. 1282–1290, 9 2001.

[107] R. Howard and F. Cegla, "Detectability of corrosion damage with circumferential guided waves in reflection and transmission," *NDT Int.*, vol. 91, pp. 108–119, 10 2017.

[108] K. Sezawa, "Dispersion of elastic waves propagated on the surface of stratified bodies and on curved surface," *Bull. Earthq. Res.*, vol. 3, pp. 1–18, 2 1927.

[109] I. A. Viktorov, "Rayleigh type waves on a cylindrical surface," *Sov. Phys. Acoust.*, vol. 4, pp. 131–136, 1958.

[110] I. A. Viktorov, "Normal plate modes in a solid cylindrical layer," *Sov. Phys. Acoust.*, vol. 9, no. 1, pp. 19–22, 1963.

[111] O. D. Grace and R. R. Goodman, "Circumferential waves on solid cylinders," *J. Acoust. Soc. Am.*, vol. 39, pp. 173–174, 1 1966.

[112] G. Liu and J. Qu, "Guided circumferential waves in a circular annulus," *J. Appl. Mech.*, vol. 65, no. 2, pp. 424–430, 1998.

[113] C. Valle, J. Qu, and L. J. Jacobs, "Guided circumferential waves in layered cylinders," *Int. J. Eng. Sci.*, vol. 37, pp. 1369–1387, 1999.

[114] S. Towfighi, T. Kundu, and M. Ehsani, "Elastic wave propagation in circumferential direction in anisotropic cylindrical curved plates," *J. Appl. Mech. Trans. ASME*, vol. 69, pp. 283–291, 5 2002.

[115] J. Fong, *A study of curvature effects on guided elastic waves.* PhD thesis, Imperial College London, London, 10 2005.

[116] J. Fong, "Leaky quasi modes in curved plates," in *Review of Progress in QNDE* (D. O. Thompson and D. E. Chimenti, eds.), vol. 760, (New York), pp. 180–187, AIP Publishing, 4 2005.

[117] D. Gridin, R. V. Craster, J. Fong, M. J. Lowe, and M. Beard, "The high-frequency asymptotic analysis of guided waves in a circular elastic annulus," *Wave Motion*, vol. 38, no. 1, pp. 67–90, 2003.

[118] P. Zuo, X. Yu, and Z. Fan, "Numerical modeling of embedded solid waveguides using SAFE-PML approach using a commercially available finite element package," *NDT Int.*, vol. 90, pp. 11–23, 9 2017.

[119] F. Treyssède, "Spectral element computation of high-frequency leaky modes in three-dimensional solid waveguides," *J. Comput. Phys.*, vol. 314, pp. 341–354, 6 2016.

[120] I. Stakgold and M. Holst, *Green's Functions and Boundary Value Problems.* Wiley, 3 ed., 2011.

[121] E. Skelton and J. James, *Theoretical Acoustics of Underwater Structures.* London: Imperial College Press, 12 1997.

[122] A. Sommerfeld, *Partial Differential Equations in Physics.* New York, NY: Academic Press Inc., 2 ed., 1953.

[123] N. N. Lebedev, *Special Functions and Their Applications.* Englewood Cliffs, NJ: Prentice-Hall Inc., 1965.

[124] G. Stokes, "On the discontinuity of arbitrary constants which appear in divergent developments," in *Transactions of the Cambridge Philosophical Society*, vol. X (I), p. 105, Cambridge University Press, 1858.

[125] R. Paknys, "Evaluation of Hankel functions with complex argument and complex order," *IEEE Trans. Antennas Propag.*, vol. 40, 5 1992.

[126] R. Paknys and D. R. Jackson, "The relation between creeping waves, leaky waves, and surface waves," *IEEE Trans. Antennas Propag.*, vol. 53, pp. 898–907, 3 2005.

[127] J. J. Bowman, T. B. A. Senior, and P. L. E. Uslenghl, *Electromagnetic and Acoustic Scattering by Simple Shapes*. Amsterdam: North Holland Publishing Company, 1 1970.

[128] G. N. Watson, *A Treatise on the Theory of Bessel Functions*. Cambridge, UK: Cambridge University Press, 2 ed., 1966.

[129] F. Olver, *Asymptotics and Special Functions*. A K Peters/CRC Press, 1 1997.

[130] M. Abramowirz and I. A. Stegun, *Handbook of Mathematical Functions*. United States Department of Commerce, National Bureau of Standards, 10 ed., 1972.

[131] L. Flax, C. Guanaurd, Guillermo, and H. Uberall, "Theory of Resonance Scattering," in *Physical Acoustics* (W. P. Mason and R. N. Thurston, eds.), vol. 15 of *Physical Acoustics*, pp. 191–294, Academic Press, 1981.

[132] G. C. Gaunaurd, "Elastic and acoustic resonance wave scattering," *Appl. Mech. Rev.*, vol. 42, no. 6, 1989.

[133] J. J. Faran, "Sound scattering by solid cylinders and spheres," *J. Acoust. Soc. Am.*, vol. 23, pp. 405–418, 7 1951.

[134] N. G. Einspruch and R. Truell, "Scattering of a plane longitudinal wave by a spherical fluid obstacle in an elastic medium," *J. Acoust. Soc. Am.*, vol. 32, pp. 214–220, 2 1960.

[135] N. H. Sun and P. L. Marston, "Ray synthesis of leaky Lamb wave contributions to backscattering from thick cylindrical shells," *J. Acoust. Soc. Am.*, vol. 91, pp. 1398–1402, 3 1992.

[136] P. L. Marston, "Scattering of a bessel beam by a sphere," *J. Acoust. Soc. Am.*, vol. 121, pp. 753–758, 2 2007.

[137] G. C. Gaunaurd and H. Überall, "Numerical evaluation of modal resonances in the echoes of compressional waves scattered from fluid-filled spherical cavities in solids," *J. Appl. Phys.*, vol. 50, no. 7, pp. 4642–4660, 1979.

[138] H. Uberall, "Modal and surface wave resonances in acoustic-wave scattering from elastic objects and in elastic-wave scattering from cavities," in *Proceedings of the 1977 IUTAM Symposium on Modern Problems in Elastic wave Propagations* (J. D. Achenbach and J. Miklowitz, eds.), (Evanston, IL), Northwestern University, 9 1977.

[139] W. G. Neubauer and D. S. Electe Jul, *Acoustic Reflection from Surfaces and Shapes*. Washington, D.C.: Naval Research Laboratory, 6 1986.

[140] J. W. Dickey and H. Überall, "Surface wave resonances in sound scattering from elastic cylinders," *J. Acoust. Soc. Am.*, vol. 63, pp. 319–320, 2 1978.

[141] H. Rhee and Y. Park, "Novel acoustic wave resonance scattering formalism," *J. Acoust. Soc. Am.*, vol. 102, pp. 3401–3412, 12 1997.

[142] E. A. Skelton and J. H. James, "Acoustics of an anisotropic layered cylinder," *J. Sound Vib.*, vol. 161, no. 2, pp. 251–264, 1993.

[143] F. Honarvar and A. N. Sinclair, "Acoustic wave scattering from transversely isotropic cylinders," *J. Acoust. Soc. Am.*, vol. 100, no. 1, pp. 57–63, 1996.

[144] W. C. Chew and W. H. Weedon, "A 3D perfectly matched medium from modified Maxwell's equations with stretched coordinates," *Microw. Opt. Technol. Lett.*, vol. 7, no. 13, pp. 599–604, 1994.

[145] W. C. Chew and Q. H. Liu, "Perfectly matched layers for elastodynamics: A new absorbing boundary condition," *J. Comput. Acoust.*, vol. 4, no. 4, 1996.

[146] U. Basu and A. K. Chopra, "Perfectly matched layers for time-harmonic elastodynamics of unbounded domains: Theory and finite-element implementation," *Comput. Methods Appl. Mech. Eng.*, vol. 192, pp. 1337–1375, 3 2003.

[147] S. Kim and J. E. Pasciak, "The computation of resonances in open systems using a perfectly matched layer," *Math. Comp.*, vol. 78, no. 267, pp. 1375–1398, 2009.

[148] F. Collino and C. Tsogka, "Application of the perfectly matched absorbing layer model to the linear elastodynamic problem in anisotropic heterogeneous media," *Geophys.*, vol. 66, no. 1, pp. 294–307, 2001.

[149] I. Harari and U. Albocher, "Studies of FE/PML for exterior problems of time-harmonic elastic waves," *Comput. Methods Appl. Mech. Eng.*, vol. 195, pp. 3854–3879, 6 2006.

[150] F. Pled and C. Desceliers, "Review and recent developments on the perfectly matched layer (PML) method for the numerical modeling and

simulation of elastic wave propagation in unbounded domains," *Arch. Comput. Methods Eng.*, vol. 29, pp. 471–518, 1 2022.

[151] E. A. Skelton, S. D. Adams, and R. V. Craster, "Guided elastic waves and perfectly matched layers," *Wave Motion*, vol. 44, no. 7-8, pp. 573–592, 2007.

[152] A. Pelat, S. Felix, and V. Pagneux, "A coupled modal-finite element method for the wave propagation modeling in irregular open waveguides," *J. Acoust. Soc. Am.*, vol. 129, pp. 1240–1249, 3 2011.

[153] A.-S. Bonnet-Ben Dhia, B. Goursaud, C. Hazard, and A. Prieto, "A multimodal method for non-uniform open waveguides," *Physics Procedia*, vol. 3, pp. 497–503, 1 2010.

[154] Y. O. Agha, F. Zolla, A. Nicolet, and S. Guenneau, "On the use of PML for the computation of leaky modes: An application to microstructured optical fibres," *Int. J. Comput. Math. Electr.*, vol. 27, no. 1, pp. 95–109, 2008.

List of Publications

[P1] E. Georgiades, M. J. S. Lowe, and R. V. Craster, "Leaky wave characterisation using spectral methods," *J. Acoust. Soc. Am.* , vol. 152, pp. 1487–1497, 9 2022.

[P2] E. Georgiades, M. J. S. Lowe, and R. V. Craster, "Computing leaky lamb waves for waveguides between elastic half-spaces using spectral collocation," *J. Acoust. Soc. Am.*, vol. 155, pp. 629–639, 1 2024.

[P3] E. Georgiades, M. J. S. Lowe, and R. V. Craster, "A unified approach for leaky circumferential wave dispersion and scattering from elastic annuli," *Submitted for publication*, 2025.